EFFICIENCY AND PRESSURE LOSS CHARACTERISTICS OF

AN ULTRA-COMPACT COMBUSTOR WITH BULK SWIRL

THESIS

James T. Radtke, ENS, USN

AFIT/GAE/ENY/07-J18

DEPARTMENT OF THE AIR FORCE
AIR UNIVERSITY

AIR FORCE INSTITUTE OF TECHNOLOGY

Wright-Patterson Air Force Base, Ohio

AFIT/GAE/ENY/07-J18

EFFICIENCY AND PRESSURE LOSS CHARACTERISITICS OF AN ULTRA-

COMPACT COMBUSTOR WITH BULK SWIRL

THESIS

Presented to the Faculty

Department of Aeronautics and Astronautics

Graduate School of Engineering and Management

Air Force Institute of Technology

Air University

Air Education and Training Command

In Partial Fulfillment of the Requirements for the

Degree of Master of Science in Aeronautical Engineering

James T. Radtke, BS

Ensign, USN

June 2007

AFIT/GAE/ENY/07-J18

EFFICIENCY AND PRESSURE LOSS CHARACTERISITICS OF AN ULTRA-

COMPACT COMBUSTOR WITH BULK SWIRL

James T. Radtke, BS
Ensign, USN

Approved:

_____ /signed/_____   _____
Dr. Paul King, PhD (Chairman)   Date

_____/signed/_____   _____
Major Richard Branam, PhD(Member)   Date

_____/signed/_____   _____
Dr. Marcus Polanka, PhD (Member)   Date

AFIT/GAE/ENY/07-J18

Abstract

Research was conducted on a novel combustor design using a highly centrifugal loaded circumferential cavity to enhance flame speeds and lower mixing time to lower overall combustion time achieving improved efficiency and stability. This Ultra-Compact Combustor (UCC) is fed air with a bulk swirl, resembling gas leaving a compressor without the final set of compressor guide vanes to straighten the flow, at higher than normal Mach numbers for a combustor. The larger Mach numbers in the combustor do not cause a total pressure loss in excess of what Rayleigh theory would dictate for the given heat addition taking place within the combustor.

Tests were conducted on the UCC with a clockwise or counter-clockwise swirl direction in the circumferential cavity using JP-8 and natural gas derived Fischer-Tropsch synthetic jet fuel with each direction. The results for lean blow out stability, combustion efficiency, and emissions proved the best configuration uses counter-clockwise swirl. The two fuels performed equally with no noticeable differences between JP-8 and the synthetic Fischer-Tropsch fuel.

To my parents, family, and friends…

Table of Contents

List of Figures

List of Tables

List of Symbols

Nomenclature

A = Area (m^2)

A_{CD} = Effective area (m^2)

AFRL = Air Force Research Laboratories

C_p = Specific heat at constant pressure (J/kg K)

CCW = Counter-clockwise

CIAC = Cavity-in-a-cavity

CO = Carbon monoxide

CO_2 = Carbon dioxide

CW = Clockwise

E = Energy

EI = Emissions index

F = Force (N)

FT = Fischer-Tropsch

g = Gravity (9.81 m/s^2)

H_c = Lower heating value of fuel (J/kg)

ITB = Inter turbine burner

LBO = Lean blow out

LP = Loading parameter

$\dot{m}$ = Mass flow rate (kg/s)

M = Mach number

NO_x = Oxides of nitrogen

P = Pressure (Pa)

Q = Heating value of fuel (J/kg)

RVC = Radial vane cavity

q = Dynamic pressure

R = Gas constant (8.314 J/mol K)

r = Radius (m)

S = Flame speed (m/s)

s = entropy (J/kg K)

SMD = Sauter mean diameter

ST = Specific thrust

T = Temperature (K)

TSFC = Thrust specific fuel consumption

TVC = Trapped Vortex Combustor

u = Velocity (m/s)

UCC = Ultra Compact Combustor

UHC = Unburned hydrocarbons

Symbols

β = Angle or bypass ratio

γ = Ratio of specific heats

η = Efficiency

π = Pressure ratio

ρ = Density

Φ = Equivalence ratio

Subscripts

a = Air or atmospheric value when paired with P or T

av = Average

b = Burner or combustor

c = Compressor

e = Exit

fab = Fuel for afterburner

fb = Fuel for burner

ftb = Fuel for turbine burner

ref = Reference

t = Turbine

tb = Turbine burner

tx = Total or stagnation value at station x

Units

F = Fahrenheit

Hz = Hertz

J = Joules

K = Kelvin

kg = Kilograms

lbm = Pounds mass

N = Newton

min = Minutes

s = Seconds

m = meters

cm = centimeters

EFFICIENCY AND PRESSURE LOSS CHARACTERISITICS OF AN

ULTRA-COMPACT COMBUSTOR WITH BULK SWIRL

I. Introduction and Overview

1.1 Historical Background

Aircraft propulsion systems have advanced dramatically since the Wright Brother's first flight in 1903. This first aircraft was powered by a propeller driven by piston engine and the propeller dominated aircraft propulsion for the next fifty years. During that time, as designers pushed to increase speed, it became clear that the propeller limited a plane to subsonic flight. The desire to increase performance created the need for a new form of propulsion that would not handicap designs in the same way as a propeller.

The jet engine was the answer to this design problem. This revolutionary form of propulsion was developed concurrently by the individual efforts of England's Frank Whittle and Germany's Hans von Ohain in the years leading up to World War II. Hans von Ohain's design first flew on August 27, 1939 becoming the first jet engine to power an aircraft (Saravanamuttoo et al., 2001:12). This achievement marked the beginning of the jet age and eventual rise to prominence of the jet engine as the premier choice for powering modern aircraft.

Since the initial invention of the turbo-jet by von Ohain and Whittle there has been a constant push to improve performance and efficiency. This drive leads to the eventual development of the turbo-fan engine to reduce Thrust Specific Fuel Consumption (TSFC). In keeping with the idea that there is always room for

improvement, today scientists and engineers are looking for ways to further develop the turbine engine. The goal is to reduce size and weight and increase efficiency and reliability while maintaining or improving the performance level of current designs. With these goals in mind, the development of the Ultra Compact Combustor (UCC) is necessary to reach the aim of an improved turbine engine.

1.2 Conceptual Design

The basic premise of the UCC is to reduce the overall size of current combustor designs. In current combustors the combustion process occurs over a portion of the axial length of the engine. The UCC seeks to have combustion occur in a cavity that wraps around the circumference of the engine using a highly swirled flow to replace the axial distance used in current design practice. A cross section of the Ultra Compact Combustor is shown below in Figure 1.
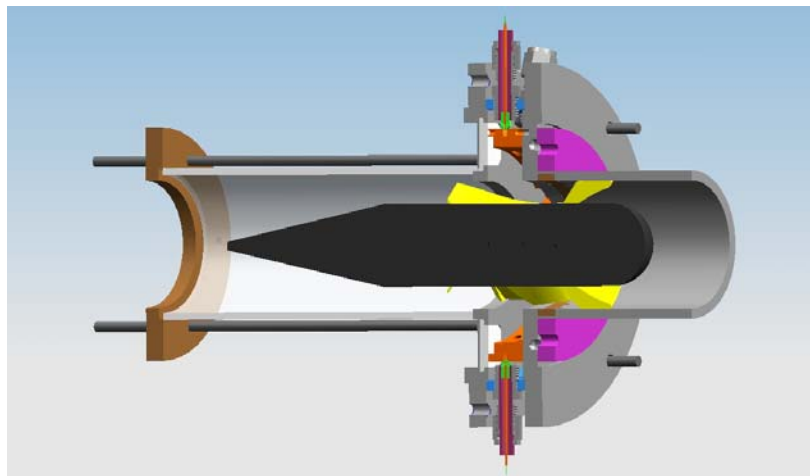
Figure 1. Ultra Compact Combustor cross-section

The current concept for a UCC consists of a cavity surrounding the outside circumference of the engine using extended turbine guide vanes as a support for a center body. The turbine guide vanes have a radial cavity that is aligned with the primary cavity

2

above the vanes and this smaller radial cavity extends to the center body. This smaller cavity acts as a secondary combustion zone. Fuel is introduced into the combustor in the primary cavity only.

The UCC builds off the lessons of the Trapped Vortex Combustor and it works by having the air flow axially along the center body where it becomes entrained into the cavity creating a vortex. This vortex increases fuel-air mixing and helps to stabilize the flame (Sturgess and Hsu, 1998:1). Air is introduced along the cavity perimeter using equally spaced injectors angled to create a highly swirled air flow in the cavity. This swirling air flow increases g-loading and reduces chemical residence time (Zelina et al., 2004:2). The UCC uses this circumferential swirl to achieve a high g-loaded flow through the primary cavity, which in turn increases flame speeds, thus reducing chemical time for combustion. This high g-loading induces a buoyant transport mechanism for flame spreading proportional to the square root of the applied acceleration above 500 g's (Lewis, 1972:413). To this end, the UCC will apply a load to the swirled flow between 500 and 3000 g depending on operating conditions to make buoyant flame transport possible (Zelina et al., 2004a:6). The bulk of the combustion process occurs in the circumferential cavity and as it is burning to completion the lower wake pressures in the main axial flow will carry the combustion products into the radial cavities imbedded in the turbine vanes (Zelina et al., 2006a:2). The combustion process will finish in the secondary zone of the radial cavities before the products are mixed with the main air and carried away to the turbine. This combustion process results in axial flame lengths approximately half of those associated with conventional combustion systems (Zelina et al., 2004b:1).

1.3 Motivation

The UCC development effort is being lead by Air Force Research Laboratory's Propulsion Directorate, Turbine Engine Division, Combustion Branch. The UCC will benefit future engines because of its smaller size and reduced weight. It does not require compressor guide vanes ahead of the combustor because swirling flow from the compressor can be used to help drive the swirl in the UCC main cavity. Also the turbine guide vanes are integral to the UCC which further reduces the length of the system (Quaale et al., 2003:2). A combustor of this described design could be almost 66% shorter than today's designs (Zelina et al., 2004a:3).

Besides offering size and weight reductions, the UCC opens the door to adding a reheat step to the Brayton cycle currently used in modern aircraft turbine engines. A UCC can be placed between the high and low pressure turbines, adding a reheat step before the vitiated flow moves through the low pressure turbine. This arrangement has been referred to as an Inter Turbine Burner (ITB) and it shows remarkable promise for increasing Specific Thrust (ST) by at least 50% with no increase in TSFC (Quaale et al., 2003:1). This small heat addition process, on the order of about 420 K, will allow for large amounts of power to be extracted in the low pressure turbine. This power can be used to drive a generator for applications that require large amounts of electricity or to power an ultra-high bypass ratio turbofan (Zelina et al., 2006b:1). The ITB also offers the prospect of being able to increase reliability and reduce time between overhauls by lowering the maximum turbine inlet temperature. Then using an ITB to add the lost heat incurred by the lowered maximum inlet temperatures (Zelina et al., 2006b:2).

The UCC has also shown promise through increases in combustion efficiency and lower pollutant outputs. Previous tests at atmospheric pressures have shown operating efficiencies between 95-99% and the promise of lower emissions than current designs (Zelina et al., 2004a:1, 8). With the push for greater efficiency, better performance, and lower pollutant emissions prevalent in the modern day design process, the technology of the UCC can be seen as one of the next possible steps in gas turbine engine development.

1.4 Method

The Ultra-Compact Combustor use of the bulk swirl from the compressor does not require compressor guide vanes at the end of the compressor to straighten the flow or a diffuser to slow the flow to lower Mach numbers. Due to the higher Mach numbers entering the UCC, excessive Rayleigh pressure losses are a concern due to their detrimental impact on overall engine efficiency. Along with an investigation into Rayleigh induced pressure loss, four different configurations of the UCC were tested to compare their lean blow out characteristics, combustion efficiency, and emissions. The tests took place at AFRL's Atmospheric Pressure Combustion Research Complex.

1.5 Content

This thesis addresses the results collected during the experiments conducted on the UCC.   The collected information has been used to examine Rayleigh induced pressure loss, combustor efficiency, emissions, and lean blow-out stability of the UCC. This information is then used to develop conclusions about the UCC pressure loss characteristics and the optimal configuration for the best performance of the UCC.

II. Background and Theory

2.1 General Combustor Principles

There are many relations that describe different aspects of combustor operation, and allow for comparison between combustors of different design. There are several that are of particular interest to this research and they are described in the following sections. These relations will be used to assist in the discussion of pertinent background material, describe operating conditions of the UCC during testing, and the discussion of results.

2.1.1 Equivalence Ratio

The equivalence ratio (Φ) is used to describe the fuel-air mixture; its definition is shown below.

$$\Phi = \frac{\dfrac{\dot{m}_f}{\dot{m}_a}}{\dfrac{\dot{m}_f}{\dot{m}_a}\bigg|_{stoich}} \tag{1}$$

An equivalence ratio equal to one represents a stoichmetric fuel-air mixture, while a ratio greater than one is fuel rich and a ratio less than one is fuel lean (Lefevbre, 1999:63)

2.1.2 Pressure Loss

A pressure loss is inherent to the combustion process and can be described two ways. The overall pressure loss across the whole combustor is represented below.

$$\frac{P_{t4} - P_{t3}}{P_{t3}} \tag{2}$$

This loss is normally represented by a percentage and typically falls between four to eight percent for most combustor designs. Pressure loss can also be described by a pressure loss factor that is a fixed property of the combustor design. This number, shown below, could be thought of as a resistance to the air flow (Lefevbre, 1999:102).

$$\frac{P_{t4} - P_{t3}}{q_{ref}} \tag{3}$$

The dynamic pressure reference value, q_{ref}, is measured at the inlet plane of the main burner.

2.1.3 Emissions Index

The emissions index (EI) is used to represent the amount of pollutants emitted by a particular engine for the quantity of fuel consumed. The nature of the calculation creates a parameter that allows for easy comparison between engines of varying size (Lefevbre, 1999:314).

$$EI = \frac{\dot{m}_{pollutants,gram}}{\dot{m}_{fuel,kg}} \tag{4}$$

2.1.4 Combustion Efficiency

The combustion efficiency, represented as a percentage, quantifies how well a given combustor operates. It can be thought of as a measure of how well the combustor releases the stored energy of the fuel into the air flow. The calculation method for this number is defined by The Society of Automotive engineers in a recommended practice for the aerospace industry (SAE, 1994: 16). This commonly accepted method of calculating combustion efficiency allows for easy comparison between works by different

7

authors. This definition of combustion efficiency, shown below, is used for all

calculations of combustion efficiency in this thesis.

$$\eta_b = \left(1.00 - 10109\frac{EI_{Co}}{H_c} - \frac{EI_{C_xH_y}}{1000}\right) \times 100 \qquad (5)$$

The number H_c represents the lower heating value of the fuel in J/kg. This definition

calculates the efficiency on an enthalpy basis by subtracting the amount of unburned fuel

and carbon monoxide, representing the inefficiencies of incomplete combustion. A value

of 100% represents complete combustion. This method does neglect the impact of NO_x

and the dissociation of combustion products (SAE, 1994:16).

2.1.5 Centrifugal Loading

The centrifugal loading in the circumferential cavity of the UCC is of particular

importance because it is used to increase mixing and decrease reaction times through

increased flame speeds. Calculating the g-loading on the UCC is a two step process

using the following equations (Zelina et al., 2004a:6).

$$V_{tan} = \frac{\dot{m}_{a,cavity}}{\rho_{cavity}A_{exit}}\frac{1}{\tan\beta} \qquad (6)$$

$$g = \frac{V_{tan}^2}{g_0 r_{cavity}} \qquad (7)$$

The angle β used in Equation 6 is calculated from a computational fluid dynamics code

and in past studies has fallen between 23 and 28 degrees. It represents the angle between

the tangential and radial velocity components of the swirling flow. It is based on past

data and has been re-calculated for the particular test rig used for this thesis.

2.1.6 Overall Fuel-Air Ratio

The mixture of fuel to air is represented by the overall fuel-air ratio (OFAR) for the entire combustor. It is typically used to describe the conditions when lean blow out occurs. The OFAR calculation is as follows.

$$OFAR = \frac{\dot{m}_f}{\dot{m}_{a,total}} \qquad (8)$$

2.1.7 Combustor Loading Parameter

Zelina et al. (Zelina et al., 2004a: 5) describes the combustor loading parameter, a number used to normalize size and pressure effects across different combustors and is related to the residence time of the flow in the combustor. The parameter is calculated below.

$$LP = \frac{\dot{m}_a}{\delta_{3.0}^{1.75} Vol_{cavity} e^{\frac{T_3}{540}}} \qquad (9)$$

$$\delta = \frac{P_{03}}{14.7} \qquad (10)$$

Typical values of the loading parameter for a conventional combustor range from 0.25 to 1.5. In the UCC the volume of the combustor is greatly reduced compared to a conventional system, so the LP for the UCC is much higher. On average, the LP for the UCC is roughly four times larger than conventional systems (Zelina et al., 2004a: 5). Increased loading parameters are indicative of smaller more compact combustor designs.

2.2 Traditional Combustor Design

Gas turbine engine combustors can take many forms depending on the intended purpose of each particular engine. Even with all the variations in design to meet specific

objectives, all combustors share some universal design features. The most common of these features are the three different combustion zones: primary, intermediate, and dilution.

The primary region is where the combustion process begins. This is where fuel injectors introduce an atomized spray to the airflow and it is characterized by a fuel rich mixture. A recirculation zone is created by swirling air around the fuel injector to anchor the flame in the primary zone. This recirculation of hot gases provides a continuous ignition source (Barnard and Bradley, 1985:253). The combustion process is essentially completed in this zone resulting in large amounts of unburned hydrocarbons and other pollutants such as carbon monoxide and nitrogen oxides.

The primary region products then flow to an intermediate zone. In this area, the fuel-air mixture becomes fuel lean with the addition of more air through the liner. The addition of this air slowly quenches the burning process by lowering the temperature to an intermediate level allowing it to finish completely. This reduces the amount of unburned hydrocarbons and carbon monoxide in the efflux gases from this region (Lefebvre, 1999:15-16).

The combustion products finally pass into the dilution zone of the combustor. This zone is where the majority of the air is added to cool the hot gases flowing from upstream of the combustor. The importance of the dilution air cannot be understated because it is used to quench the reaction, improve the pattern factor of the hot gases, and lower the gas temperature to prevent damage to the turbine blades before entering the high pressure turbine (Lefebvre, 1999:16).

The UCC incorporates these same combustion zones in a much smaller design. According to Zelina et al. (Zelina et al., 2006a: 2) the circumferential cavity acts as the primary combustion zone, the radial cavities in the turbine guide vanes operate as an intermediate area, and the dilution zone is created by the circumferential strut flame-holder. In this manner the UCC operates with the same principle as any other combustor.

2.3 Trapped Vortex Combustor

The Trapped Vortex Combustor (TVC) is the predecessor of the UCC. The concepts explored during the TVC development are directly applicable to the UCC. The TVC was developed with the intent of lowering emissions and creating a more compact and simpler combustor design.

In the first design iteration of the TVC, a vortex is trapped within a cavity to stabilize a flame. Air and fuel are also introduced into this cavity to strengthen the vortex and further stabilize the flame. The cavity acts as a shielded pilot to ensure that the main combustor has a constant stable source of ignition, thus eliminating the primary combustion zone. This shielded pilot allowed for a wider operating range and lead to improved combustion efficiency (Roquemore et al., 2001: 1-2).

Subsequent generations of the TVC led to a design using a double vortex, as seen below in Figure 2, on either side of the main combustion chamber. This design injects all of the fuel into the two cavities that hold the vortices (Roquemore et al., 2001: 9).

11
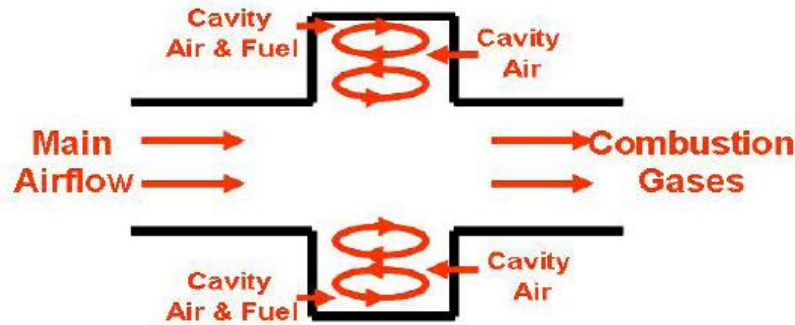
Figure 2. Trapped Vortex Combustor concept (Greenwood, 2005:1-2)

The vortices in the cavities improve fuel-air mixing and the support struts that sit flush with the front plane of the cavities act as bluff bodies to draw combustion products out of the cavities. These bluff bodies create a recirculation zone that mixes the cavity products with the main air flow. The cavities operate in a very fuel-rich environment and the recirculation zone created by the struts acts as lean burn zone in the TVC design. The lean burn area allows combustion of unburned hydrocarbons and carbon monoxide to finish, thus reducing emissions. The combustors that are part of the TVC class all display good lean blow out limits and are easier to relight at altitude because of the shielded nature of the cavity (Roquemore et al., 2001: 5).

The UCC incorporates the idea of using a vortex trapped within a cavity to enhance mixing of the fuel and air, as well as better flame stability. The UCC adds a highly centrifugally loaded swirling flow in the circumferential cavity to enhance flame speeds in combination with the trapped vortex. The UCC synthesis of these two concepts has lead to an improved combustor design for future engines.

2.4 Centrifugal Force Enhanced Combustion

Flame speeds fall into two different categories based on their burning rate and method of propagation. The two categories are laminar and turbulent. Each name

12

denotes different flame characteristics and a range of inherent speeds for that type of flame. It is hypothesized a third regime of flame transport exists: bubble or buoyant burning. This method relies on buoyant forces to help transport the flame and may be considered an enhanced turbulent flame speed. Current combustors rely on turbulence to induce higher speed turbulent flames in comparison to the speed of a laminar flame. To increase flame speeds and decrease reaction times, the UCC creates buoyant transport conditions in the circumferential cavity through an applied centrifugal force field.

Lewis (Lewis, 1973:1) is responsible for most of the basic research that lead to the idea of using centrifugal force to enhance flame speeds. In normal gravity, the buoyant force of hot rising gases in cool air is too small to overcome the laminar and turbulent flame spreading rates. The buoyant force is calculated by the following equation (Lewis, 1973:1).

$$F_B = \rho_a g \left[1 - \frac{\rho_f}{\rho_a} \right] \tag{11}$$

This force is generally ignored because it is so small. The easiest way to increase the buoyant force of a flame is increase the centrifugal force, g, acting on the combustible mixture. As this force increases it will eventually cause a bubble of hot burning gas to move faster than the laminar or turbulent flame speeds becoming the dominant flame transport mechanism (Lewis, 1972:416). After running a series of tests using a combustion centrifuge, Lewis found below 200 g the buoyant force has little to no effect on a combusting mixture (Lewis, 1973:1). As the centrifugal force is increased beyond 200 g to 500 g a transition starts to occur as the buoyant force starts to become more dominant. Beyond 500 g the buoyancy force has induced a bubble, i.e., buoyancy transport mechanism, and the overall flame speed starts to increase proportional to the

square root of the g-loading acting on the mixture (Lewis, 1972:415). Lewis found his

data for the bubble velocity of the flame to fit the expression (Lewis, 1973:2),

$$S_B = 1.25\sqrt{g} \qquad (12)$$

Equation 12 implies flame speed can be continually increased through a growing g-

loading, however; it was found the flame speed will peak around a centrifugal loading of

3500 g. After that the flame speed starts to decrease until the flame extinguishes itself

around 5000 g (Lewis, 1972:415-418). Data published by Lewis shows the g-loading at

flame extinction grows with the inherent laminar flame speed for a specific mixture

(Lewis, 1972:419). Later work by Athenien and Zelina (Athenien and Zelina, 2006:3-4)

exploring the combustion regime found in the UCC demonstrated that as the g-load

increases in the circumferential cavity the turbulent Reynolds number decreases. This

decrease indicates a relaminarization of the flow, leading to a large drop in flame speed

and consequently extinction because the flame cannot spread fast enough to stay lit.

2.5 Inter-Turbine Burning

The development of the UCC will make it possible include a reheat step in the

Brayton cycle to gain enhanced performance. Sirignano and Liu (Sirignano and Liu,

1998:1-2) pioneered the idea of inter-turbine burning when they proposed a constant

temperature cycle that uses a constant heat addition process in the turbine. This proposed

constant temperature cycle, shown below in Figure 3, would allow for smaller

afterburners, lowered thrust specific fuel consumption (TSFC) in comparison to the use

of an afterburner, and an increase in specific thrust (ST) (Liu and Sirignano, 2000:1).
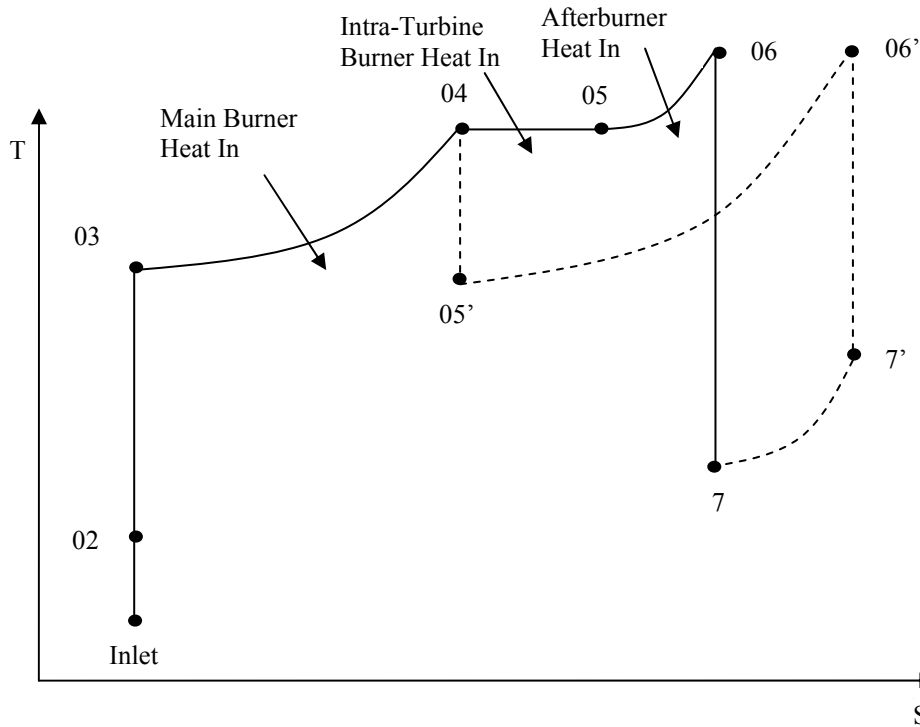
**Figure 3. Conventional (dashed line) and constant temp (solid line) cycle T-s diagram
(Adapted from Sirignano and Liu, 2000:9)**

To demonstrate the advantages of their proposed constant temperature cycle,
Sirignano and Liu (Sirignano and Liu, 1998:2-3) carried out a cycle analysis. Parts of
their cycle analysis are replicated in the following passages to demonstrate the benefits
gained by inter-turbine burning. During their analysis several assumptions were made:

1. No air is bled from the compressor

2. The gases are completely expanded at the nozzle exit

3. No auxiliary power is extracted in the turbine, so the turbine work balances with
   the compressor power demands

4. A perfect gas with constant properties, including specific heat

5. A constant stagnation temperature is maintained in the turbine through organized
   heat addition.

15

For the sake of brevity, only the details of the main burner, a conventional turbine, a turbine-burner, and engine performance criteria will be explored. Conventional cycle analysis techniques were used to analyze engine components that are noted in the following discussion.

2.5.1 Main Burner

The heat addition relation for the main combustor assumes the enthalpy and kinetic energy of the incoming fuel is negligible and is shown in Equation 13.

$$\dot{m}_{fb} Q_R \eta_b = C_p T_{04} (\dot{m}_a + \dot{m}_{fb}) - C_p T_{t3} \dot{m}_a \tag{13}$$

Using the heat addition relation for the main combustor the following relationship between the fuel mass flow rate and the air mass flow rate can be established.

$$\frac{\dot{m}_{fb}}{\dot{m}_a} = \frac{C_p (T_{t4} - T_{t3})}{Q_R \eta_b - C_p T_{t4}} \tag{14}$$

Equation 14 relates the fuel mass flow and temperature rise across the combustor. The heat addition is limited in this equation because the burner exit temperature is set by material limits in the combustor and downstream assemblies, consequently having a direct effect on ST and TSFC. The combustion process itself has an inherent pressure loss that is described below by Equation 15.

$$P_{t4} = \pi_b P_{t3} \tag{15}$$

2.5.2 Conventional Turbine

The turbine assembly must generate enough power to supply the power demands of the compressor. Work must be balanced between these two engine components and it is shown below.

$$\dot{m}_t C_{pt}(T_{t4} - T_{t5}) = \dot{m}_c C_{pc}(T_{t3} - T_{t2}) \tag{16}$$

The associated temperature and pressure drops across the turbine from the work balance are detailed in the following.

$$\frac{T_{t5}}{T_{t4}} = 1 - \frac{\dot{m}_c C_{pc}(T_{t3} - T_{t2})}{\dot{m}_t C_{pt} T_{t4}} \tag{17}$$

$$\frac{P_{t5}}{P_{t4}} = \left[1 - \frac{1}{\eta_t}\left(1 - \frac{T_{t5}}{T_{t4}}\right)\right]^{\frac{\gamma}{\gamma-1}} \tag{18}$$

2.5.3 Turbine-Burner

The turbine-burner would augment a conventional turbine by allowing controlled combustion to take place within the turbine to maintain a constant stagnation temperature as the gases expand through the turbine.

$$T_{t5} = T_{t4} \tag{19}$$

Equation 19 takes the place of Equation 17 during an analysis of a turbine burner engine, compared to a conventional cycle, because the added energy from intra-turbine combustion is transformed directly into the work extracted by the rotor, not into increasing the gas temperature; thus, the gas remains at a constant stagnation temperature. The required fuel flow to accomplish this condition is detailed in the following equation.

$$\dot{m}_{ftb} = \frac{Turbine \quad power \quad requirement}{Q_R \eta_{tb}} \qquad (20)$$

An average temperature can be used to represent the heat added to the flow if an average

Mach number is used to represent the flow speed through the turbine-burner.

$$T_{av} = \frac{T_{t4}}{1 + \frac{\gamma - 1}{2} M_{av}^{\;2}} \qquad (21)$$

Using this average temperature an entropy calculation is performed below for use in

calculating the turbine-burner pressure ratio.

$$s_5 - s_4 = \frac{\dot{m}_{ftb} Q_R \eta_{tb}}{(\dot{m}_a + \dot{m}_{fb}) T_{av}} = \frac{Power_{Turbine}}{(\dot{m}_a + \dot{m}_{fb}) T_{av}} \qquad (22)$$

$$\frac{P_{t5}}{P_{t4}} = e^{\frac{s_5 - s_4}{R}} \qquad (23)$$

Due to the complicated combustion characteristics that will take place in an intra-turbine

burner a pressure recover factory, π_{tb}, is introduced. This factor accounts for the

stagnation pressure loss that will occur from the combustion and flow interactions with

the turbine while burning.

$$\frac{P_{t5}}{P_{t4}} = \pi_{tb} e^{\frac{s_5 - s_4}{R}} \qquad (24)$$

2.5.4 Engine Performance Criteria

When describing a turbine engine there are two main criteria used to evaluate its

performance, specific thrust and thrust specific fuel consumption. For an engine using

intra-turbine burning, ST and TSFC calculations are completed below.

$$ST = \frac{Thrust}{\dot{m}_a} = \left[\left(1 + \frac{\dot{m}_{fb}}{\dot{m}_a} + \frac{\dot{m}_{ftb}}{\dot{m}_a} + \frac{\dot{m}_{fab}}{\dot{m}_a} \right) u_e - u \right] \qquad (25)$$

$$TSFC = \frac{\dot{m}_f}{Thrust} = \frac{\dot{m}_{fb} + \dot{m}_{ftb} + \dot{m}_{fab}}{ST \times \dot{m}_a} \qquad (26)$$

After Sirignano and Liu (Sirignano and Liu, 1998:5) completed their analysis, they found

performance improvements using their constant temperature cycle. A large increase in

ST took place without a large gain in TSFC; when comparing a turbine-burner engine to

an afterburning engine for a 20% increase in ST the turbine-burner configuration only

showed a 10% gain in TSFC while the afterburning engine showed nearly a 50% gain in

TSFC for the same increase in ST. A discrete heat addition between the turbine stages,

illustrated below in Figure 4, would not see quite the same performance increases as the

constant temperature engine, but it will open the window to significant performance

improvements over current engine designs.
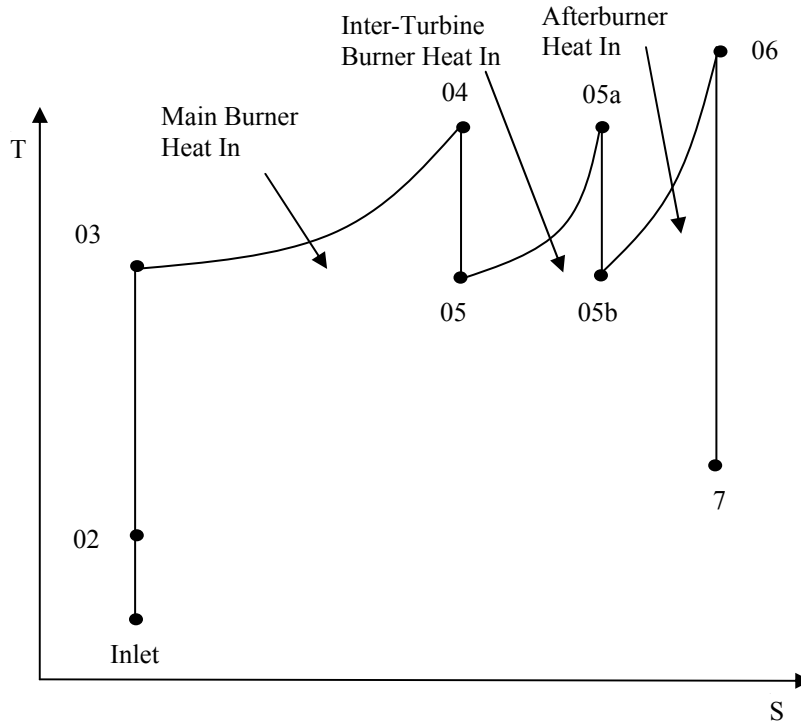
Figure 4. Single stage ITB T-s diagram (adapted from Sirignano and Liu, 2000:9)

2.5.5 Single Stage ITB Performance Study

An analysis of a dual-spool turbofan and a turboshaft engine was completed to compare the performance benefits that could be gained from using an ITB between the high and low pressure turbines. A code was written as part of this thesis using the method outlined by Hill and Peterson (Hill and Peterson, 1992:171-189) to analyze each engine cycle. This analysis used variable specific heats through each engine component and component efficiencies supplied by Mattingly et al. (Mattingly et al., 2002:107). The equations, specific heats, and component efficiencies used can be found in Appendix A. This cycle analysis is considered ideal because it does not include losses that are inherent through turbine cooling, drive shaft inefficiencies, and blade tip effects at high speeds. The analysis used a single-point on-design calculations with the overall compressor pressure ratio and turbine inlet temperature set as constants. The maximum temperature rise for the ITB was chosen to be 420K, or 300°F, in accordance with results published by Zelina et al. (Zelina et al., 2006b:1) for optimum work extraction from the low pressure turbine.

To demonstrate the utility of the ITB in accordance with its purpose, to make it possible to extract large amounts of power from the low pressure turbine, the fan pressure ratio and bypass ratio were varied for the turbofan engine. These two variables were chosen because each directly impacts the amount of work that has to be extracted from the low pressure turbine. In each study, these variables were increased until the low pressure turbine could not provide enough energy to supply the increased power demands from the corresponding design variable change. The MATLAB script written to perform this analysis used an if statement that broke the loop when the low pressure turbine tried

to expand the gases beyond atmospheric pressure, the limit for power extraction from a turbine.

The first study varied the fan pressure ratio. During theses calculations the bypass ratio was held as a constant at a value of five. This pressure ratio is proportional to the amount of work the lower pressure turbine has to extract to power the fan. The results of the comparison in form specific thrust and thrust specific fuel consumption are shown below in Figure 5.
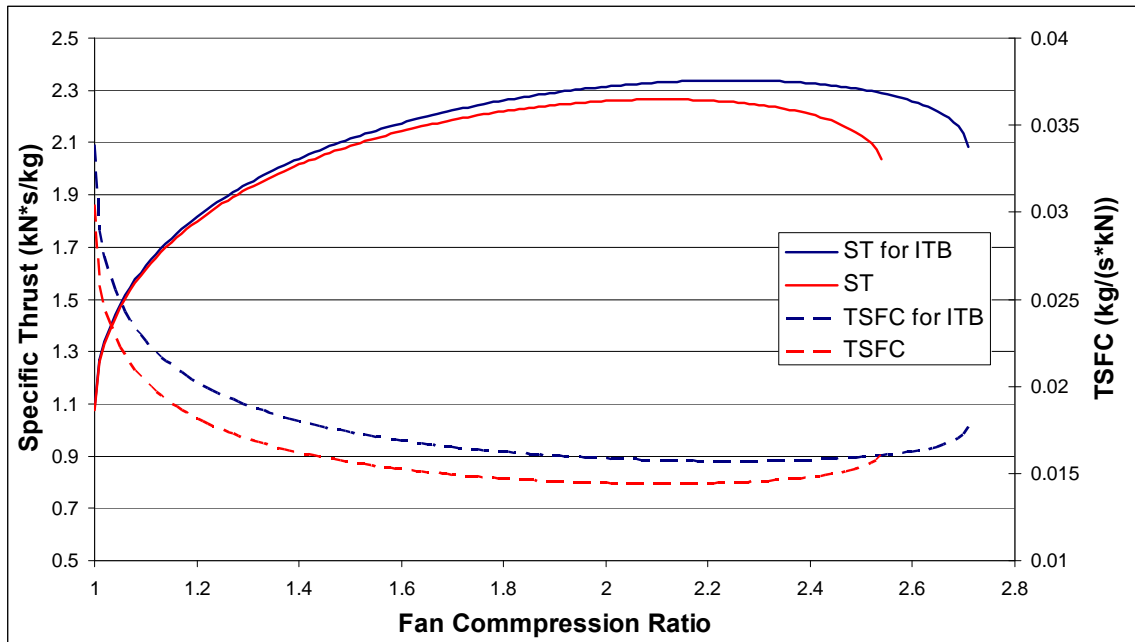
Figure 5. ITB impact on ST and TSFC for a varied fan pressure ratio

On average using an ITB increased the ST by 2.5% for a TSFC increase of 10.45%. The maximum of the ST curves corresponds to the minimum TSFC for that particular engine and represents the ideal operating point for this engine. Comparing these points between the two cycles showed a gain of 3.22% in ST and a 9% gain in fuel consumption. This marginal gain in performance for such a large jump in fuel consumption shows using an ITB to increase the fan compression ratio is impractical. It would also be less efficient to increase the fan pressure ratio and consequently the fan air stream exit velocity because it

21

is more efficient to move a large mass of air over a smaller velocity increment; hence the idea of increasing the bypass ratio to make more efficient engines.

More encouraging results were found when the bypass ratio was varied with a set fan pressure ratio of 1.5. Figure 6 displays the results of a varied bybass ratio in the form of ST and TSFC.
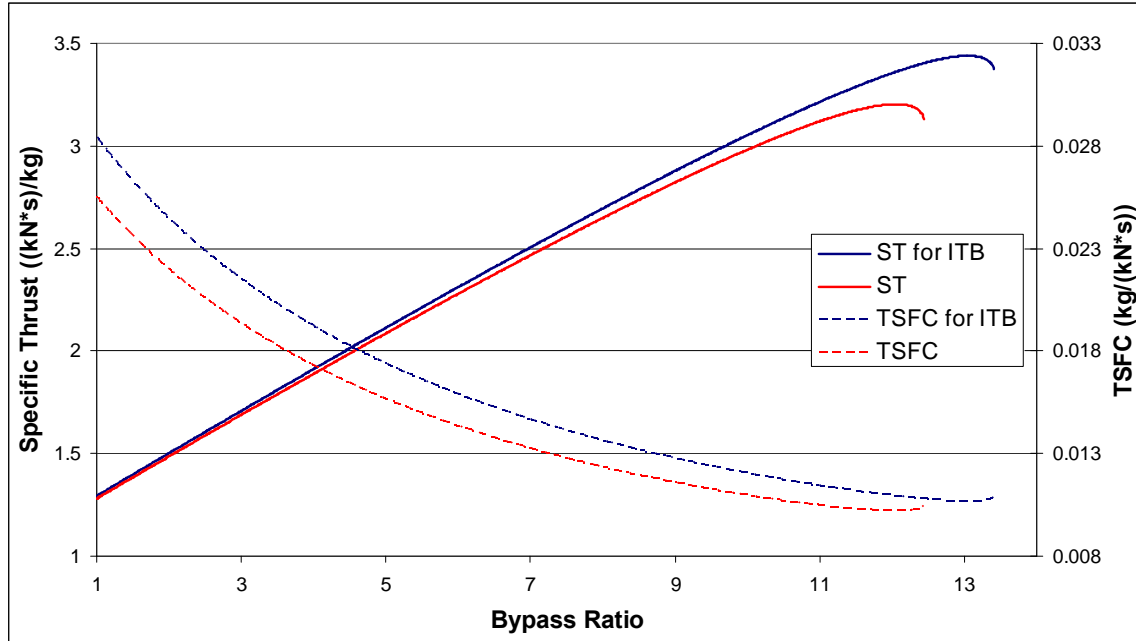
Figure 6. ITB impact on ST and TSFC for a varied bypass ratio

On average a 1.93% gain in ST was found for a 10.33% gain in fuel consumption over the entire graph. This is due to the fact that at low bypass ratios the ITB is not operating since the extra power is not needed to drive the fan. As the bypass ratio increases, there is a much larger increase in ST between the engines for a more reasonable jump in TSFC. At the maximum point on the ST curve, a corresponding minimum on the TSFC curve is found representing the most efficient operating point for this particular engine. In the case of the ITB engine, the ST curve peaked at a bypass ratio of 13.05 and the conventional engine peaked with a bypass ratio of 12.04. Comparing the ITB and non-ITB engine at these points for each curve showed at 7.37% jump in ST for only a 4.9%

rise in TSFC. These results show a positive performance gain versus fuel burn, but they are marginal improvements at best, and reflect assertions made by Zelina et al. (Zelina et al., 2004a:1) that an ITB could be used to power ultra-high bypass ratio engines. In addition to the performance gains, the ITB engine, for these particular engine parameters, allows for a larger maximum bypass ratio than the conventional engine. The larger available bypass ratios will allow more efficient engine designs to become available in the future.

Another possible use for ITB engines it to supply large amounts of power through a low-pressure turbine to a generator or the rotor of a helicopter. Consequently, the impact of an ITB on a turboshaft engine was examined. This engine used the same efficiencies, specific heats, and other assumptions as the turbofan analysis and the steps are shown in Appendix A. The high-pressure turbine drives the compressor while the low-pressure turbine would be considered a free turbine used for power generation. The gases were assumed to be completely expanded to atmospheric pressure, reflecting the maximum amount of work that can be extracted from the power turbine. The compressor pressure ratio was lowered to reflect the low-pressure ratios seen in current turboshaft engines.

Using an ITB in a turboshaft engine had a large impact on the available power from the engine. It increased the specific power of the engine, for the parameters studied, by 22.68% for only a 9.12% rise in power specific fuel consumption. This further proves the concept that an ITB would be extremely useful in application where large amounts of work must be extracted from an engine to power generators, helicopters, or any other power intensive future application.

2.5.6 Mission Comparison using an ITB and Non-ITB Engine

A simple mission profile was created to compare the use of a turboshaft engine with an ITB to a conventional engine with out an ITB. Using an ITB to supply power for energy intensive applications like takeoff, climb, and maneuvering will allow for a smaller core that can be designed to run at its design point to provide cruise power with the ITB off. This design point represents the most efficient operating point of that engine. The second engine was designed to provide the same power output as the ITB engine, but it must run at reduced throttle to supply cruise power. This oversized engine will consume more fuel at lower power settings because of the larger required air mass flow to produce the same amount of power as the ITB engine at full throttle and engines running at off-design points typically are not as efficient, further increasing fuel consumption at that point.

The mission profile demonstrated the advantages of the ITB engine and its fuel savings. The mission includes a takeoff and climb, cruise to an operating area, maneuvers, cruise back to the starting point, and a descent and landing. The takeoff, climb, and maneuvers are all performed at full throttle for both engines. The cruise phases do not use the ITB and the core of the engine runs at full throttle, the oversized engine operates at a lower throttle setting to match the power output of the ITB engine core. During the descent and landing both engines operate at half of the full power output.

The fuel consumption rate for each engine at the design point was found during the design point calculations. The off-design point fuel consumption rate for both engines was found using a MATLAB script that reduced the maximum turbine inlet

temperature while holding the temperature ratio across the high-pressure turbine constant.

The high-pressure turbine temperature ratio can be held constant because the downstream

power turbine is assumed to be choked during all operating conditions meaning the

upstream gas generator turbine operates at a non-dimensional fixed point, correlating to a

fixed temperature ratio (Saravanamuttoo et al., 2001:388). The iteration method is shown

in Appendix A.

The resulting fuel mass flow rates and the total amounts of fuel for each mission

leg are shown below in Table 1 and Table 2.

Table 1. Fuel flow at varying throttle settings

Engine	Fuel Consumption (kg/s)		
Type	Full Power	Cruise Power	Landing Power
Non-ITB	0.3774	0.33005	0.2417
ITB	0.4118	0.3076	0.2241

Table 2. Fuel consumed during mission

		Fuel Consumed (kg)	
Leg	Duration (min)	Non-ITB Engine	ITB Engine
Takeoff & Climb	10	226.44	247.08
Cruise	60	1188.18	1107.36
Maneuvers	10	226.44	247.08
Cruise	60	1188.18	1107.36
Land & Descend	10	145.02	134.46
Total Consumed		2974.26	2843.34

Using a turboshaft engine augmented with an ITB to produce maximum power when

needed results in a net fuel savings of 4.4% over a traditional Non-ITB engine. The

majority of the savings occurs during the cruise legs of this mission. The cruise legs

alone use 6.8% less fuel when the ITB engine is employed. Those fuel savings are

representative for the mission shown above in Table 2; however, more fuel can be saved

by reducing the amount of time the ITB engine runs at full power. Any sort of

application that involves extended periods at cruise power will result in a greater fuel savings.

2.6 Radial Vane Cavity Interactions

The radial vane cavity (RVC) serves to increase the transportation of combustion products. These products flow out of the circumferential cavity into the RVC and subsequently mix with the main airflow. Previous work by Zelina et al. (Zelina et al., 2004a:4-8) compared a vane with no RVC to one that has an RVC. An example of a vane with a RVC is shown below in Figure 7.
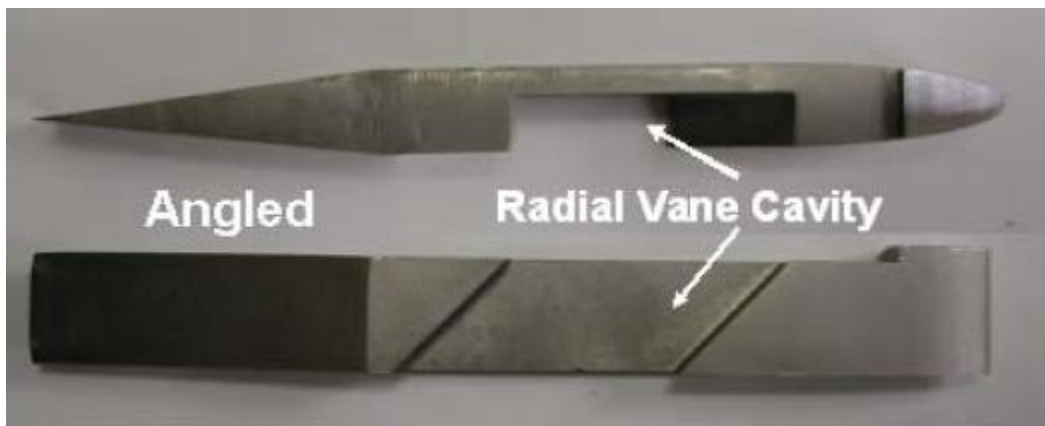
Figure 7. Vane with the RVC (Zelina et al., 2006a:4)

They found that the RVC increases mixing with the main air flow and consequently this design had higher combustion efficiency since the cavity creates a leaner secondary combustion zone for the fuel-air reactions to burn to completion. Along with better performance, the cavity helped to create lower emissions than a normal vane with no cavity and it also displayed better lean blowout behavior (Zelina et al., 2004a:6-8).

After the investigation into the effects of a RVC. another set of tests was conducted by Zelina et al. (Zelina et al., 2006a) to determine how the shape of the cavity

26

would affect performance. A contoured cavity was compared to the RVC shown in

Figure 7. An example of the contoured vane geometry is shown below in Figure 8.
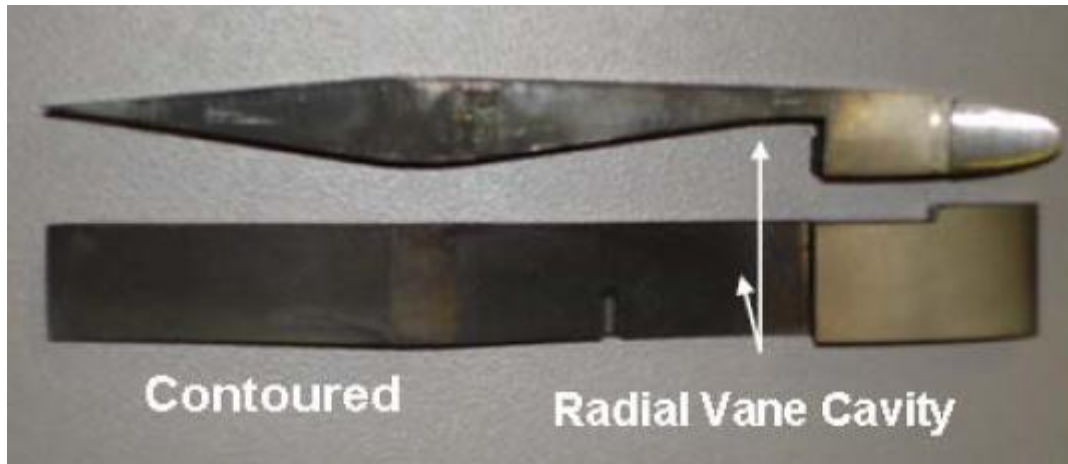
Figure 8. Vane with a contoured RVC (Zelina et al., 2006a:4)

The reason for the test of a contoured vane was the hope it would reduce the pressure loss

along the main airflow in the combustor during operation (Zelina et al., 2006a:4). At the

completion of testing to compare these two vane designs, it was found that the contoured

vane had poorer performance against its counterpart, the angled vane. In comparison to

the angled RVC it had poor lean blowout characteristics, higher emissions, and it did not

promote mixing of the cavity airflow with the main airflow as well as the angled vane

(Zelina et al., 2006a:7-8).

The vanes used during testing for this thesis are designed to more accurately

represent turbine guide vanes found in jet engines, unlike the straight vanes tested in

those previous tests. The curvature creates a pressure and a suction side on the new vane

design. A radial vane cavity was built into the suction of the vane for this thesis. It is

expected that the cavity on the suction side will perform the best because the pressure is

lower on that side which will enable the radial vane cavity to transport hot gases from the

circumferential cavity down the radial vane cavity and into the main flow. A more

detailed description of the vane design tested can be found in Chapter 3.

2.7 Efficiency Improvements

Previous work performed on the UCC has shown enhanced efficiency because of

greater mixing and shorter times for combustion as a result of the g-loading. Zelina et al.

(Zelina et al., 2006a:6-7) found an angled radial vane cavity helped to create combustion

efficiencies approaching 99% over a wide range of g-loadings and the higher g-loadings

yield better efficiency. They also expect operational efficiency will improve at higher

operating pressures due to increased reaction rates defined by the Arrhenius rate

equation.

$$k = A \cdot \exp(-E/RT) \tag{27}$$

The high pressure will result in increased temperatures driving the exponent term towards

unity and a higher reaction rate.

In 2005, Zelina et al. (Zelina et al., 2005:5) reported results for high-pressure tests

of the UCC showing favorable results. They found the UCC should operate at 97 to 99%

efficiency over a wide range of operating conditions. The data also showed the

efficiency is almost independent of the combustor loading parameter and OFAR. This

finding is very important because if the UCC is to be used as an ITB it would operate

under high combustor loading conditions, due to the reduced combustor volume of the

UCC, at low OFARs because analysis has shown, as stated earlier, only a small rise in

temperature is needed for a performance benefit.

Numerical simulations (Anisko et al., 2006: 8) conducted on UCC models have shown some interesting results. Namely, the combustion efficiency can be affected by the width of the circumferential cavity and narrower cavities show efficiency improvements.

2.8 Lean Blowout Characteristics

Lean blowout characteristics have been explored during testing of the UCC. These characteristics are a good indication of stability and performance. According to Lefebvre (Lefebvre, 1999:148), lean blowout (LBO) occurs when the combusting mixture becomes too fuel lean to support combustion. This is an important operating statistic because it determines the operating envelope of the engine and consequently its stability. This characteristic is very important to the UCC, especially if it is to operate as an ITB. The ITB must have a wide operating range due to its nature, location in a vitiated flow, and the requirement of very low OFAR for efficient ITB operation.

Atmospheric testing of the UCC has found that LBO limits have been reduced by a factor of 3 to 4 over conventional designs at a loading parameter of approximately 1 (Zelina et al., 2006b:7). Zelina et al. hypothesized the lower LBO limits could be because the circumferential cavity is shielded from the main airflow allowing the recirculation of combustion products to stabilize the flame in the cavity. This recirculation creates a higher Φ in the cavity than the overall Φ helping to reduce the LBO limit (Zelina et al., 2006b:7).

High-pressure testing of the UCC has yielded similar results to those tests conducted at atmospheric pressure. At combustor loadings of approximately 1.7 the LBO

limit for the UCC was reduced by a factor of 3 compared to typical engines in service. It

was also shown that the UCC could operate at LPs of three times greater than

conventional systems and still have better LBO characteristics (Zelina et al., 2005:5).

2.9 Emissions Reductions

Emissions data was collected during previous testing of the UCC. Its unique

design has shown lower pollutant emissions as the growing focus on climate change and

global warming has caused engine designers to become more environmentally conscious.

The process of combustion produces many products including water vapor, carbon

dioxide, carbon monoxide (CO), unburned hydrocarbons (UHC), and oxides of nitrogen

(NO_x). Emissions of CO, UHCs, and NO_x have had the most effort expended on them to

reduce the quantity emitted by the engine. The emissions of any engine are directly tied

to operating temperature and the efficiency of the combustor, causing the UCC to show

promise for lowered pollutant outputs because of its increased combustion efficiency.

Typically, emissions of CO and UHC are the highest at idle and low power

settings due to the relatively low burning rates and peak temperatures caused by a low

equivalence ratio, and poor mixing because of lower air flow rates. At high power

settings, the release of these two pollutants is at a minimum because of the more

complete combustion taking place at these high power settings. The amount of CO and

UHCs emitted is a direct measurement of the completeness of the combustion process

(Lefebvre, 1999:317-320).

Reducing NOx emissions is a particular challenge to designers because of the

different mechanisms generating NO_x. It is the main pollutant released during flight and

has the most effort of the three directed to its reduction (Lefebvre, 1999:314). In general, NO_x creation is controlled by the flame temperature and residence time in the combustor. NO_x production is at a minimum at low power settings because of reduced temperatures and shorter residence times and reaches higher levels at high and cruise throttle settings.

The UCC has shown promise for reduced emissions of CO and UHC because of increased efficiency and longer residence times for cold, unreacted mixtures pulled to the outer diameter of the main cavity due to the effects of centrifugal loading holding the heavier reactants in the cavity to finish combusting while releasing the lighter weight products into the main air flow. This inherent design feature produces these desirable results at a wide range of throttle settings. The release of NO_x has also shown potential to be reduced with this design, though pressure has a great effect on its production (Zelina et al., 2006a:7-8). The high pressure tests showed NO_x emissions decreased with increased g-loads because of a shorter residence time and better turbulent mixing of the flow in the circumferential cavity (Zelina et al., 2005:6-7).

2.10 Rayleigh Flow

A critical component of understanding how the UCC will function in practical use is its Rayleigh loss characteristics. The UCC has a complicated shape and the flow through the combustor is at higher Mach numbers than current designs making it much more susceptible to Rayleigh losses. Rayleigh flow describes how heat addition to a flowing gas will cause a change in velocity. For a subsonic flow, the heat addition will drive the speed to Mach 1 and for a supersonic flow it will cause the speed to drop toward Mach 1. The heat addition causes a pressure drop and this differential changes the flow

speed (Saravanamuttoo et al., 2001:451). The UCC has an inherent pressure drop

induced by the swirling flow and its complicated shape. Introducing heat will cause

further pressure loss and this loss has been quantified in this thesis to help understand the

performance characteristics of the UCC and its viability as an innovative combustor for

future engines.

2.11 Synthetic Fischer-Tropsch Fuel

The Fischer-Tropsch (FT) process was discovered in Germany and developed by

Drs. Franz Fischer and Hans Tropsch (Corporan et al., 2007:2). It uses a gas-to-liquid

process that converts coal or natural gas to a refined liquid fuel similar to diesel or jet

fuel. This refined product is almost free of sulfur, nitrogen, and aromatics (Corporan et

al., 2007:2). This technology provides a way to produce aviation fuels without the need

for crude oil, reducing the military's dependence on imported oil in a crisis.

Besides the national security implications, this fuel has performance

characteristics similar to its petroleum based counterpart. The Fischer-Tropsch fuel can

be tailored to meet the standards for JP-8, as shown below in Table 3, and can be used in

current engines with no modification.

Table 3. Comparison of FT fuel to ASTM Standards for JP-8 (Corporan et al., 2007:6)

ASTM Test	Standard	JP-8 (POSF 3773)	Synthetic Fuel (POSF 4734)
Total Acid Number, mg KOH/g (D3242)	Max 0.015	0.000	0.001
Aromatics, %vol (D1319)	Max 25.0	15.9	0.0
Total Sulfur, % mass (D4294)	Max 0.30	0.06	0.00
Distillation-Residue, % vol (D86)	Max 1.5	1.3	1.4
Distillation-EP, °C (D86)	Max 300	256	271
Freezing Point, °C (D5972)	Max -47	-51	-59
Existent Gum, mg/100mL (D381)	Max 7.0	4.6	0.20
Viscosity @ -20°C, cSt (D445)	Max 8.0	4.1	4.6
Specific Gravity @ 15.5°C (D4052)	0.775-0.840	0.799	0.757
Smoke Point, mm (D1322)	Min. 19.0	25.0	>50
Flash Point, °C (D93)	38	48	49
Heat of Combustion, BTU/lb (D3338)	18400	18597	18965

The fuels are almost identical as shown above, but there are some differences in their chemical make-up. JP-8 mainly consists of a blend of normal and iso-paraffins along with small amounts of cycloparaffins, olefins, and aromatics. The FT derived synthetic jet fuel consists only of normal and iso-paraffins (Corporan et al., 2007:6).

Tests conducted using the synthetic fuel on a T63 turbine engine at WPAFB, OH showed no adverse operating effects on the engine. Its fuel consumption did not change using fully synthetic fuel.   These tests have shown dramatically reduced particulate emissions and oxides of sulfur are practically non-existent since the fuel is nearly sulfur free. The fuel did not have an impact on other gaseous emissions and has combustion characteristics similar to JP-8 (Corporan et al., 2007:16). The potential for future implementation of this technology to provide fuel for the aviation industry dictates a test of its combustion characteristic in the UCC.

III. Experimental Configuration and Methods

3.1 UCC Experimental Set-Up

The UCC testing rig is installed in Room 151 of AFRL's Atmospheric Pressure Combustion Research Complex at Wright Patterson AFB, OH. The test rig, shown in Figure 9, is operated at atmospheric pressure because it eliminates the need for complex pumps and auxiliary equipment needed to simulate the actual operating conditions of a normal combustor. This lack of complexity reduces the cost of testing and makes the proof of concept investigation into the UCC easier to perform. The rig is instrumented to collect relative data concerning emissions, pressures, and temperatures.
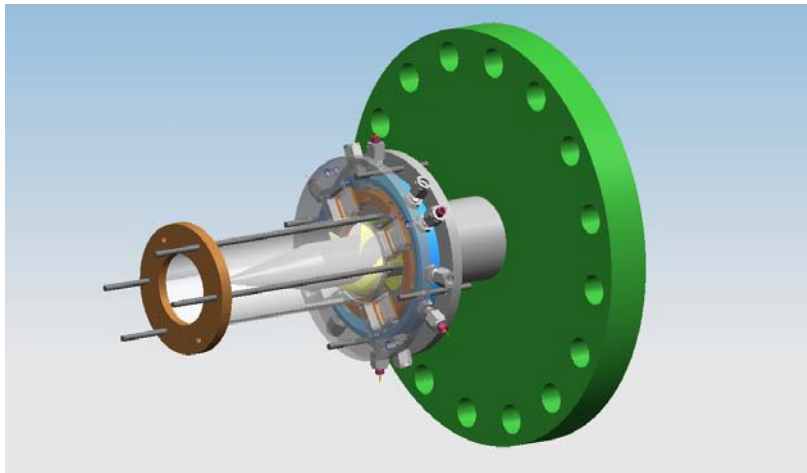
Figure 9. Complete Ultra Compact Combustor

The UCC consists of a front and rear flange that create a sandwich around the combustion cavity. The interior of the UCC consists of a centerbody that simulates the turbo machinery that would pass through the center of the combustion section in a turbine engine. The vanes on the centerbody consist of a set of pre-swirlers and a curved set of simulated turbine guide vanes. The interior of the UCC is shown below in a cross section depicted below in Figure 10.
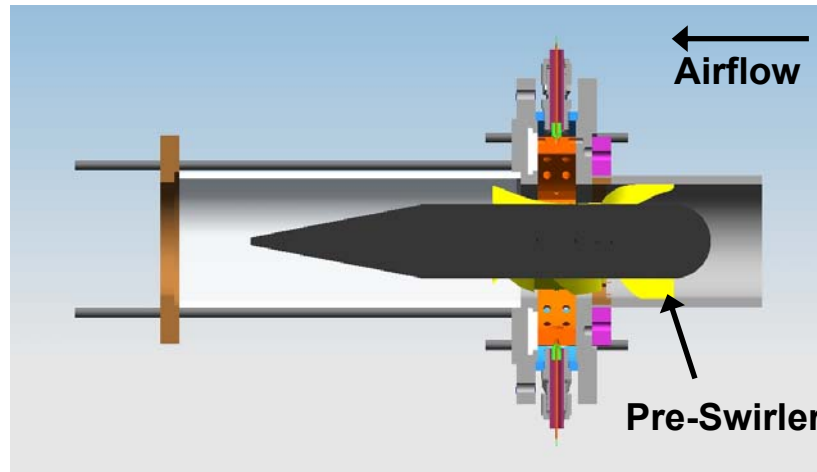
Figure 10. Cross section view of Ultra Compact Combustor

3.1.1 Front Flange

The main purpose of the front flange is to attach the test rig to the air supply and provide a smooth airflow to the combustor. To this purpose the flange is mounted to an entry pipe that has an inner diameter of 7.684 cm (3.025 inches). The pipe is also fitted with notches to help align the pre-swirlers and hold them in place during operation.

3.1.2 Centerbody

The centerbody simulates the engine core. It is 4.948 cm (1.948 inches) in diameter and 30.798 cm (12.125 inches) long overall. A 1.365 cm (0.5 inch) entry annulus is created between the centerbody and combustor walls. It has a bullet nose facing into the air flow for minimal disruption of the flow as it enters the combustor. The constant diameter section mounts the pre-swirlers and the simulated turbine guide vanes. It has a gently tapered body extending out of the combustor to prevent separation of the flow as the gases are exhausted.

These vanes serve a dual purpose. They support the centerbody and hold it in place within the combustor. Figure 11, seen below, shows the centerbody with mounted turbine guide vanes.
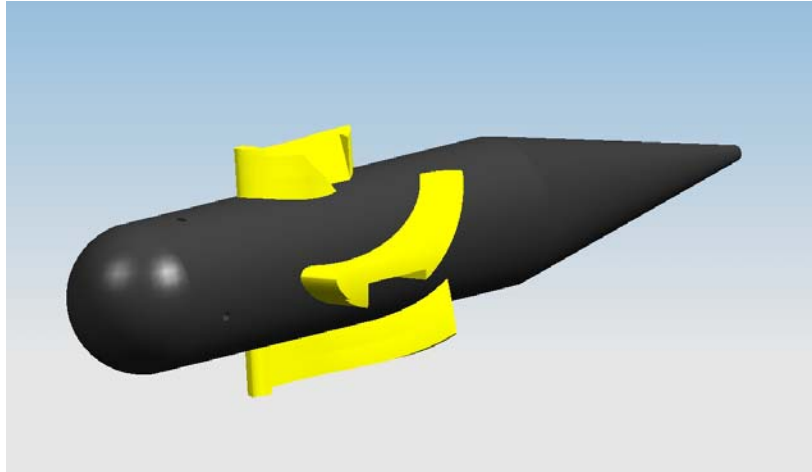
Figure 11. Centerbody with mounted turbine guide vanes

Besides supporting the centerbody, the pre-swirlers are used to provide a counter-clockwise bulk swirl to the airflow. Swirl direction is observed from the rear of the combustor. This simulates the swirl the airflow would have moving from the compressor to the combustor because the UCC does not require the flow to be straightened through the use of compressor guide vanes.

The pre-swirlers and turbine guide vanes were designed by Peter Koch of AFRL. The pre-swirlers are designed in to give the correct inlet conditions for the turbine guide vanes. The angle of incidence between the pre-swirlers and guide vanes was designed to be zero degrees. The designer of the vane assembly rotated the pre-swirlers slightly about the centerline to direct the flow to the stagnation point of the turbine guide vanes. Therefore, there may be a non-zero angle of incidence, but it was not quantified by the designer (Koch, 2007). If the angle is non-zero, it is most likely positive because of the flow separation seen on the suction side of the vanes during testing. The arrangement of

the guide vanes on the centerbody gives a solidity of 1.56. The turbine guide vanes will be described in more detail later in this chapter.

3.1.3 Pressure Ring

The pressure ring is the outside ring of the UCC. It is mounted between the front flange and rear flange. This ring is designed to mount all of the fuel injectors, the air feeds, and an igniter securely in place. To this extent there are six holes drilled through the pressure ring in the radial direction for the fuel injectors at 60 degree intervals. Another six holes are drilled in the same manner as the fuel injector mounts to attach air feeds to provide airflow for the cavity injection air. The holes for the air supply are paired with a fuel injector hole and are offset from the fuel injector mount by approximately 20 degrees. The ring has an outer diameter of 17.463 cm (6.875 inches), an inner diameter of 16.193 cm (6.375 inches), and a width of 2.54 cm (1.00 inches).

3.1.4 Combustor Ring

The combustor ring is the inner liner of the Ultra Compact Combustor. This ring, shown below in Figure 12, is mounted concentrically inside the pressure ring and is sandwiched between the front and back flanges forming the outer circumference of the circumferential combustion cavity.
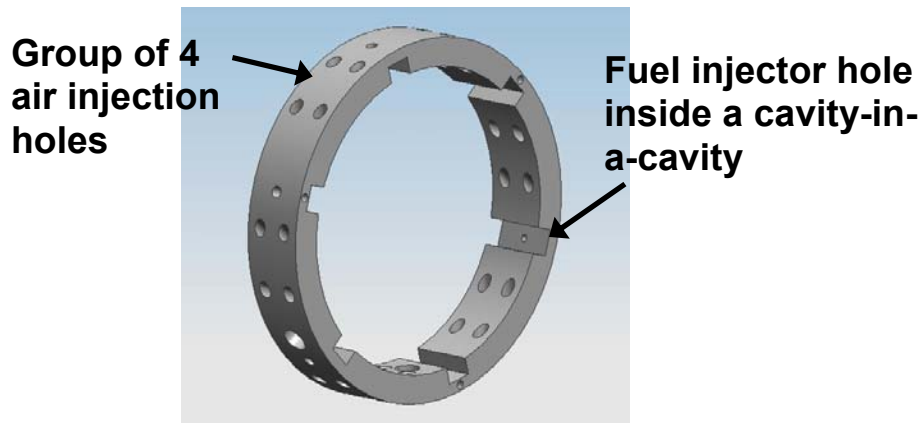
Figure 12. Combustor ring

It contains 24 air injection holes that are angled 45 degrees off of the radial. These holes are grouped together in fours and each group is placed between the fuel injectors. The holes for the fuel injectors are again spaced every 60 degrees. Pressure atomizing fuel injectors will spray through each hole into a small rectangular cavity, also known as a cavity within a cavity, which is cut into the ring. Each cavity is 0.635 cm (0.25 inches) deep and 1.106 cm (0.400 inches) wide. The ring itself has an outer diameter of 13.97 cm (5.5 inches) and an inner diameter of 11.760 cm (4.63 inches). It is 2.540 cm (1 inch) wide.

3.1.5 Turbine Guide Vanes

This design of the UCC features curved support vanes that are a better representation of the turbine guide vanes found in a turbine engine when compared with the straight vanes found in previous UCC designs. These vanes, as mentioned earlier, support the centerbody and are approximately 1.27 cm (0.50 inches) in height and bridge the annulus created by the centerbody and inner surface of the UCC. The vanes have a chord length of 7.62 cm (3.00 inches). Figure 13 shows a drawing of the curved vane used during the testing conducted for this thesis.

38
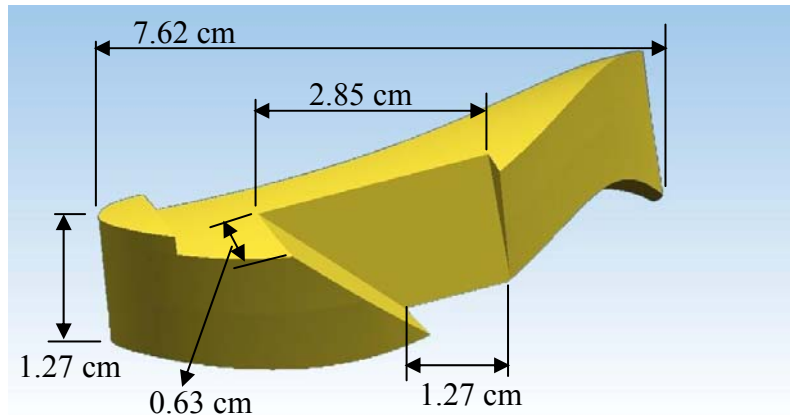
Figure 13. Turbine guide vane

This design has a radial cavity on the suction side of the vane. The cavity is 2.85 cm (1.125 inches) long on the top of the vane and at the vane base it is 1.27 cm (0.50 inches) long. At its deepest, the RVC is cut 0.63 cm (0.25 inches) deep into the vane. The radial vane cavity is intended to help transport hot gases out of the circumferential cavity and mix those gases with the main airflow. The vane curve causes exhaust gases to circulate in a clockwise manner when viewed from the rear of the combustor. Figure 14, shown below, defines the swirl direction illustratively for the ease of the reader.
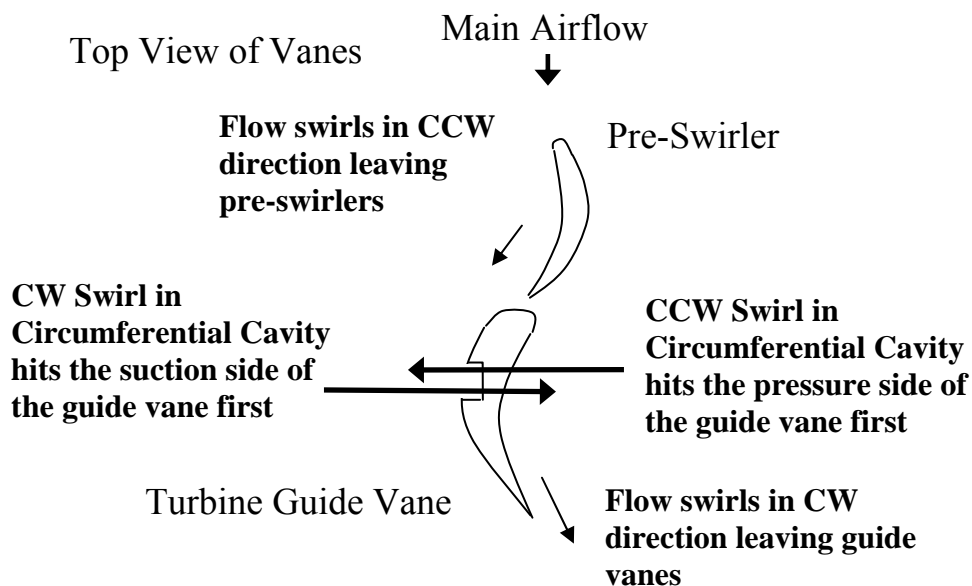
Rotation Direction is viewed from the end of the combustor at the exhaust

Figure 14. Swirl direction definitions

3.1.6 Quartz Observation Windows

Quartz glass is used in two locations on this test rig to allow for observation of the interior of the UCC. The most obvious location is the quartz exhaust tube that fits around the aft portion of the centerbody. This tube has an outer diameter of 9.081 cm (3.575 inches), an inner diameter of 8.255 cm (3.25 inches), and is 22.860 cm (9.00 inches) long.

There are 4 small quartz windows mounted on the back flange that allow for direct optical access to the circumferential cavity. These windows are 2.540 cm (1.00 inch) square and are spaced at 90 degree angles around the rear flange. Two windows were purposely positioned right in front of a fuel injector to observe how the flame behaves around the fuel injector.

3.1.7 Fuel Injectors

Fuel was injected into the circumferential cavity using six pressure-atomizing fuel injectors. The injectors are located in the combustion ring and inject along the radius of the ring. The same type of fuel injector was used for both POSF 3773 JP-8 and the synthetic Fischer-Tropsch fuel. Each injector has a flow number of 0.3 for a total flow number of 1.8 using all six injectors. The injector spray patterns are similar to those depicted below in Figure 15 and Figure 16 with the axis referenced to the centerline of the fuel injector.
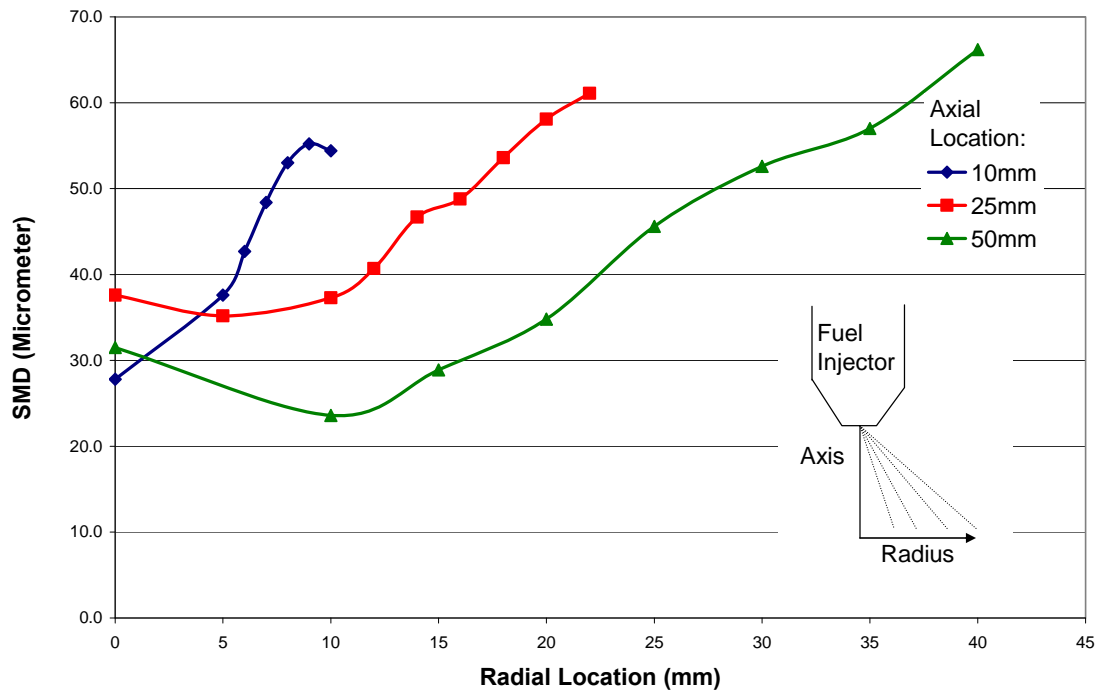
Figure 15. Fuel droplet size at 0.827 MPa (Mao, 2003)
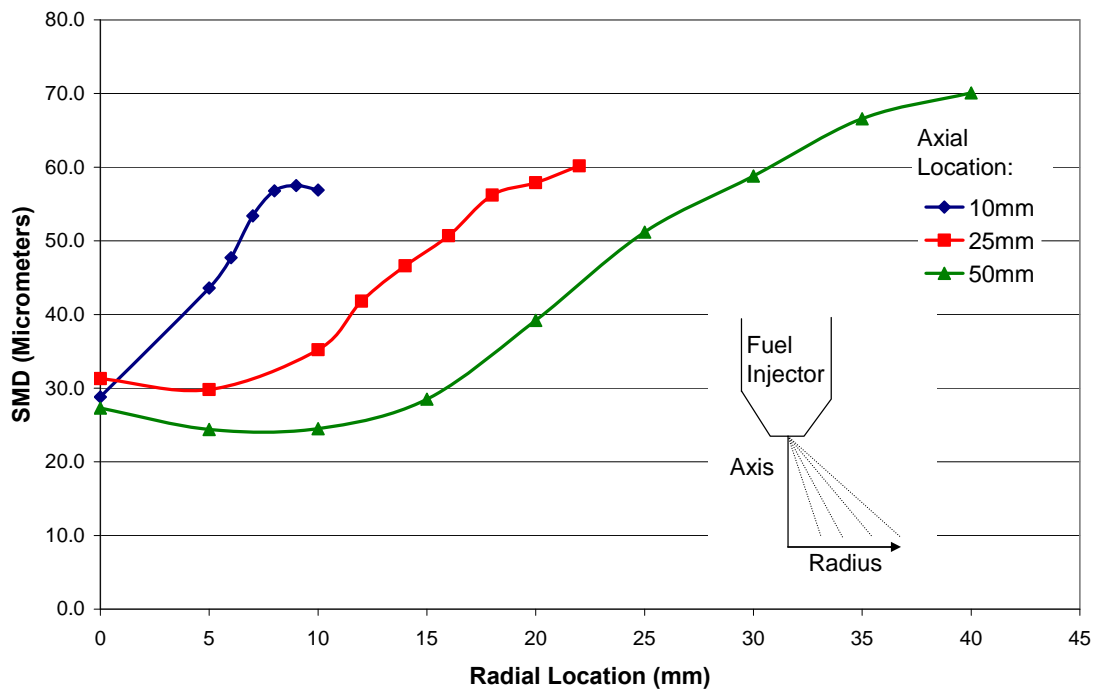
Figure 16. Fuel droplet size at 0.783 MPa (Mao, 2003)

To prevent coking from affecting the performance of the UCC and the resulting information collected during testing; every time fuel is shut off to the combustor a nitrogen purge system is turned on to prevent deposits from forming in the injectors. The injector tips were also changed when the rig was opened to change configurations. The used injectors are then cleaned and refurbished in-house or sent back to the manufacturer. This way the injectors are used in a rotation to achieve consistent performance from the fuel injection system over all the tests and minimize the fuel injector effects on the tests. Figure 17 shows the assembled UCC with the fuel injectors, combustion ring, and pressure ring.
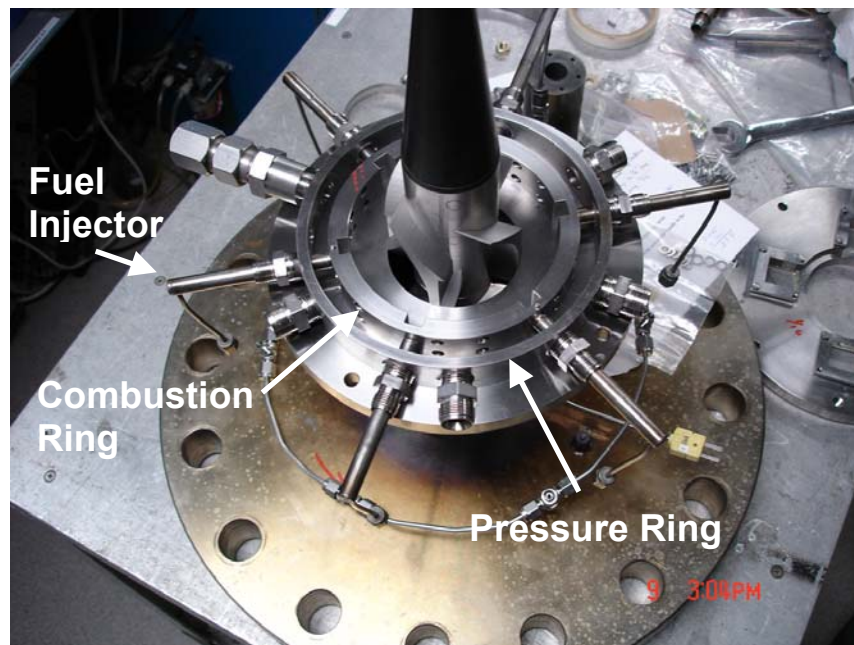
Figure 17. Assembled UCC without the back flange or quartz tube.

3.2 Facility Description

Tests were carried out at AFRL's Atmospheric Pressure Combustion Research Complex at Wright Patterson Air Force Base, Ohio. This facility is capable of delivering 0.454 kg/s (1 lbm/s) of air at atmospheric pressure to an experiment. The air can be split

between 3 independently controlled feeds to divide the flow as needed. For example, air can be split into a main, circumferential cavity, and dilution supply for the test rig. This air supply can be electrically heated to temperatures approaching 588 K (Zelina et al., 2006b:6).

Fuel is provided by an on site fuel farm to the test cell through two separate independent fuel systems. Each system can feed fuel to the test stand at pressures of 6.89 MPa (1000 psia) and at a flow rate of 2.27 kg/min (5 lbm/min). The facility is capable of using liquid fuel or gaseous propane for its studies (Zelina et al., 2006b:6).

3.3 Emissions Analysis and Data Collection

Emissions data is collected via a single element oil-cooled probe placed at the exit plane of the combustor. This probe delivers samples that are analyzed for CO, CO_2, NO_x, and unburned hydrocarbons (UHC) (Zelina et al., 2006b:6). The probe is maintained at 422 K to properly quench reactants and prevent condensation of combustion products to improve measurement accuracy. The information produced from the samples are directly displayed in the control room to facilitate data acquisition and experiment control. All of the emissions analysis equipment is accurate to within 0.1% at full scale reading.

3.3.1 NO_x Measurements

This lab uses an Eco Physics CLD 700 EL to detect and measure the amount of NO_x present in the combustor efflux. This machine is a two channel NO_x analyzer that measures hot samples taken directly from the combustor. To prevent condensation of water vapor in the sample before analysis, its pressure is dropped below atmospheric

levels. The sample is then directed into one of two chambers; one for NO and the other

for NO_x. The pollutant levels are then measured using a chemiluminescence detector. To

reduce error the pressure is regulated through the use of a motorized bypass system

(Ehret, 2002:44-45).

3.3.2 Carbon Monoxide Measurements

Carbon Monoxide levels are measured using a California Analytical Instruments

Model ZRF. This is a Non-Dispersive Infrared Analyzer. The machine can operate on

one or two IR absorbing spectrums through the use of a mass flow detector. To measure

CO levels an IR beam is emitted from its source and passes through a rotating single-

point beam chopper revolving at 9 Hz. This split beam is then directed through a sample

cell and a reference cell. The reference cell contains a non-IR absorbing gas. After

passing through the sample or reference cell, the beams converge on a micro-flow

detector that measures the intensity difference between the sample and reference. This

intensity difference is used to determine the amount of CO contained in the combustor

efflux (Ehret, 2002:45).

3.3.3 Carbon Dioxide Measurements

The California Analytical Instruments Model ZRH is used to measure CO_2

emissions. Like the ZRF, it is a Non-Dispersive Infrared Analyzer and operates in much

the same way. However, this unit uses a single beam optical system with a dual cell

transmission detector to minimize any error from other gases in the sample (Ehret,

2002:46).

3.3.4 Unburned Hydrocarbon Measurements

The quantity of unburned hydrocarbon fuel emitted from the combustor is measured using a Beckman Model 402 Hydrocarbon Analyzer. This instrument uses a hydrogen flame to ionize any hydrocarbons in the sample. This ionization creates a current flow measured by an electrode surrounding the flame in the sample chamber. The strength of this current is proportional to the amount of UHCs contained within the sample. The current is converted to a voltage for easy measurement (Ehret, 2002:46).

3.3.5 Pressure and Temperature Measurements

Pressure and temperature measurements are crucial for determining the operating characteristics of the UCC. To this end, the test rig is instrumented to collect pressure data using pressure transducers and temperatures using thermocouples as shown below in Figure 18.
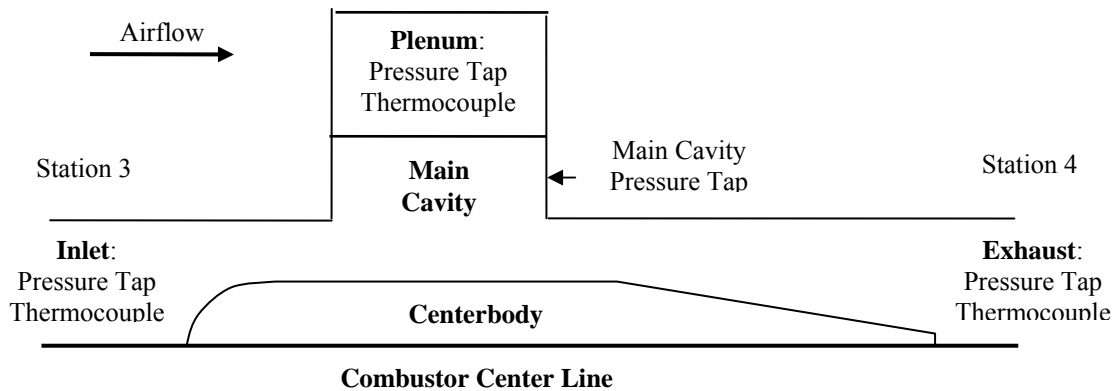
Figure 18. Instrumentation locations on the UCC

Pressure transducers were placed upstream of the entrance to the pre-swirlers, referenced as station 3, in the plenum between the pressure ring and combustor ring, on the back flange of the UCC to sample the pressure from the main circumferential cavity, and

downstream of the combustor cavity and guide vanes at the end of the quartz exhaust tube, referenced as station 4. These pressure taps measure static pressure through flush mounted sampling points along the UCC test rig. The pressure taps are connected by tubing to individual Sensotec transducers remotely located in an instrumentation cabinet. These transducers are accurate to 0.25% of their full scale value.

Thermocouples are co-located with the pressure transducers; however, due to the extreme temperatures in the main combustor cavity a temperature probe could not be placed with the pressure transducer in that location. All of the thermocouples are manufactured by Omega and are of type K. The thermocouple at station four, due to its design, will measure a temperature that is very near to the total temperature. Though, the sensor at the combustor exit plane will not measure a total condition, because it black body radiates in the high temperature exhaust gases.

One of the operating characteristics of the UCC is a pressure drop that takes place in the main airflow and another occurring in the circumferential cavity. The pressure drop for the main airflow is measured between the inlet and exhaust pressure taps. The pressure drop for the circumferential cavity is measured between the pressure taps located in the plenum and the exhaust.

3.3.6 Flow Measurements

Measuring the airflow and fuel flows through the experiment are critical to controlling the combustor operation as well as determining its operating characteristics. The mass flow rate for the fuel is measured directly using a coriolis meter located upstream of the fuel manifold. This meter is accurate to within 0.05% of its reading and

46

is made my Micromotion. Airflow rates are determined indirectly using an orifice meter

at the flow control valve upstream of the combustor. The measurements from this orifice

meter are used in combination with Bernoulli's Equation to derive the mass flow rate.

The orifice plate is accurate to within 0.6% of its reading. The main air supply and cavity

air supplies are independently controlled and measured so separate mass flow rates can

be measured for each air supply.

3.3.7 Data Collection

Data is collected using a Labview program specifically written for the

instrumentation on the UCC. The program was written by Jeff Stutrud, an in-house

expert at AFRL. It displays all of the pressure, temperature, mass flow, and emissions

measurements allowing the operator to easily observe and control the operation of the test

rig. These measurements are saved at user controlled intervals by clicking a data

collection button within the program. This data is saved to a text file that can be

imported into Microsoft Excel. All of the instruments were electronically calibrated

before testing each day by the laboratory technicians.

3.4 Experimental Plan

A series of tests were designed to investigate the behavior of the UCC. The

specifics of each test are explained later in this chapter, but tests were performed to

explore the Rayleigh losses, lean blow out characteristics, steady-state emissions and the

operating profile. Before any of these trials could begin, isothermal tests, discussed in

section 3.5.1, were completed using a counter-clockwise rotation in the circumferential

cavity to determine the effective areas of the cavity and the main passage of the combustor. These areas were used during the analysis of data from the Rayleigh flow experiments. All of these tests were performed with the 2.54 cm wide circumferential cavity and the turbine guide vane that has a radial vane cavity on the suction side of the vane. Table 4 summarizes the test plan in matrix form.

Table 4. Summary of test matrix

		Swirl Direction	
		CCW	CW
Fuel	JP8	Rayleigh Emissions LBO	Emissions LBO
	FT	Emissions LBO	Emissions LBO

During the first part of the testing the combustion ring was installed so it caused the flow to swirl in a counter-clockwise direction. In this way the pressure side of the turbine guide vane leans into the rotating flow of the main circumferential cavity. With the flow rotating in this way the Rayleigh flow, lean blow out, and steady-state emissions tests were performed with JP-8. Once these tests were completed, the fuel supply system was purged and refilled with Fischer-Tropsch synthetic fuel. Using this artificial jet fuel, the lean blow out and steady-state emissions tests were performed. The Rayleigh flow tests were carried out once to see if the Rayleigh loss characteristics were different for this combustor. The different configuration does not change the pressure loss characteristics, as they are a function of the combustor design and heat addition, not the fuel supplying the heat source.

After completing the initial tests, the combustor was dissembled and the combustor ring was re-installed so it would rotate the main combustion cavity flow in a clockwise direction. This direction of rotation causes the swirling flow to lean against

the suction side of the turbine guide vanes. With this new rotation direction, the lean blow out and steady-state emissions tests were performed with the synthetic fuel while the fuel system was still primed with it. Once those tests were completed the fuel system was purged and refilled with JP-8. Finally, the lean blow out and steady-state emissions experiments were completed. Again, the Rayleigh flow tests were not repeated because it was assumed the pressure loss characteristics were the same as the first part of the experiment.

To maintain consistent operating characteristics and to control as many variables as possible the combustor was inspected each day for problems before operation. These preventative maintenance steps included inspecting the windows for cracks or chips, checking the fuel injectors for blockage or coking, and all data connections. Experience showed the fuel injectors coked up during tests, especially after the Lean Blow-Out tests. To combat this problem, the peanut tips were replaced on a regular interval to maintain adequate flow numbers. The four quartz observation windows had a tendency to coke up and chip or crack over time from thermal stress experienced during operation. The bad windows were replaced with spares that were ordered in anticipation of this happening during testing.

3.5 Experimental Methods

Each type of test used a separate method for running the experiment, but all tests began with a set of common procedures. Each day of testing, airflow was turned on to the rig and it was preheated by the air flowing from the heaters to the test section. The rig was warmed to approximately 533 K for all tests. This temperature accomplished two

goals; first it simulated heated airflow coming from a compressor and second the heated air helped to aid the combustion process by vaporizing and pre-heating the fuel as it is injected. After the rig is hot, the flow conditions for each individual test were set using the pressure drop across the main air flow and through the circumferential cavity. These pressure drops were used to set flow conditions because they are easier to replicate from test to test, make data analysis more convenient, and allow this combustor design to be more easily compared with other designs.

For the lean blow out and emissions tests, the pressure drops for the main and cavity airflow were set to be identical. They were set in this manner for two reasons. First, if the main airflow pressure drop is greater than the pressure drop of the cavity airflow, the main airflow would expand into the circumferential cavity breaking down the circumferential swirl resulting in the cavity extinguishing itself. Second, if the cavity pressure drop is greater than the main airflow pressure drop, the cavity airflow will expand out of the circumferential cavity into the main airflow essentially blowing the cavity contents into the main flow before they can combust. Equal pressure drops across both flows are needed to balance the circumferential cavity airflow and the main airflow for proper operation of the UCC.

Certain tests required the combustor to be lit off at this point, others did not, but lighting it involves introducing fuel to the main cavity and triggering the igniter. The fuel flows and airflows were varied if needed to achieve stable operation and then reset to the test conditions if varied for lighting the combustor. If the combustor ever purposely or accidentally blows out during testing, the fuel was immediately shut off and a nitrogen purge of the fuel system was started to prevent the fuel injectors from coking and

becoming blocked. At this point, the next steps in the testing procedure varied from test to test and are further explained below.

3.5.1 Isothermal Test Procedure

To compute the effective area of the combustor a series of isothermal tests were run. The combustor inlet temperature was maintained at 533 K and no heat was added through combustion. A series of different pressure drops were set and the corresponding mass flows were recorded for use later in determining the effective area.

3.5.2 Rayleigh Flow Test Procedures

The Rayleigh flow tests were conducted in two separate steps. First, a pressure drop was set for the main airflow while the cavity mass flow was held constant through all tests. The constant cavity mass flow was chosen to prevent the pressure drop across the cavity from becoming too large and consequently blowing the burning gases out of the cavity and into the main airflow. For the purposes of this test, the combustion needed to stay inside the cavity to simulate a heat source adding energy to the main flow. Once the desired pressure drop was achieved a data point was taken and the mass flow rates were recorded. All of those measurements were taken under cold flow conditions, meaning the combustor was not lit at the time.

The second step of this test involved lighting the combustor to get data during hot-flow conditions. At each test condition, the mass flows for the cavity and main air were set to match those from the cold-flow tests for that particular condition. Since, the pressure drops were the item of interest for this test and a heat addition will further

increase them, the mass flow rates had to be identical to duplicate the flow conditions for each data point. A comparison of the resulting pressure drops with those from the cold-flow is used to determine how Rayleigh flow affects the combustor.

3.5.3 Lean Blow Out Test Procedures

The lean blow out (LBO) characteristics of this design was investigated through a series of tests to record when LBO occurs. LBO is defined as the moment when the combustion process in the UCC is completely extinguished. The pressure drop was varied for each test because it influences the overall loading of combustor and the centrifugal loading of the circumferential cavity. Each test was conducted by first setting identical pressure drops for the main airflow and combustion cavity for the reasons described earlier. Then, the combustor was lit and stabilized at an overall fuel-air ratio (OFAR) of 0.03. This OFAR was chosen as a starting point for each test because it is a stable operating point and it maintains consistency in testing procedures. After stabilization, the fuel flow was slowly reduced until LBO was achieved. At that moment, a data point was collected for later use in the analysis of the combustor stability characteristics.

3.5.4 Steady-State Test Procedures

Tests of the UCC in steady-state operation were used to determine its emissions characteristics and combustion efficiency. These tests were conducted with the main and cavity airflows set so the pressure drops are matched for reasons explained previously. Each of a series of different pressure drops was run with a variety of OFARs to

investigate the performance of the UCC. At each test point the UCC was allowed to run

and stabilize at that operating condition before information on the emissions and

efficiency of the combustor was collected. In this way, the data on the combustor is

collected during steady-state operation and is used to help understand its operation.

IV. Results and Analysis

4.1 Observations

Observations of the Ultra-Compact combustor taken while operating helped to characterize its behavior and supplement information collected from the instrumentation monitoring the rig. All of the observations and tests were conducted with the 2.54 cm wide combustor cavity and the turbine guide vanes with a radial cavity on the suction side. These observations help to understand the physical phenomenon that occur during operation and make it easier to quantify the information presented in the data. Several important observations concerning the UCC and its operation are detailed below.

4.1.1 UCC in Operation

Using the quartz windows in the back flange and the quartz exhaust tube it was very easy to observe how the combustor operated and its characteristics. While in operation, the flames could be seen swirling around the main combustion cavity, transporting down the radial vane cavities, and traveling down the exhaust tube as shown below in Figure 19.
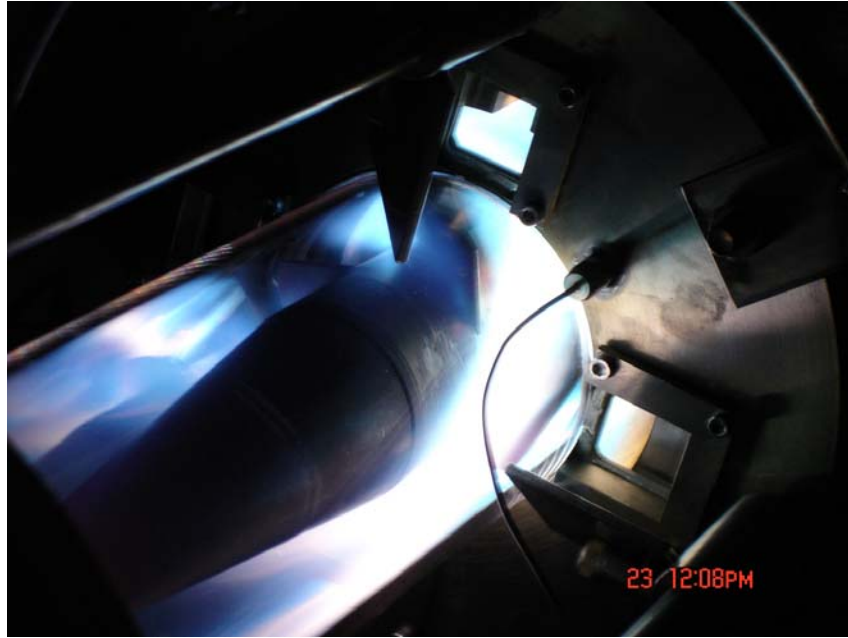
Figure 19. UCC during operation

Figure 19 shows the UCC running on JP-8 with a counter-clockwise swirl in the cavity.

The turbine guide vanes turn the exiting flow inducing a swirl in the exhaust.

Unfortunately, this swirl is hard to see in pictures, but Figure 20 shows the swirl induced

by the guide vanes while operating at high OFAR.
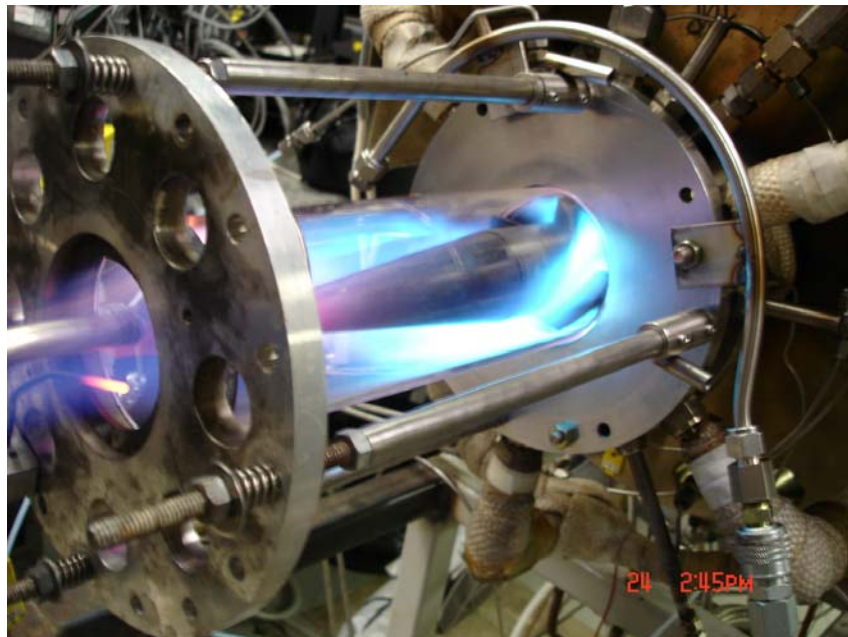
Figure 20. UCC showing flame lengths at high OFAR and swirl in flame

High OFARs lead to long flame lengths in the exhaust tube as combustion completed in the axial distance of the test rig. Lower OFARs had the opposite result and showed shorter flame lengths. These flames are long right now, but once the combustor operates in a pressurized environment, the flame length will decrease because of the increased reaction rates dictated by the Arrhenius rate law. Both figures show the combustor producing a bright blue flame; this flame was consistently seen at all operating conditions, except right before lean blow out, and it indicates an efficient and uniform combustion taking place without cold spots in the combustor. Compared to a conventional swirl stabilized combustor, the UCC produces shorter flame lengths and a clean, blue flame.

The acoustics were also used to provide clues to the operating stability of the UCC. As the combustor started to operate erratically, the combustor would begin to emit a low rumble. As the instability grew, the rumble would increase in volume and speed until the flame extinguished. No laboratory data was taken on the characteristic acoustics of the UCC, but observation with a human ear helped to better understand it operation.

4.1.2 Distinguishing JP-8 and Fishcer-Tropsch Fuel Characteristics

Two different fuels were tested in the UCC to compare their performance characteristics. JP-8 and a synthetic jet fuel derived from natural gas using the Fischer-Tropsch process were tested. Physically, the two fuels have the same handling requirements concerning combustible materials and display no differences in appearance or smell. Other than purging the fuel supply system when switching fuels to ensure the desired fuel was being fed to the UCC with out contamination, using the FT fuel required

56

no modification of the test rig. The Air Force hopes to make this fuel a transparent

replacement to JP-8 and during initial visual observation it appears to satisfy that

requirement. Actual performance characteristics and emissions differences are quantified

later in this thesis.

Visual observation of the differences between the two fuels produced a few

notable differences during the tests. When Fischer-Tropsch (FT) fuel was in use, the

flames were a noticeably brighter blue, as shown below in Figure 21 in comparison to

Figure 19 and Figure 20.
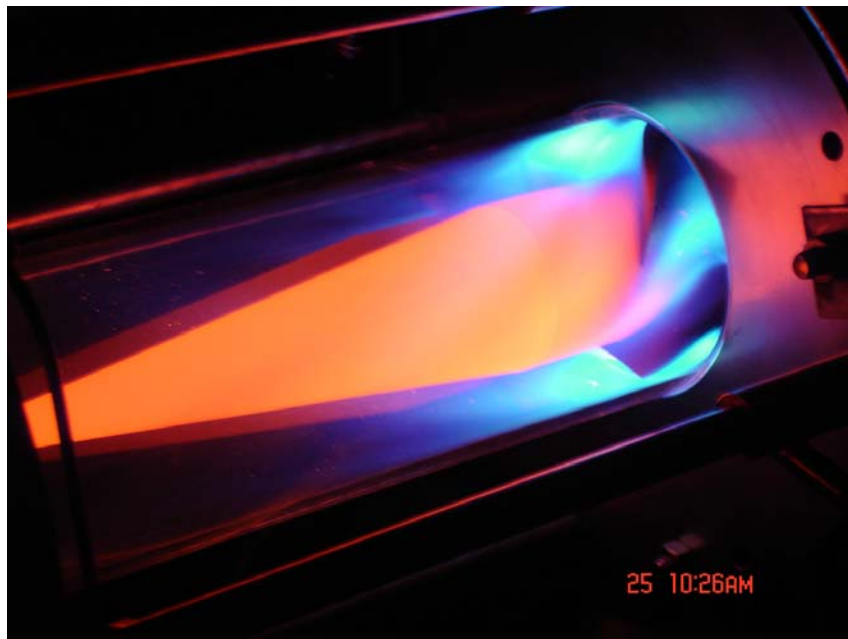
Figure 21. UCC burning synthetic FT fuel

The FT fuel burned noticeable cleaner than the pure JP-8. The JP-8 used in these tests did

not include the +100 additive package developed to reduce particulate emissions and

coking of engine components. The FT fuel coked the quartz observation windows and

fuel injectors at a noticeably slower rate than the JP-8. While burning FT fuel, the fuel

injectors maintained their flow numbers longer before coking up and causing injector

performance to suffer. Even during lean blow out tests, which rapidly degraded the

injector flow number due to coke deposits, the fuel injectors did not coke up nearly as quickly using FT fuel, maintaining their flow numbers unlike they did using JP-8 during the same tests.

The quartz windows last longer using FT fuel because it cokes the windows at a slower rate than JP-8. Figure 22, below, shows the coke deposits on one of the two quartz observation windows centered on a fuel injector and the cavity-in-a-cavity (CIAC) after running several tests using JP-8. If FT fuel was used, there would have been coke deposits, but no where near the same amount of deposits as the JP-8 creates in the same amount of running time. This coking of the quartz windows made it necessary to replace them at regular intervals to maintain optical access into the circumferential cavity.

Figure 22. Cavity-in-a-cavity seen through a quartz observation window

It also seemed to have a cleansing effect when in use, as it cleaned up some of the coke deposits in the combustor left by the combustion of JP-8. The lower rate of coke production from combustion of FT fuel might be attributed to the lack of aromatics and other heavier molecules that produce much of the soot in smoke seen in engines burning JP-8 (Corporan et al., 2007:7).

4.1.3 Cavity-In-A-Cavity Observations

Using the quartz observation windows centered on the cavity-in-a-cavity, shown previously in Figure 22, the behavior of the flow within that secondary cavity could be observed. The CIAC was previously described in section 3.1.4. The idea behind the CIAC is create a secondary vortex below the fuel injector to help anchor the flame in that small cavity. In this way, the CIAC acts as a pilot for the main circumferential cavity. Observations showed a vortex did anchor here, but unfortunately the fuel spray cone would hit the sides of this cavity, degrading the performance of the vortex within the CIAC. In Figure 23, below, a high speed image taken during operation, shows the vortex anchored in the CIAC. The arrows illustrate the flow direction seen during the video.
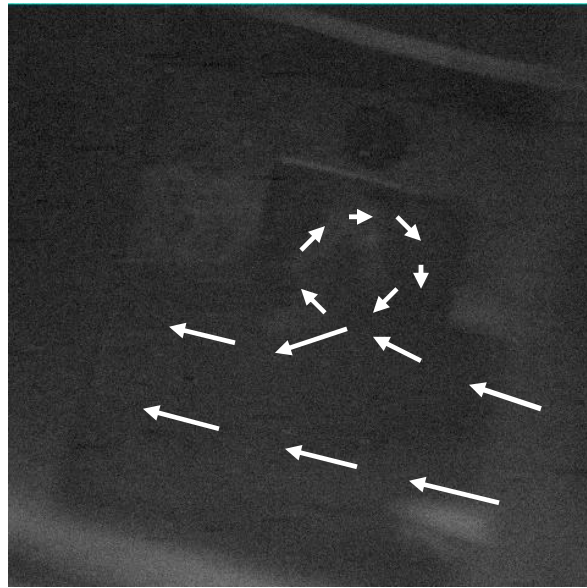
Figure 23. High speed image of a vortex in the CIAC

Visual observation through the quartz window allowed a person to see this phenomenon happen, but due to the luminosity of the flame, a normal color picture could not capture the vortex. The high-speed videos were able to record the flame behavior in the secondary and main cavities. These videos will be used for further analysis of the UCC that will take place outside of the scope of this thesis.

4.2 Isothermal Results

The goal of the isothermal tests was to determine an effective area for the combustor. It is used to determine the exit conditions of the combustor and provides a reference area for the combustor at uniform temperature. This area, A_{CD}, is the area the airflow physically sees as it travels through the combustor. It represents the smallest or most constricted area that the flow sees as it moves through the combustor. In the case of this design, the smallest area the flow will see is in the turbine guide vanes at the exit of the combustor. The effective area takes into account the boundary layer and any other phenomenon that would restrict the air flow.

Using information gathered during the isothermal testing, the effective area was calculated using the following equation, derived from incompressible flow theory.

$$A_{CD} = \frac{\dot{m}_{a,total}}{1.099} \frac{1}{\sqrt{\dfrac{P_3(P_3 - P_4)}{T_{ave}}}} \sqrt{\left(1 - \left(\frac{A_{CD}^2}{A_3^2}\right)\right)} \tag{28}$$

It assumes the entry and exit Mach numbers are much less than one and density is constant. Since density is not constant through the UCC, an average density is used where this equation is applied. The mass flow is units of lbm/s, pressures are in psia, and the temperature is in degrees Rankine resulting in inches squared to be converted to metric units to report in this thesis. The derivation of this equation is included in Appendix B. The data was taken at two different inlet temperatures, 292 K and 405 K, over pressure drops measured from the inlet pressure for both the main and cavity ranging from $\Delta P = 1.5\%$ to 6% in half percent increments.

Analysis of the data results in an effective area of 11.195 cm^2 (1.735 inches square). In comparison, the physical area of the exit of the turbine guide vanes is 16.155 cm^2 (2.504 inches square) and the entrance area of the combustor is 20.103 cm^2 (3.116 inches square). This represents a reduction of 30.69% in the exit area due to the complex shape of the combustor and separated flow along the turbine guide vanes.

4.3 Rayleigh Pressure Loss Results

The addition of heat to any airflow will result in an increase in speed for a subsonic flow resulting in a given loss in total pressure. This pressure loss is not desired in the constant pressure Brayton cycle because it represents a loss in potential work and efficiency. The pressure loss is quantified in this study of the Rayleigh pressure loss characteristics for the Ultra Compact Combustor.

Using the data collected for cold flow and hot flow conditions from the method described in Chapter 3, the pressure losses of the UCC were quantified. The initial cold flow pressure drops, measured from the inlet pressure of the main and cavity air supplies, were 1.5% and 2%. The hot flow data was collected using the mass flows from the cold flow conditions and overall fuel-air ratios of 0.015 and 0.025 resulting in two different temperature ratios. The hot flow pressure drop minus the cold flow pressure drop quantifies the pressure loss due to Rayleigh flow. The Rayleigh pressure losses for the UCC are then compared with theoretical Rayleigh flow. More data points were attempted, but at higher pressure drops, stable combustion could not be maintained because the combustor was operating outside of its stability curve, described later in this chapter with the lean blow out results.

4.3.1 Rayleigh Mach Increase

The analysis of the collected data began by calculating the entry and exit Mach numbers of the UCC. This had to be done to calculate a change in Mach number, defined in the following equation, to compare to Rayleigh theory.

$$\Delta M = M_{Exit} - M_{Entrance} \tag{29}$$

This initial analysis was done using a simple continuity calculation in combination with the Ideal Gas Law to find the entry and exit Mach number. The results of these bulk calculations, shown in Table 5, were used to get an initial estimate of the flow characteristics through the combustor. The exit Mach number is measured at the end of the turbine guide vanes. Appendix C contains more information on the employed method. Condition 0A and 1A represent the same entry conditions into the combustor, but with differing heat additions denoted by the hyphenated number on each condition symbol.

Table 5. Results of bulk Mach number calculations using continuity

Condition	ΔT	Entry Mach #	Exit Mach #
0A-1	2.94	0.0707	0.2957
1A-1	2.93	0.0883	0.3464
0A-2	3.44	0.0699	0.3109
1A-2	3.41	0.0872	0.3696

Of course, these calculations do not represent any physical phenomenon occurring within the combustor itself; the intermediate values found for the calculation represent numbers that satisfy the continuity equation. There is quite a bit of error involved in these calculations due to their nature, but they show the Mach number is high enough that compressibility could come into play, especially with the complex shape of the UCC.

To get a much better estimation of the air speeds entering and exiting the UCC, compressibility was taken into account through the use of the following equation.

$$\dot{m} = \frac{AP_t}{\sqrt{T_t}}\sqrt{\frac{\gamma}{R}}M\left(1+\frac{\gamma-1}{2}M^2\right)^{-\frac{\gamma+1}{2(\gamma-1)}} \qquad (30)$$

From the data sets for these tests the mass flow, pressure, and temperature are known. Unfortunately, the instrumentation only measures a static pressure and a gas temperature from a flush mounted thermocouple. The pressure is corrected to total pressure using the isentropic relationship, shown below, which is substituted into Equation 30.

$$P_t = P\left(1+\frac{\gamma-1}{2}M^2\right)^{\gamma/\gamma-1} \qquad (31)$$

The temperature measured at station 3 is still just that, a measured temperature, but it will have less error between it and stagnation because of the low entry Mach numbers. The temperature used to calculate the Mach number at the exit of the turbine guide vanes is computed from a curve fit for the adiabatic flame temperature using the overall equivalence ratio. Using all of this information, the Mach number was found using an inline solver.

The area term at the exit of the combustor will decrease due to the growth of a boundary layer from the heat addition. The boundary layer displacement will have the most effect at the exit of the turbine guide-vanes at the high exit temperatures, further decreasing the exit area represented by the effective area found in the first round of tests. The displacement was calculated on the surface of the guide vanes, assuming the displacement grows proportionally to the square root of the Reynolds number along the length of the vane, the area displacements at the end of each vane were used to calculate a

reduction in the effective area found during the isothermal tests. Table 6 shows the

resulting reduction in area the boundary layer displacement causes at each condition with

details on how this reduction was found in Appendix C.

Table 6. Reduction in exit area from boundary layer displacement

Condition	Exit Area Reduction
0A-1	3.612%
1A-1	3.237%
0A-2	3.671%
1A-2	3.332%

Since, this area reduction has been quantified the new resulting area is used in the

calculation of the exit Mach number, thus eliminating a possible source of error.

With the use of the collected data, the reduced areas due to displacement, and the

corresponding specific heat ratio an iterative solver was employed to solve for the Mach

number in Equation 30 yielding the results displayed below in Table 7.

Table 7. Flow speeds using compressibility

Condition	Entry Mach #	Exit Mach #
0A-1	0.0711	0.2785
1A-1	0.0888	0.3223
0A-2	0.0703	0.3245
1A-2	0.0877	0.3845

The resulting entry and exit Mach numbers do not match the speeds found using the bulk

calculations. The bulk method made the assumption of an incompressible gas.

Considering compressibility, as is done in Equation 30, results in higher Mach numbers,

but it is also more realistic and could be considered a better representation of the different

flow conditions through the combustor. With the available information the data

presented in Table 7 is the best estimation, with minimal error, of the flow speeds found

in the UCC.

The combustor itself acts as a nozzle due to the decrease in area from entrance to exit. The area decreases by roughly 47% when using the effective area as the exit area and with heat addition the area contraction will decrease by three to four percent more because of the displacement boundary layer. The decrease in area from entry to exit will account for part of the acceleration through the combustor. Table 8 displays the exit Mach numbers for a contraction in area using isentropic relations, the calculated entry Mach numbers from Table 7, the entrance area, the exit area without heat addition, and the assumption of constant mass flow through the combustor.

Table 8. Exit Mach numbers resulting from a decrease in area with no heat addition

Condition	Entry Mach #	Exit Mach #
0A-1	0.0711	0.1285
1A-1	0.0888	0.1612
0A-2	0.0703	0.1271
1A-2	0.0877	0.1591

In reality, the mass flow through the UCC is not constant because of mass additions from air and fuel in the circumferential cavity. The rest of the increase in Mach number at the exit of the UCC is due to the heat addition driving the Mach number towards unity.

The heat addition and speed increase is governed by Rayleigh flow theory. Rayleigh theory assumes a constant area pipe with heat addition; however, with the UCC as described early there is a change in area associated with this heat addition. The theoretical resulting Mach number for both of these factors is governed by the following equation from Saad (Saad, 1985:263).

$$\frac{dM}{M} = \frac{1+\frac{\gamma-1}{2}M^2}{M^2-1}\frac{dA}{A} - \frac{\left(\gamma M^2+1\right)\left(1+\frac{\gamma-1}{2}M^2\right)}{2\left(M^2-1\right)}\frac{dT_t}{T_t} \tag{32}$$

An estimate of the exit Mach number was calculated using a computer code derived from Saad's equation, but it is applied in a more practical manner for computational ease. The

code calculated the exit conditions by using an isentropic nozzle feeding a constant area

Rayleigh duct with heat addition.
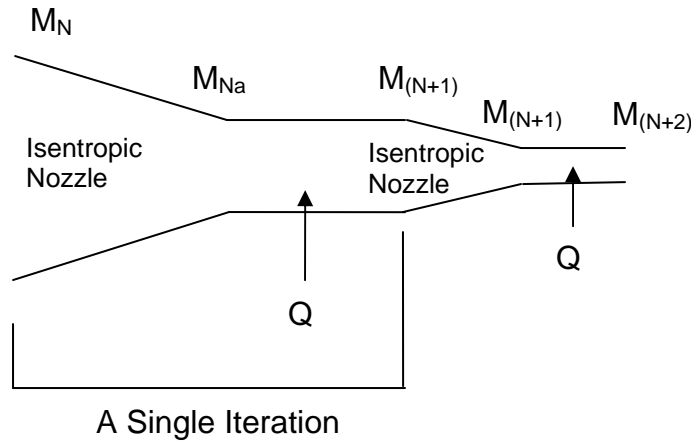
Figure 24. Graphical illustration of Rayleigh flow computer code method

These nozzles and ducts were stacked together in many iterations resulting in a numerical

estimate for the result of the exit conditions. The entry Mach number for the theory

calculation is the average of the individual entrance Mach numbers for each condition

regardless of the heat addition. More details on this numerical estimation can be found in

Appendix C. The results of this code are displayed in Table 9.

Table 9. Results of Rayleigh theory computer code based on equation 32

Condition	Entry Mach #	Exit Mach #	ΔM
0A-1	0.0710	0.2351	0.1641
1A-1	0.0890	0.2993	0.1796
0A-2	0.0710	0.2506	0.2103
1A-2	0.0890	0.3112	0.2222

Using the results of this computer program, shown in Table 9, and comparing those

results with the information computed from experimental data yields Figure 25 seen

below.
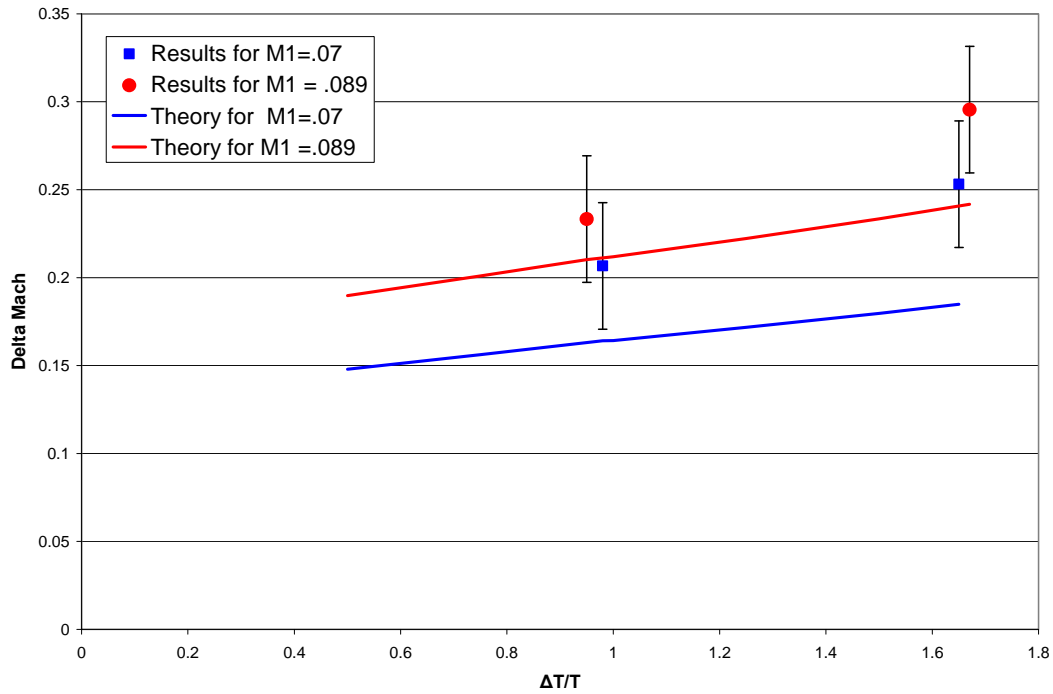
Figure 25. Comparison of experimental and theoretical Rayleigh flow

The experimental results do not match what Rayleigh theory suggests should be the exit

Mach number. In all four cases, the exit Mach number is below what theory would

dictate. Comparing the experimental results to theory for the same entry conditions and

heat addition results in the percentage differences shown in Table 10.

Table 10. Comparison of Rayleigh theory and experimental results

Condition	Experimental Exit Mach #	Theoretical Exit Mach #	Error %
0A-1	0.2785	0.2351	25.97%
1A-1	0.3223	0.2993	10.94%
0A-2	0.3245	0.2506	40.91%
1A-2	0.3845	0.3112	26.62%

The error between the theory and experimental results can mostly be accounted

for in several assumptions made by the theory and during the analysis. The Rayleigh

flow theory assumes frictionless, one-dimensional flow through the combustor without

any mass addition (Saad, 1985:261). The effective area was used in the theory

calculation because it is the area that the cold flow sees and provides a baseline for the comparison of the boundary layer changes. In reality, the flow through the combustor experiences friction forces that will reduce the speed of the flow accounting for a percentage of the error. The friction also induces a boundary layer that causes displacement of the flow narrowing the exit area as discussed earlier. Including that boundary layer displacement reduces the error between theory and the experimental data because it accelerates the flow due to a nozzle like effect.

More of the error can be accounted for in the assumption of laminar uniform flow through the UCC. The flow along the turbine guide vanes is not uniform and appears to be highly separated during actual operation. The back of the suction side of each turbine guide vane shows signs of separated flow, such as carbon deposits and wear marks different from the center of the channel. In Figure 26, signs of separation can be seen on the centerbody.
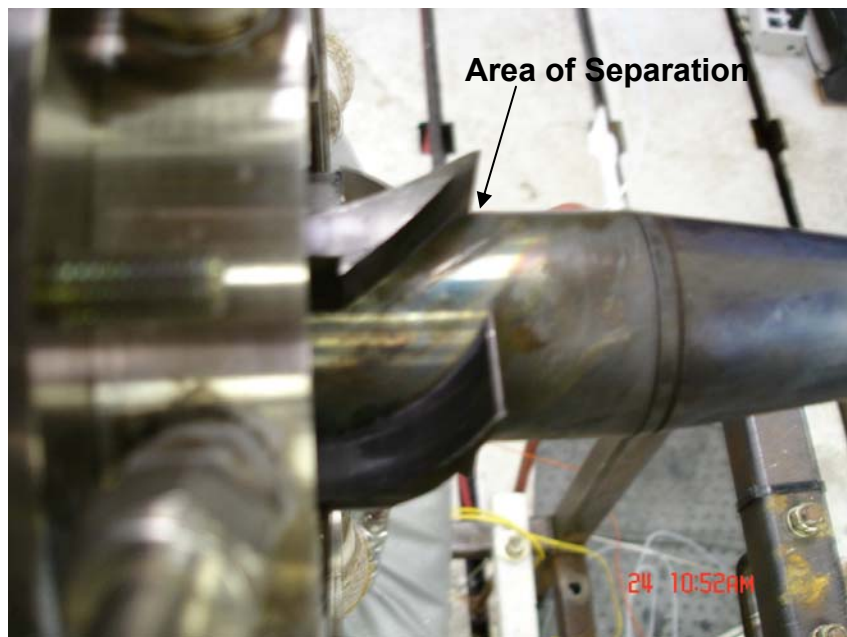
Figure 26. Turbine guide vanes showing signs of separated flow

This separation creates a much higher speed flow near the end of the suction side when compared to the pressure side of the adjacent guide vane where the flow is attached. This attached flow means the Reynolds number will be lower and consequently lead to a larger displacement of the flow by the boundary layer. In actuality, the exit Mach numbers may be higher than calculated with the assumption of uniform flow, eliminating more error.

It is reasonable to conclude, the UCC does follow Rayleigh theory for heat addition in relation to the expected change in Mach number. Knowing the UCC does conform to Rayleigh flow in that respect allows for a comparison of experimental and theoretical pressure losses due to the heat addition process.

4.3.2 Rayleigh Pressure Losses

The pressure losses due to combustion within the Ultra Compact-Combustor are computed by finding the difference between the hot and cold pressure drops recorded during testing. This pressure drop is represented in the following equation and Appendix C contains more information on how the hot or cold pressure drops are calculated.

$$\left.\frac{\Delta P}{P}\right|_{Rayleigh} = \left.\frac{\Delta P}{P}\right|_{Hot} - \left.\frac{\Delta P}{P}\right|_{Cold} \tag{33}$$

This difference is the drop in pressure induced by the heat addition from the combustion taking place within the UCC. Table 11 shows the pressure loss experienced within the UCC increases with larger entry Mach numbers and an increase in heat addition, corresponding to Rayleigh theory.

Table 11. Pressure losses in the UCC due to heat addition

Condition	Experimental %ΔP/P Hot Loss
0A-1	0.779%
1A-1	1.048%
0A-2	1.175%
1A-2	1.738%

Using the theoretical exit Mach numbers computed early to prove Rayleigh flow is valid for the UCC a hypothetical pressure drop can be computed using Rayleigh flow theory, outlined in Appendix C. The theory calculations assume a constant area frictionless pipe with uniform heat addition. In reality, the UCC has a contracting area, but the contraction is assumed to be isentropic so it does not affect the pressure drop. Therefore, it is reasonable to assume the pressure drop in the UCC is only from the heat addition process and does not involve any losses due to the area contraction. The theory lines are corrected for the area contraction of the UCC by accelerating the resultant Mach numbers through an isentropic nozzle with the same areas as the UCC. Figure 27, seen below, displays the pressure loss as a function of the Mach number at the exit of the turbine guide vanes.
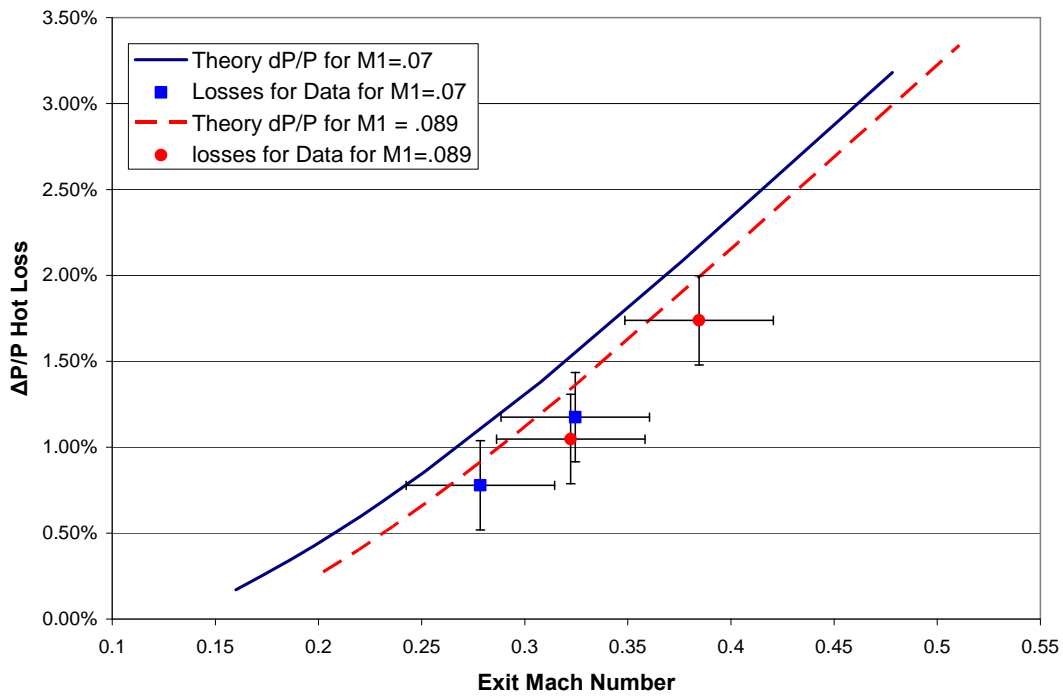
Figure 27. Comparison of Rayleigh pressure losses for the UCC

The data shows that UCC loses less pressure than it should according to Rayleigh theory, Table 12 details the theoretical values for a given temperature rise and inlet condition and compares them to the collected data.

Table 12. Hot pressure loss comparison for Rayleigh flow

Condition	Experimental %ΔP/P Hot Loss	Theoretical %ΔP/P Hot Loss	% Difference
0A-1	0.779%	0.335%	132.481%
1A-1	1.048%	0.512%	104.873%
0A-2	1.175%	0.565%	108.134%
1A-2	1.738%	0.902%	92.670%

The UCC, in reality, does not come close to resembling a tube with uniform heat addition. In the Ultra-Compact Combustor, the heat is added very rapidly on one side of the flow from the main circumferential cavity. On the other side of the flow is the relatively cold centerbody acting as a heat sink. The way the heat is added may reduce

71

the pressure loss experienced by this new combustor design. The presence of the boundary layers in the UCC may also serve to reduce the loss of total pressure as well. The theory also does not take into account the mass addition of air and fuel that takes place in the circumferential cavity. This mass addition may serve to preserve the total pressure and prevent its loss due to the heat addition.

The way this test is designed may also account for why the pressure drop is below what would be expected according to Rayleigh. In a real engine, the combustor is fed pressurized air from the compressor at Mach numbers around 0.2 before being diffused for entry into the combustor. This test relies on a pressure drop across the UCC to increase the entry Mach number. This reliance on pressure drop may be removing some of the pressure loss due to heat addition, when in fact it could be higher if the UCC was fed high velocity air, like that coming off a compressor rotor.

In conclusion, the Ultra-Compact Combustor does experience pressure losses from combustion; however, it appears these losses are less severe than Rayleigh theory would predict. At the very least, it is safe to assert the UCC will not have pressure loss characteristics greater than what Rayleigh would predict for the given heat addition.

4.4 Lean Blow Out Results

The combustion process in any conventional burner is subject to instabilities from flight conditions and throttle settings. This series of tests explores the stability of the UCC and its operating envelope, specifically its lean blow out characteristics. These characteristics are of particular importance since it could operate as an inter-turbine burner. The importance of good LBO characteristics is because the ITB only needs a

small temperature rise and thus operates near LBO when compared to conventional systems. During this discussion, it is important to remember the pre-swirlers in front of the combustor entry add a counter-clockwise bulk swirl to the flow when viewed from the rear of the combustor.

This series of tests compare the lean blow out characteristics of JP-8 and FT with two different directions of swirl in the circumferential cavity, clockwise (CW) and counter-clockwise (CCW). Each set of tests started at a 6% pressure drop and decreased in half percent increments to 1% following the method outlined in Chapter 3. Using the data collected at the point of lean blow out (LBO) the cavity g-loading, cavity equivalence ratio, and combustor load parameter were calculated. The g-loading was calculated following the method outlined in Chapter 2 using an angle of 25 degrees. This angle was taken from past data experiments on older variations of the UCC. For the combustor loading parameter, defined in Chapter 2 as Equation 9, the volume used in the denominator comes from the cavity volume projected down to the centerbody, demonstrated below in Figure 28, with the volume that the four turbine guide vanes occupying in that region subtracted.
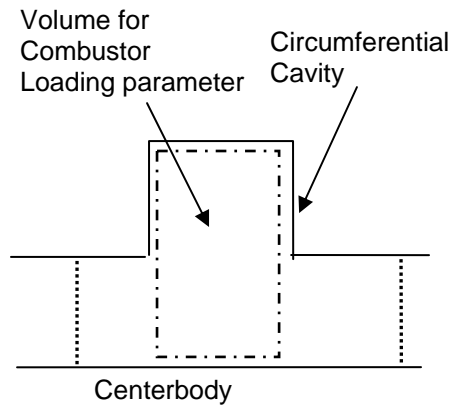
Figure 28. Volume for combustor loading parameter

The best way to compare the collected information in this case is graphical, plotting the OFAR and cavity equivalence ratio at LBO against the combustor loading parameter and the g-loading in the cavity. The configuration with the best LBO performance, and consequently the widest stability envelope, will be the one that has the lowest OFAR or cavity equivalence ratio at LBO and the highest loading parameter or g-loading. The g-loading is important because it can keep unburned fuel in the cavity through a centrifugal effect, thus reducing the LBO limit.

The first step towards deciding which configuration, fuel and rotational direction, provides the best operating stability is comparing the four configurations. The LBO trials were completed once for each configuration. Figure 29 and Figure 30 display all the LBO limits for that particular cavity loading parameter and g-loading, respectively, for each of the configurations.
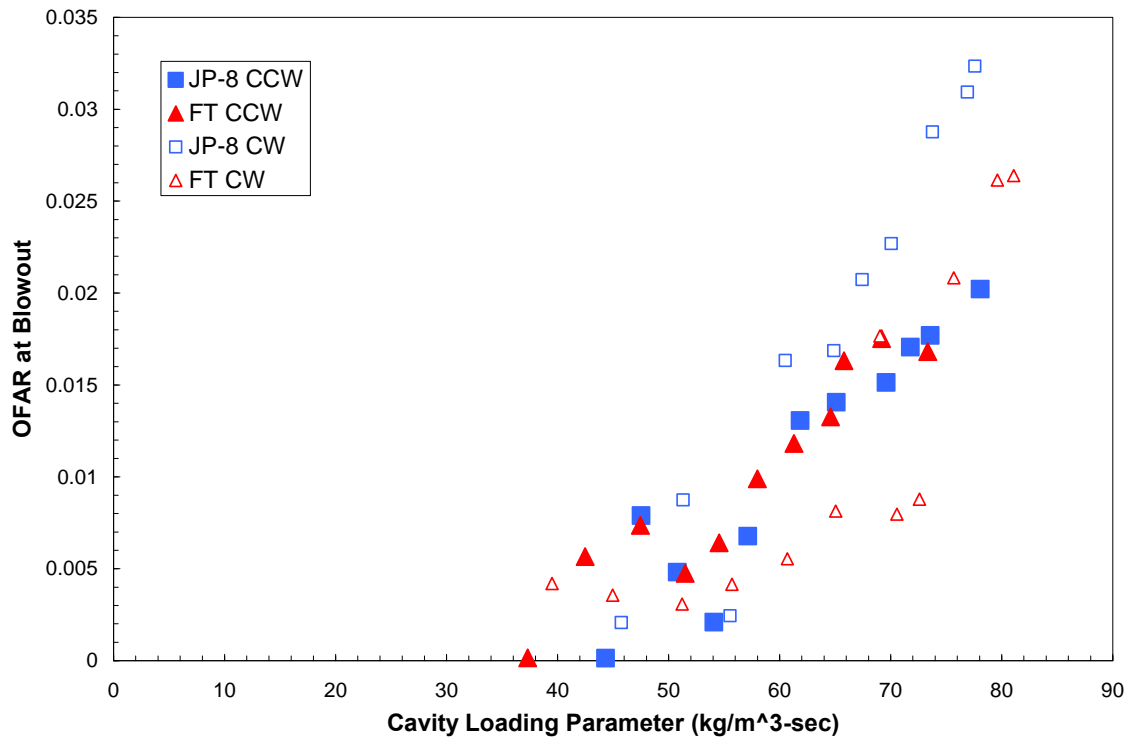
Figure 29. LBO performance as a function of cavity loading
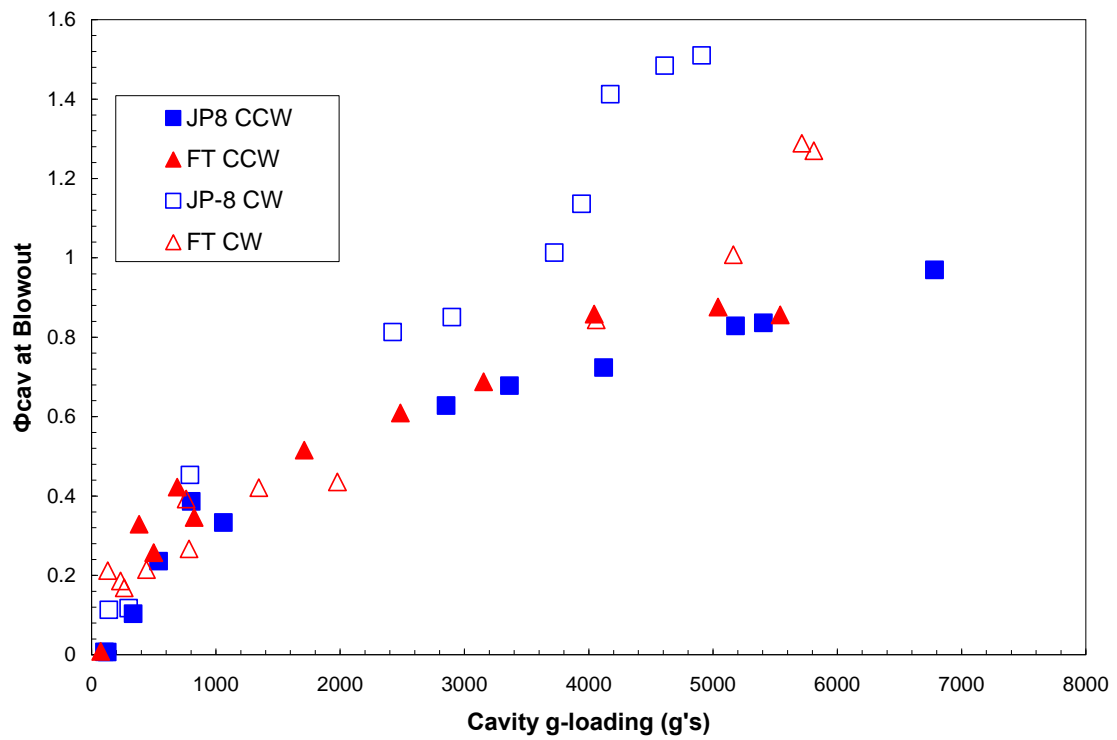
Figure 30. LBO performance as a function of cavity g-loading

75

The information presented in Figure 29 leads one to believe the counter-clockwise configuration using either JP-8 or FT fuel performs very similar in terms of lean blow out. While the CCW configuration shows a very small performance difference between the two fuels, the CW configuration performs very differently with respect to fuel choice. Examination of the clockwise configuration shows the FT fuel performs better than the petroleum based JP-8 in that configuration.

Examination of Figure 30 shows a much more distinguishable and coherent trend for the stability of the UCC. At low g-loadings the different configurations are indistinguishable from one another. As the g-loading increases, around 3000 g's the CW swirl burning JP-8 starts to diverge from the other three with higher cavity equivalence ratios at blow out. At 5000 g's the CW Fischer-Tropsch configuration performance begins to suffer, while both CCW configuration are able to sustain higher g-loadings before extinguishing the flame at significantly lower cavity equivalence ratios, and consequently a much lower OFAR. Since the UCC is designed to operate at high cavity g-loading to improve mixing and consequently efficiency, it appears the counter-clockwise configure provides the most consistent performance over the broadest range of g-loading and cavity loading parameters.

The clockwise configuration may perform worse because the swirl in the cavity is competing against the direction of the counter-clockwise bulk-swirl of the incoming main air (Refer to Figure 14, page 39, for illustration of flow directions). During tests with that configuration, looking into the cavity through the quartz observation windows, one could see what could be described as a dead-zone located where the circumferential cavity interfaces with the main air flow. The competing nature of the two swirls leads to the

flow becoming disorganized in the combustor, unlike the CCW configuration where a clear rotation is visible through the quartz windows. Therefore, the CCW rotation is the desired rotation for the best stability and lean blow out performance. It provides the most consistent operational trend for lean blow out and the different fuels have minimal impact on its performance.

The difference between the performances of the two fuels is marginal if not indistinguishable as shown previously in Figure 29 and Figure 30. However, Table 13 shows there is more of a difference between the configurations.

Table 13. Average lean blow out values for the UCC across all g-loads and cavity loading parameters

Fuel	Rotation Direction	Average OFAR	Average Cavity Equivalence Ratio
JP-8	CCW	0.0099	0.4779
	CW	0.2668	0.8902
FT	CCW	0.0100	0.5243
	CW	0.0114	0.5589

In the clockwise configuration, the synthetic fuel has a definite performance advantage over JP-8. This might be because the FT fuel has a lower surface tension and atomizes better helping to maintain a stable flame longer. Though, as mentioned earlier the clockwise configuration does not perform as desired at high loading parameters and g-loadings when compared to the CCW rotation in the main cavity. In the CCW configuration, the fuels are nearly identical in their performance, so a definitive recommendation on a fuel for use with the UCC cannot be made for the CCW configuration in relation to stability and lean blow out characteristics. The fuel choice will most likely be dictated by other performance measures such as efficiency and emissions.

Previous work done by Zelina et al. showed the LBO limits for the UCC were three to four times lower compared to conventional swirl stabilized combustors at a loading parameter of one (Zelina et al., 2006b:7). The design of the UCC tested for this thesis includes bulk swirl and curved turbine guide vanes, two design items not included in previous iterations of the UCC. A comparison between the current design and previous LBO results from an older UCC design yielded Figure 31 (Zelina et al., 2006a:5).
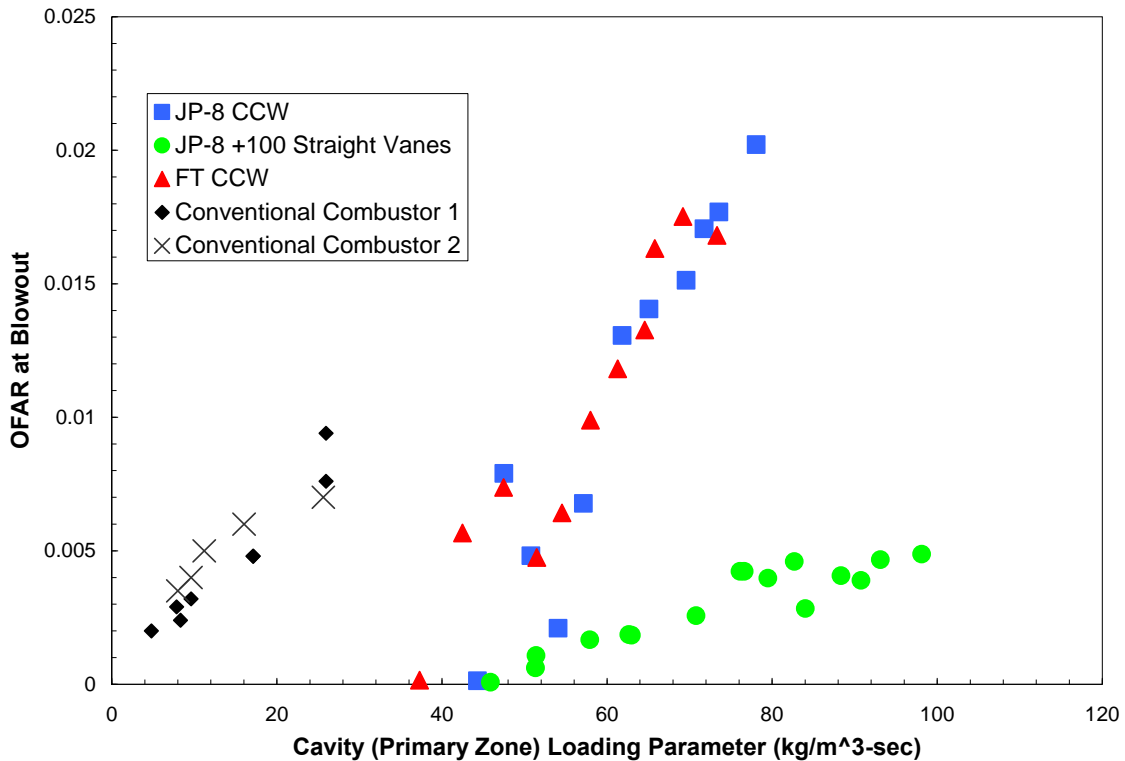
Figure 31. Comparison of conventional combustors and different UCC designs LBO limits (Zelina et al., 2004b:7)

The old UCC design with straight vanes, no bulk-swirl, and a 3.81 cm (1.5 inch) cavity, in comparison to the 2.54 cm (1 inch) cavity being tested, had better LBO performance. The design used for this thesis is more realistic to how a real world implementation of this concept would behave. One of the main principles behind the UCC is to save space

by removing the last set of compressor guide vanes and use the bulk swirl from the compressor to help drive the loading in the cavity. This design tests this principle combining it with curved vanes that resemble a true turbine guide vane; the LBO results found for the present design are more realistic for how an applied UCC would perform in an engine. During these tests the fuel spray hit the walls of the cavity adversely affecting LBO performance. Even though LBO performance suffered with the curved vanes and bulk swirl, it operated at higher cavity loading parameters at the expense of higher OFARs at lean blow out.

4.5 Efficiency Results

The efficiency of the UCC is measured by collecting exhaust samples and analyzing those samples for carbon monoxide and unburned hydrocarbons. The combustion efficiency is then calculated from the ASME Recommended Aerospace Practice described in Chapter 2. Data was collected on all four configurations of the UCC. The tests varied pressure drop from 5% to 1% and used OFARs at each pressure drop spanning 0.035 down to 0.015. Using this information the g-loading was calculated using the same method employed during the evaluation of the LBO characteristics.

The easiest way to analyze the different efficiencies of the UCC under varying operating conditions and configurations is through graphic plotting of the data to compare how g-loading and cavity equivalence ratio affect the combustion efficiency. A plot of the g-loading versus combustion efficiency, shown in Figure 32, does not present any discernable trend relating the g-loading to performance.
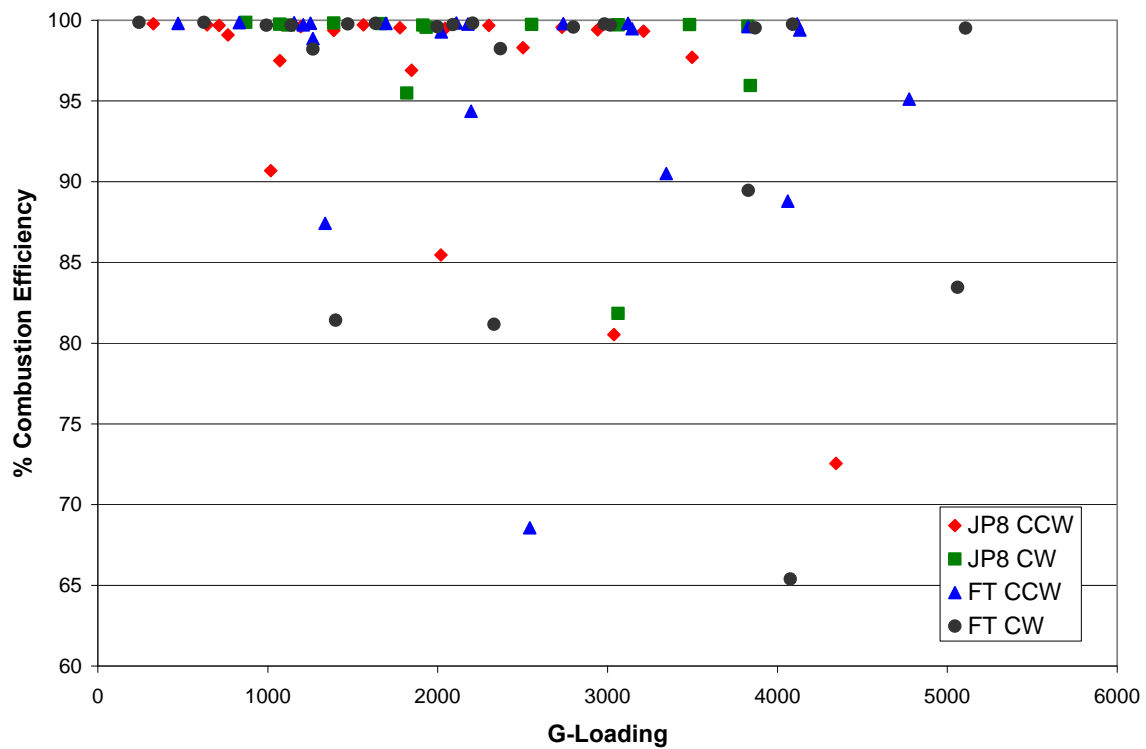
Figure 32. Combustion efficiency of the UCC as a function of g-loading

The maximum combustion efficiency displayed in Figure 32 is 99.8%. In most

combustors, the efficiency is sensitive to the equivalence ratio and it can have a large

effect on the performance of that component. The UCC is not above this trend and it

displays sensitivity to equivalence ratio, especially in the main circumferential cavity. It

is designed to operate with a rich cavity and when the cavity equivalence ratio replaces g-

loading, as shown before in Figure 32, a general trend develops for the performance,

displayed below in Figure 33.
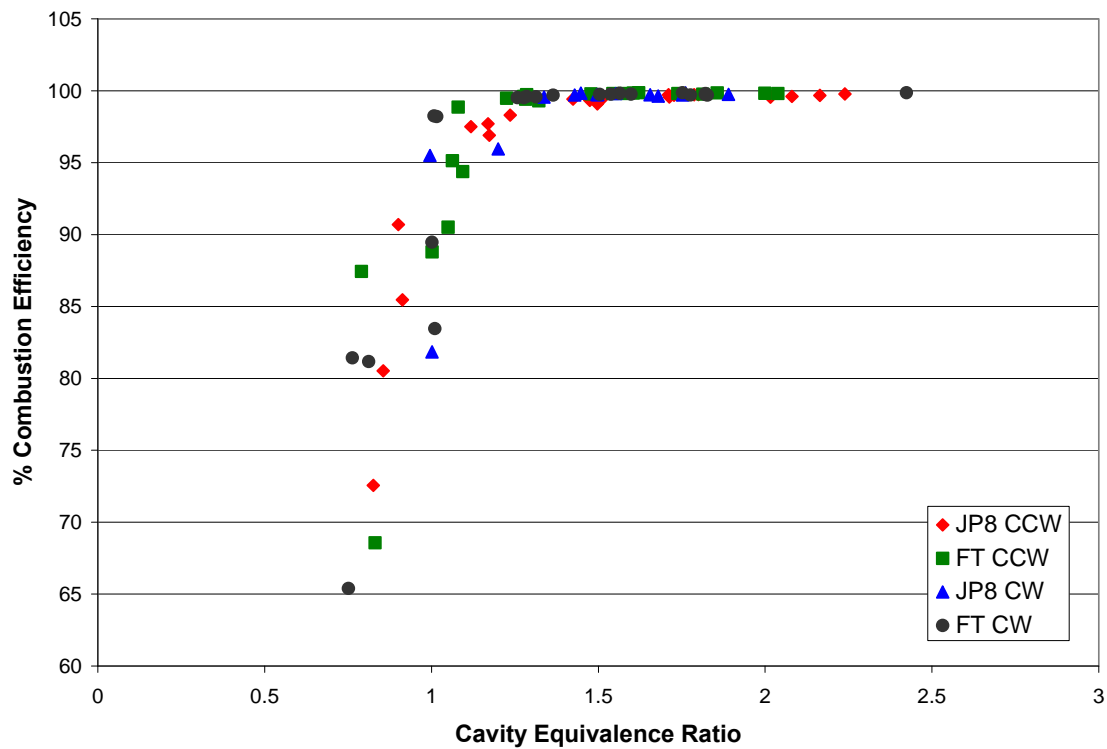
Figure 33. Combustion performance of the UCC as a function of cavity equivalence ratio

This trend supports the design philosophy of operating with a rich cavity, with cavity equivalence ratios above 1.25 the UCC operates at 99+% efficiency for all configurations. The circumferential cavity burns rich in the same manner as the primary combustion zone of a conventional combustor design, burning rich in the same manner as a conventional design should not affect specific fuel consumption. As the cavity equivalence ratio decreases below 1.25 a quick drop off in combustion efficiency occurs.

The information presented in Figure 33 can be broken down by the individual configuration and plotted in a similar manner. The efficiencies in the following plots are broken up by the g-loading that the combustor operated at for each individual data point. The following four figures, Figure 34, Figure 35, Figure 36, and Figure 37, present the results for each individual configuration.
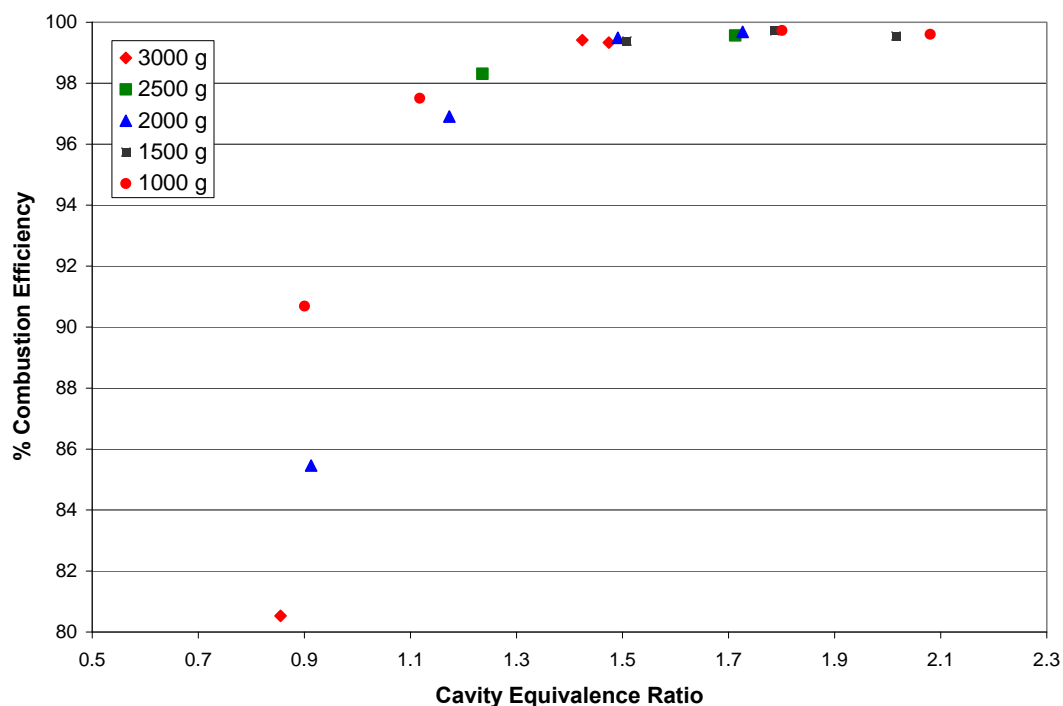
Figure 34. Efficiencies of the UCC in the JP-8 CCW configuration as a function of cavity equivalence ratio
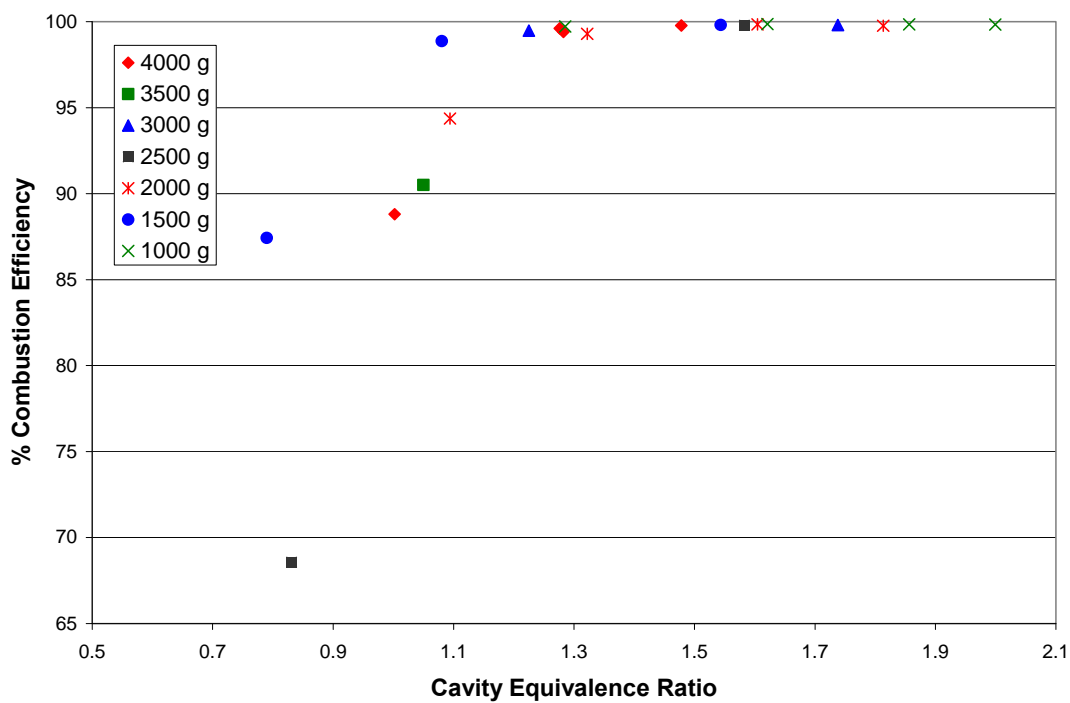
Figure 35. Efficiencies of the UCC in the FT CCW configuration as a function of cavity equivalence ratio
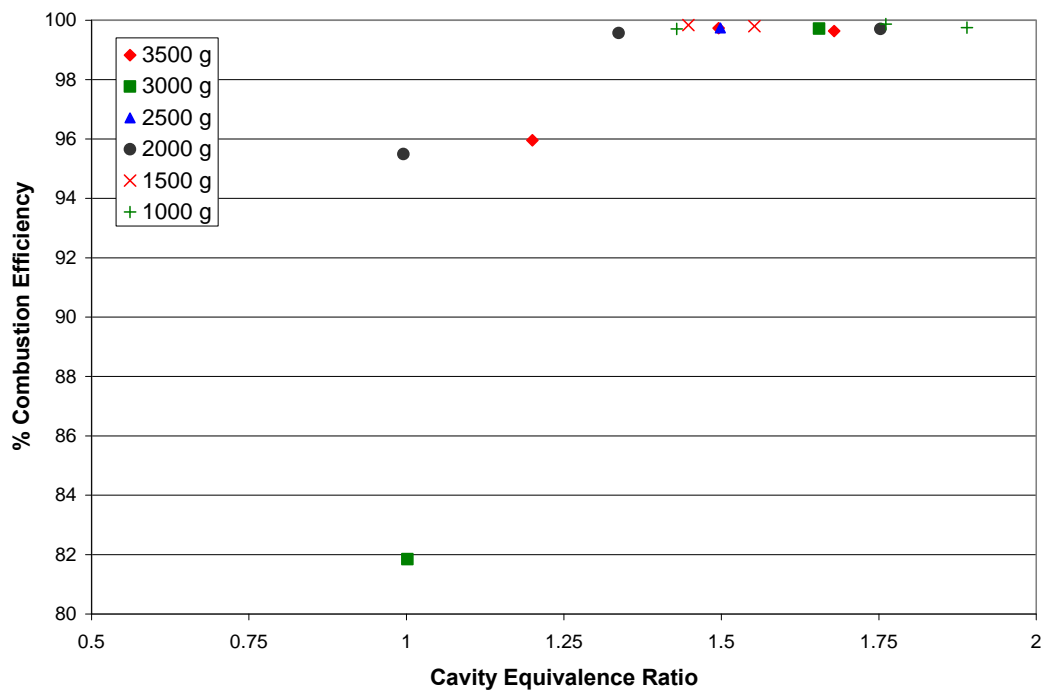
Figure 36. Efficiencies of the UCC in the JP-8 CW configuration as a function of cavity equivalence ratio
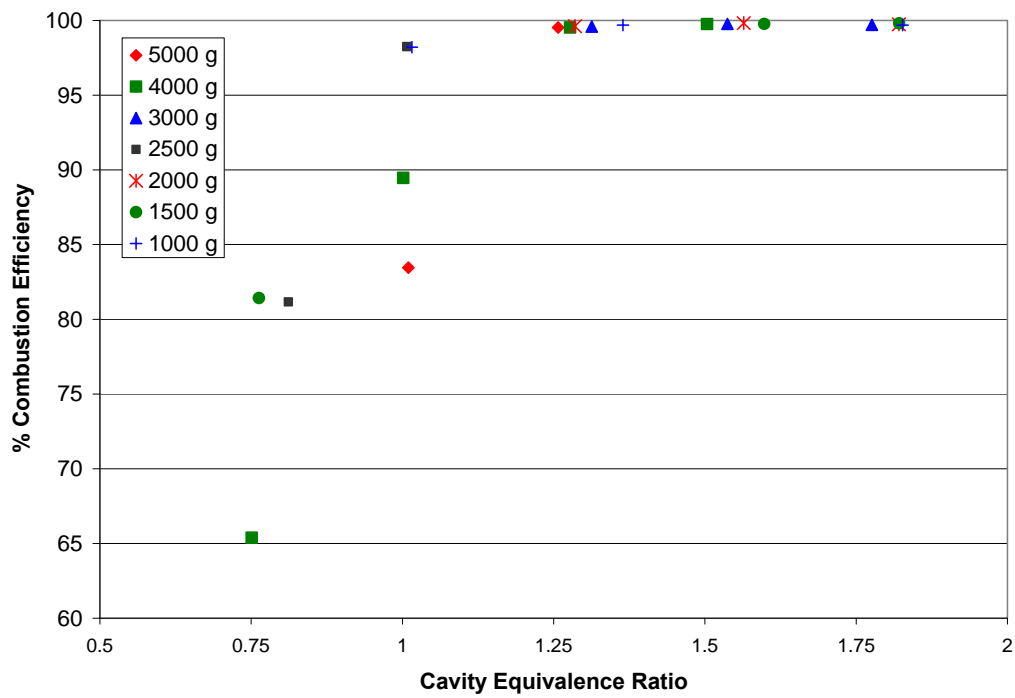
Figure 37. Efficiencies of the UCC in the FT CW configuration as a function of cavity equivalence ratio

Examination of Figure 34, Figure 35, Figure 36, and Figure 37 show both clockwise configurations start to suffer a drop in efficiency around a cavity equivalence ratio of 1.25 or earlier. The JP-8 CCW configuration, shown in Figure 34, suffers an efficiency drop at roughly the same equivalence ratio as the clockwise configurations; however, the FT CCW configuration, shown in Figure 35, maintains its efficiency to a lower equivalence ratio. The performance of the clockwise configurations may suffer due to the competing nature of the cavity swirl direction and the bulk swirl of the incoming air, as mentioned earlier during the lean blow out discussion.

The results of the lean blow out tests showed a counter-clockwise swirl in the main cavity is necessary to achieve the widest stable operating range for the UCC. Therefore, the discussion following will be focused on the counter-clockwise configuration and the performance differences of the JP-8 and synthetic fuel. Further plots of the combustion efficiency broken down by cavity equivalence ratio for both configurations are included in Appendix D for the reader's reference.

The two plots displayed in Figure 34 and Figure 35 show at high cavity equivalence ratios over a broad range of g-loadings the UCC maintains its efficiency with either fuel. However, as the equivalence ratio decreases the configuration burning JP-8 starts to suffer greater efficiency losses before the one using FT fuel. The configuration in Figure 45 still suffers a combustion efficiency loss at low cavity equivalence ratios, but compared to the JP-8 configuration it maintains more of its efficiency over a broader range of cavity equivalence ratios.

From the graphs, it appears the two fuels have equal performance. This assertion holds true when the average combustion efficiency, computed over all cavity equivalence ratios and g-loadings for the CCW configurations is compared in Table 14.

Table 14. Average combustion efficiency for CCW swirl

Fuel	Average Combustion Efficiency
JP-8	96.063%
FT	96.332%

The Fischer-Tropsch synthetic fuel has an average and maximum efficiency equal to JP-8, as seen in Table 15.

Table 15. Maximum efficiencies of the UCC in CCW configuration

Fuel	Maximum Combustion Efficiency
JP-8	99.777%
FT	99.864%

The efficiencies reported above in Table 14 and Table 15 are so close together that a clear choice can not be determined. The lack of a clear performance difference is encouraging, because the Air Force wants to use Fischer-Tropsch fuel as a transparent alternative to petroleum based JP-8. The data shows, for the UCC, either fuel could be used without a noticeable impact on performance. These results are for a combustor operating at atmospheric pressure only. If it were to be operated under pressure, as it would be in a normal turbine engine, the efficiencies will increase because of increased reaction rates due to the pressure.

4.6 Emissions Results

Pollutant emissions were collected simultaneously with the information needed to compute combustion efficiencies of the Ultra-Compact Combustor. All of this information was collected over the same range of pressure drops and fuel-air-ratios as in the emissions tests. The emissions information is presented in terms of an emissions index (EI), described in Chapter 2, which non-dimensionalizes the emissions based on the amount of fuel burned for easy comparison between throttle settings and different combustor designs.

Two pollutants of concern to combustor designers are carbon monoxide (CO) and oxides of nitrogen (NOx). Both of these are strong functions of the cavity equivalence ratio. In general, especially with the UCC, high cavity equivalence ratios produce higher amounts of NOx and lower amounts of CO.   The low amounts of CO at high cavity equivalence ratios possible come from the combusting mixture burning out in the main flow to finish the process. This trend reverses itself with lower cavity equivalence ratios. The following two figures, Figure 38 and Figure 39, illustrate this trend.
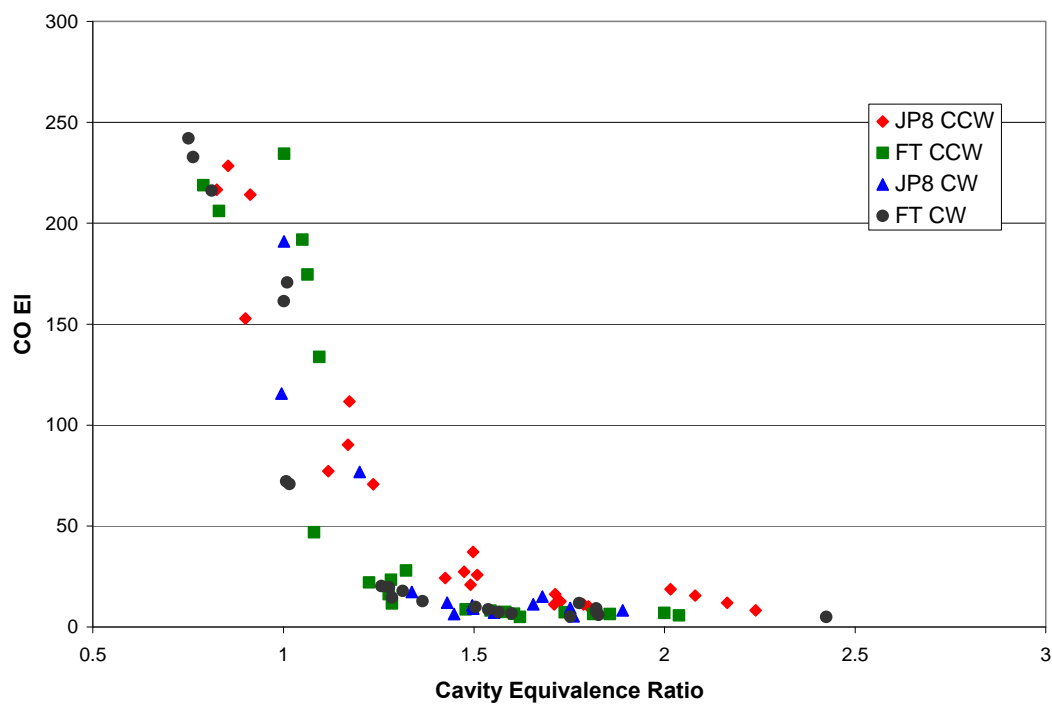
Figure 38. CO emissions for the UCC
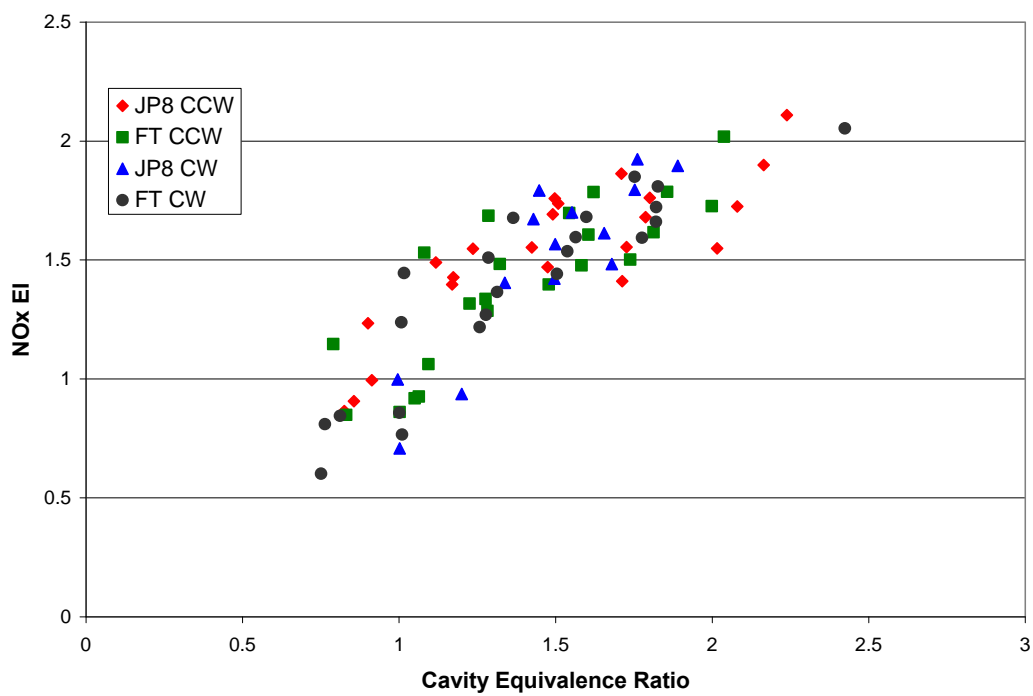
Figure 39. NOx emissions for the UCC

CO and UHC emissions for the UCC should improve when it is tested under pressure. The production of NOx is a strong function of pressure and residence time. Increasing pressure will raise NOx production, because it increases the rate constants in the Zeldovich mechanism, one of the chief mechanisms responsible for NOx production. Even with this rise in NOx production, the decreased residence times of the UCC, in comparison to conventional combustor designs will lower NOx emissions. CO is a by-product of incomplete combustion and can be considered a form of unburned fuel in a combustor. Higher pressures increase reaction rates, helping to burn the CO and consequently lower its emission form the UCC.

Another way to view the overall emissions characteristics is through the use of a plot with both emissions indexes plotted on the same graph. This emissions trade, seen below in Figure 40, shows the inter-relation of CO and NOx production in a burner.
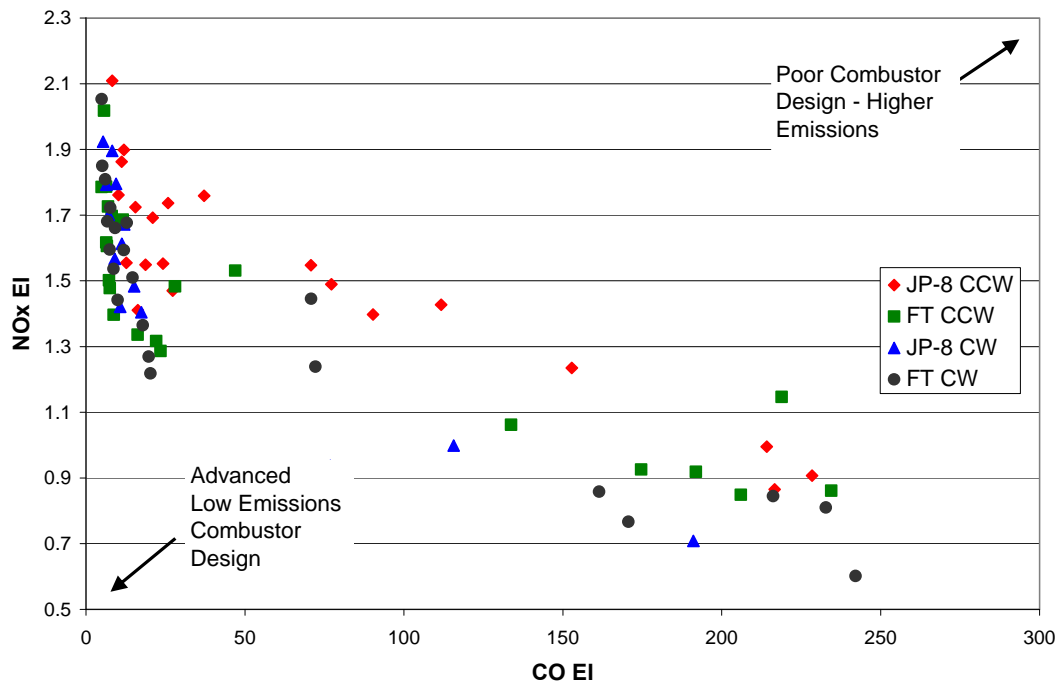
Figure 40. Emissions trade for the UCC

Any move of the curve to the lower left represents a design with improved emissions characteristics. The cluster of data points on the NOx EI axis of Figure 40 represents the points of highest combustion efficiency and the desired operating range for this combustor. The spread of data along the CO EI axis represents data collected at lower operating efficiencies.

An examination of Figure 38, Figure 39, and Figure 40 does not show a readily apparent best configuration in terms of emissions. In fact, it appears all the configurations perform nearly the same in this respect. An examination of average pollutant emissions, for the entire range of cavity equivalence ratios and g-loadings for each configuration, in Table 16 shows the clockwise configuration has lower pollutant emissions, but only marginally less.

Table 16. Average pollutant emissions for the UCC

Fuel	Swirl Direction	CO Emissions Index	NOx Emissions Index
JP-8	CCW	64.248	1.528
	CW	35.422	1.494
FT	CCW	62.568	1.410
	CW	60.411	1.389

The average CO emissions for the JP-8 with CW swirl is below all the other averages for CO, though this is not a true representation of that configuration. During testing of that configuration less data was acquired because of problems stabilizing the combustor at some of the testing points where the performance of other configurations were lower, so with less data over a narrower operating range, covering the more efficient operating points, it appears to have better emissions performance. If the combustor had been stable

enough to gather all the data, it might have had a CO emissions index on the same order or higher than the other configurations.

The emissions values for the FT fuels show a decrease in CO and NOx. The clockwise swirl configuration shows marginally lower emissions when compared to the counter-clockwise set-up. This could be due to the chemical make-up of the FT fuel, but previous work by Corporan showed there is little difference in emissions characteristics between JP-8 and FT fuel (Corporan et al., 2007:16). The lowered emissions of the FT fuel seen in the UCC are most likely due to the greater combustion efficiency. Again, the differences between the JP-8 and FT fuel are marginal and the lack of a decisive difference between the two fuels prevents a choice of fuel with regards to emissions from being made.

V. Conclusion

5.1 Rayleigh Flow Conclusions

The Ultra-Compact Combustor does follow Rayleigh flow theory for the tests conducted in this thesis. The heat addition process did increase the exit Mach number of the gases passing through the UCC in accordance with what Rayleigh flow dictates for the change in Mach number. Since, the heat addition process and Mach number change follow Rayleigh theory the pressure losses due to that speed change should follow Rayleigh theory. However, the hot pressure losses for the UCC were consistently below what Rayleigh theory would dictate. As mentioned, this could be due to the way the pressure drop is used to increase the speed of the air flow prior to entering the inlet unlike in a normal engine, where the compressor provides a high Mach flow from the work done during the compression process. Consequently, the pressure losses could be greater than found from the collected data. Though, since the UCC follows Rayleigh theory for heat addition and its resulting Mach increase, it is reasonable to assert the upper limit of the pressure loss is set by Rayleigh flow theory.

5.2 Lean Blow Out Conclusions

When compared with the clockwise swirl configuration, the lean blow out tests show the counter-clockwise cavity rotation configuration has a wider, more consistent operating range with better LBO limits. The difference between JP-8 and FT fuels in this configuration is minimal. The two fuels perform close enough to each other that a definitive choice between the two cannot be made for this test. The UCC continued to exhibit improved lean blow out limits in comparison to conventional combustors

currently employed in modern gas turbine engines; however, when compared to a previous design of the UCC without bulk swirl or curved turbine guide vanes it does not perform nearly as well. Again, the fuel spray hitting the cavity walls probably impacted the LBO performance. The design iteration tested for this thesis is the most realistic design incorporating the bulk swirl a UCC would see without compressor exit guide vanes or a diffuser in front of it and curved guide vanes simulating vanes found in operating engines. Therefore, the results presented here are more indicative of how a UCC would operate if installed in a turbine engine.

5.3 Efficiency Conclusions

The combustion efficiency of the UCC with counter-clockwise swirl is greater when compared to the opposing swirl direction. The CCW design maintains higher efficiencies over a wider operating range of cavity equivalence ratios when compared to the CW design. Again, the performance differences between JP-8 and the synthetic FT fuel are indistinguishable. For all practical purposes, the two fuels perform identically in the combustor, which means a fuel selection to increase efficiency cannot be accomplished.

5.4 Emissions Conclusions

Surprisingly, the clockwise swirl direction had average lower emissions when compared to the counter-clockwise configuration. These differences were slight, with the CW configuration having a slim emissions reduction in both CO and NOx. A

comparison of the two fuels shows they performed equally. With the almost identical performance of the two fuels, a fuel choice with regards to emissions cannot be made.

5.5 UCC Configuration Conclusion

A larger variation in results was expected with the changing swirl direction. Changing the flow dramatically in that way would seem to have caused a big difference in performance. The fact that it did not may indicate the cavity operates independently of the main flow. Using the results of the lean blow out, efficiency, and emissions tests a conclusion can be drawn recommending one specific configuration for the UCC.

The LBO and efficiency tests showed a counter-clockwise swirl is clearly better. It appears the UCC performs better when the circumferential cavity rotates in the same direction as the bulk swirl coming off the compressor. In this case, the UCC operated at its best with the CCW cavity rotation possibly due to the matching CCW bulk swirl from the pre-swirl vanes. Even though the emissions were slightly better for the competing swirl directions, operational reliability and performance dictates a choice of the counter-clockwise swirl for this design.

The choice of fuel for powering the UCC is not as clear cut as the swirl direction decision. In all the tests cases, the natural gas derived Fischer-Tropsch synthetic jet fuel performed identically to the JP-8 with only minor variations in LBO, efficiency, and emissions results. However, these variations are so small that a decisive choice between the JP-8 and FT is not possible.   The lack of difference between these fuels is important to the Air Force because Fischer-Tropsch synthetic fuel is seen to be a transparent alternative to petroleum based JP-8. From these tests it appears to fulfill that desire,

providing a transparent alternative to JP-8 that does not have any performance penalties, while reducing the Air Force's dependence on petroleum.

5.6 Recommendations for Future Work

Future work supporting the development of the UCC needs to include high pressure tests. Testing at high pressure will give a truer efficiency and emissions profile due to the effects pressure has on the results. The Rayleigh flow tests should also be repeated at high pressure to see if the UCC still follows Rayleigh theory. If possible, those tests should be conducted with a nozzle or orifice plate in front of the combustor to increase the Mach number to values that approach the exit Mach numbers coming off a compressor. This will place the UCC in an environment that has a closer resemblance to the operating environment of turbine engine and it should lead to results that are more indicative of how a UCC might behave in that environment.

As mentioned previously, the fuel spray was hitting the sides of the circumferential cavity and walls of the cavity-in-a-cavity. This most likely had an adverse effect on performance. To fix this problem a fuel injector with a smaller spray angle could be used. Widening the cavity-in-a-cavity, in combination with a narrower spray cone from new fuel injectors, should prevent any fuel from hitting the sides of the circumferential cavity or those in the cavity-in-a-cavity.

Work should also proceed on building a large model of the UCC that has more turbine guide vanes and a greater circumferential cavity diameter. A very preliminary design of this larger UCC model is shown below in Figure 41.
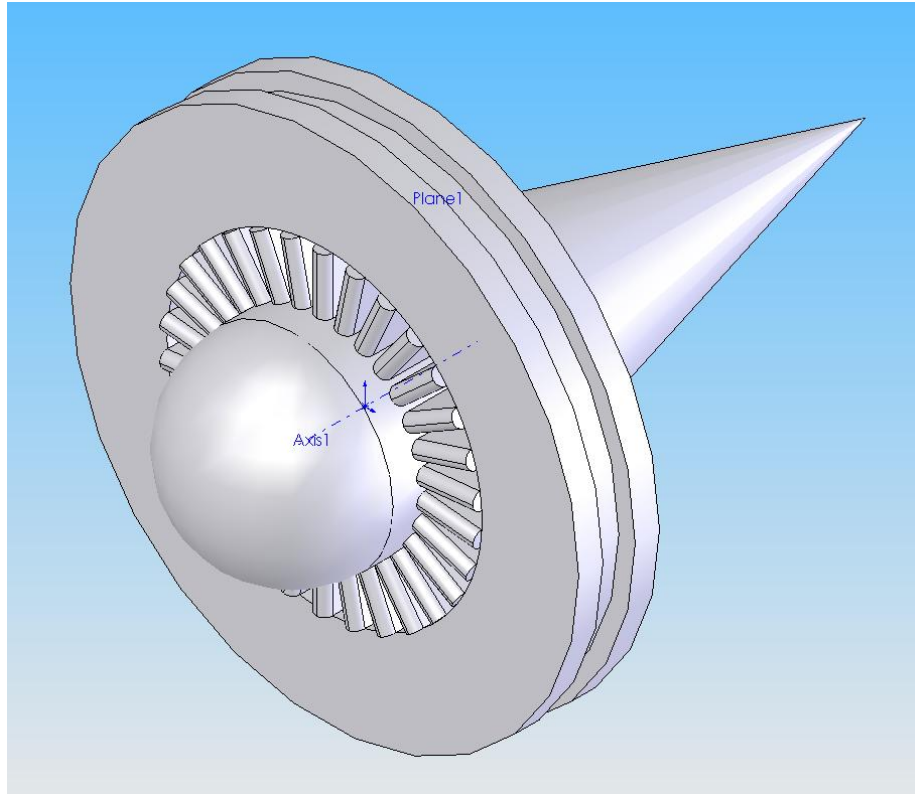
Figure 41. Notional larger UCC design for future testing

This larger scale rig will improve the understanding of cavity-vane interactions and the complex flow phenomenon taking place within the UCC. It will bring the UCC one step closer to a full scale installation in a turbine engine for testing. This larger model should be equipped with more extensive instrumentation. These extra instruments should be placed to collect temperature information at the exit of the turbine vanes. Using this information, a temperature distribution for the exit of the guide vanes can be collected to examine the temperature pattern factor before the gas enters a turbine rotor.

If the UCC is supposed to operate as an inter-turbine burner, more investigations need to be completed on how the combustor will function in a high speed vitiated flow coming from the high-pressure turbine. Theses tests should be conducted at atmospheric pressure with the current UCC design and then be completed in a high pressure environment to quantify its performance as an inter-turbine burner. If these tests are

successful, it opens the door to all of the performance improvements and advantages of a re-heat step in the Brayton cycle.

Appendix A: Single Stage ITB Study

A.1 Component Details

The single stage ITB study used the following component details for all constants such as efficiencies, specific heats, and pressure ratios. The specific heats can be found in Hill and Peterson (Hill and Peterson, 1992:171-189) and the efficiencies are taken from Mattingly et al. (Mattingly et al., 2002:107).

Table 17. Component specific heats, efficiencies, and pressure ratios

Component	Gamma	Cp (J/kg K)	Efficiency	Pressure Ratio
Diffuser	1.4	1004.5	0.96	
Fan	1.4	1004.5	0.86	
Low Pressure Compressor	1.37	1062.7	0.88	3
High Pressure Compressor	1.37	1062.7	0.88	10
Combustor	1.35	1107	0.99	0.94
Turbine	1.33	1156.7	0.89	
Nozzle	1.36	1084.2	0.86	

Table 18. Engine parameters

Maximum Turbine Inlet Temperature	1780 K
Maximum ITB Temperature Rise	420 K
Lower Heating Value of Jet A	43400 kJ/kg
Gas Constant for Air	287 J/(kg K)
Mass Flow through Core	100 kg/s

The tests were conducted at sea-level static conditions. Under these conditions atmospheric pressure is 101325 Pa and the temperature is 288 K. All of these values apply for both the turbofan comparison and the turboshaft comparison.

A.2 Conventional Cycle Analysis

The conventional on-design turbofan analysis was conducted using the following station numbers and equations from the method outlined by Hill and Peterson (Hill and

Peterson, 1992:171-189). It was carried out two times. The first time the fan pressure

ratio was varied then the bypass ratio was varied. The collected information was used to

compute specific thrust (ST) and thrust specific fuel consumption (TSFC) to make a

comparison to the ITB cycle engine.

Table 19. Conventional turbofan engine station numbers

Station #	Description
a	Atmospheric Properties
1	Atmospheric Conditions/Diffuser Inlet
2	Diffuser Outlet/LP Compressor Inlet/Fan Inlet
2b	Fan Outlet
3	LP Compressor Outlet/HP Compressor Inlet
4	HP Compressor Outlet/Combustor Inlet
5	Combustor Outlet/HP Turbine Inlet
6	HP Turbine Outlet/LP Turbine Inlet
7	LP Turbine Outlet
8	Nozzle Exit Plane

Station 1:

$$T_1 = T_a \tag{34}$$

$$P_1 = P_a \tag{35}$$

Station 2:

$$T_{t2} = T_1(1 + \frac{\gamma - 1}{2}M^2) \tag{36}$$

$$P_{t2} = P_1\left[1 + \eta_{Compressor}\left(\frac{T_{t2}}{T_{t1}} - 1\right)\right]^{\frac{\gamma}{\gamma-1}} \tag{37}$$

Station 2b:

$$T_{t2b} = T_{t2}\left[1 + \frac{1}{\eta_{Fan}}\left(\pi_{Fan}^{\frac{\gamma-1}{\gamma}} - 1\right)\right] \tag{38}$$

$$P_{t2b} = P_{t2}\pi_{Fan} \tag{39}$$

$$u_{exit,fan} = \sqrt{2\eta_{Fan} \frac{\gamma}{\gamma-1} RT_{t2b} \left[1 - \left(\frac{P_a}{P_{t2b}}\right)^{\frac{\gamma-1}{\gamma}}\right]} \tag{40}$$

Station 3:

$$T_{t3} = T_{t2} \left[1 + \frac{1}{\eta_{Compressor}} \left(\pi_{LPC}^{\frac{\gamma-1}{\gamma}} - 1\right)\right] \tag{41}$$

$$P_{t3} = P_{t2} \pi_{LPC} \tag{42}$$

Station 4:

$$T_{t4} = T_{t3} \left[1 + \frac{1}{\eta_{Compressor}} \left(\pi_{HPC}^{\frac{\gamma-1}{\gamma}} - 1\right)\right] \tag{43}$$

$$P_{t4} = P_{t3} \pi_{HPC} \tag{44}$$

Station 5:

$$T_{t5} = \text{Turbine Inlet Temperature Limit} \tag{45}$$

$$P_{t5} = P_{t4} \pi_{Burner} \tag{46}$$

$$f = \frac{\dfrac{T_{t5}}{T_{t4}} - 1}{\dfrac{\eta_{Burner}Q}{C_{p,Burner}} T_{t4} - \dfrac{T_{t5}}{T_{t4}}} \tag{47}$$

$$\dot{m}_{fuel} = f\dot{m}_{air} \tag{48}$$

Station 6:

$$T_{t6} = T_{t5} - \frac{\dot{m}_{Compressor} C_{p,Compressor} \left(T_{t4} - T_{t3}\right)}{\dot{m}_{Turbine} C_{p,Turbine}} \tag{49}$$

$$P_{t6} = P_{t5} \left[1 - \frac{1}{\eta_{Turbine}} \left(1 - \frac{T_{t6}}{T_{t5}}\right)\right]^{\frac{\gamma}{\gamma-1}} \tag{50}$$

Station 7:

$$T_{t7} = T_{t6} - \frac{\dot{m}_{Compressor} C_{p,Compressor} \left(T_{t3} - T_{t2}\right) + \beta \dot{m}_{Compressor} C_{p,Fan}\left(T_{t2b} - T_{t2}\right)}{\dot{m}_{Turbine} C_{p,Turbine}} \quad (51)$$

$$P_{t7} = P_{t6} \left[1 - \frac{1}{\eta_{Turbine}} \left(1 - \frac{T_{t7}}{T_{t6}}\right)\right]^{\frac{\gamma}{\gamma-1}} \quad (52)$$

Station 8:

$$u_{exit} = \sqrt{2\eta_{Nozzle} \frac{\gamma}{\gamma-1} RT_{t7} \left[1 - \left(\frac{P_a}{P_{t7}}\right)^{\frac{\gamma-1}{\gamma}}\right]} \quad (53)$$

Specific Thrust and Thrust Specific Fuel Consumption Calculations:

$$Thrust = \dot{m}_a \left[\left(1+f\right)u_{exit} + \beta u_{exit,fan} - \left(1+\beta\right)u\right] \quad (54)$$

$$ST = \frac{Thrust}{\dot{m}_{air}} \quad (55)$$

$$TSFC = \frac{\dot{m}_{fuel}}{Thrust} \quad (56)$$

A.3 ITB Cycle Analysis

The on-design ITB turbofan cycle analysis was conducted using the following

station numbers and equations from the method outlined by Hill and Peterson (Hill and

Peterson, 1992:171-189). It was carried out two times. The first time the fan pressure

ratio was varied then the bypass ratio was varied. The collected information was used to

compute specific thrust (ST) and thrust specific fuel consumption (TSFC) to make a

comparison to the conventional turbofan engine.

Table 20. ITB turbofan engine station numbers

Station #	Description
1	Atmospheric Conditions/Diffuser Inlet
2	Diffuser Outlet/LP Compressor Inlet/Fan Inlet
2b	Fan Outlet
3	LP Compressor Outlet/HP Compressor Inlet
4	HP Compressor Outlet/Combustor Inlet
5	Combustor Outlet/HP Turbine Inlet
6	HP Turbine Outlet/ITB Inlet
7	ITB Outlet/LP Turbine Inlet
8	LP Turbine Outlet
9	Nozzle Exit Plane

Station 1:

$$T_1 = T_a \tag{57}$$

$$P_1 = P_a \tag{58}$$

Station 2:

$$T_{t2} = T_1 \left(1 + \frac{\gamma - 1}{2} M^2\right) \tag{59}$$

$$P_{t2} = P_1 \left[1 + \eta_{Compressor}\left(\frac{T_{t2}}{T_{t1}} - 1\right)\right]^{\frac{\gamma}{\gamma - 1}} \tag{60}$$

Station 2b:

$$T_{t2b} = T_{t2} \left[1 + \frac{1}{\eta_{Fan}}\left(\pi_{Fan}^{\frac{\gamma - 1}{\gamma}} - 1\right)\right] \tag{61}$$

$$P_{t2b} = P_{t2} \pi_{Fan} \tag{62}$$

$$u_{exit,fan} = \sqrt{2\eta_{Fan} \frac{\gamma}{\gamma - 1} R T_{t2b} \left[1 - \left(\frac{P_a}{P_{t2b}}\right)^{\frac{\gamma - 1}{\gamma}}\right]} \tag{63}$$

Station 3:

$$T_{t3} = T_{t2}\left[1 + \frac{1}{\eta_{Compressor}}\left(\pi_{LPC}^{\frac{\gamma-1}{\gamma}} - 1\right)\right] \tag{64}$$

$$P_{t3} = P_{t2}\pi_{LPC} \tag{65}$$

Station 4:

$$T_{t4} = T_{t3}\left[1 + \frac{1}{\eta_{Compressor}}\left(\pi_{HPC}^{\frac{\gamma-1}{\gamma}} - 1\right)\right] \tag{66}$$

$$P_{t4} = P_{t3}\pi_{HPC} \tag{67}$$

Station 5:

$$T_{t5}=Turbine\ Inlet\ Temperature\ Limit \tag{68}$$

$$P_{t5} = P_{t4}\pi_{Burner} \tag{69}$$

$$f = \frac{\dfrac{T_{t5}}{T_{t4}} - 1}{\dfrac{\eta_{Burner}Q}{C_{p,Burner}}T_{t4} - \dfrac{T_{t5}}{T_{t4}}} \tag{70}$$

$$\dot{m}_{fuel} = f\dot{m}_{air} \tag{71}$$

Station 6:

$$T_{t6} = T_{t5} - \frac{\dot{m}_{Compressor}C_{p,Compressor}\left(T_{t4} - T_{t3}\right)}{\dot{m}_{Turbine}C_{p,Turbine}} \tag{72}$$

$$P_{t6} = P_{t5}\left[1 - \frac{1}{\eta_{Turbine}}\left(1 - \frac{T_{t6}}{T_{t5}}\right)\right]^{\frac{\gamma}{\gamma-1}} \tag{73}$$

Station 7:

$$T_{t7}=T_{t6}+ITB\ Temp\ Rise\ \underline{or}\ Maximum\ Turbine\ Inlet\ Temp \tag{74}$$

$$P_{t7} = P_{t6}\pi_{Burner} \tag{75}$$

$$f = \frac{\dfrac{T_{t7}}{T_{t6}} - 1}{\dfrac{\eta_{Burner}Q}{C_{p,Burner}}T_{t6} - \dfrac{T_{t7}}{T_{t6}}} \tag{76}$$

$$\dot{m}_{fuel,ITB} = f\dot{m}_{air} \tag{77}$$

Station 8:

$$T_{t8} = T_{t7} - \frac{\dot{m}_{Compressor}C_{p,Compressor}\left(T_{t3} - T_{t2}\right) + \beta\dot{m}_{Compressor}C_{p,Fan}\left(T_{t2b} - T_{t2}\right)}{\dot{m}_{LP,Turbine}C_{p,Turbine}} \tag{78}$$

$$P_{t8} = P_{ty}\left[1 - \frac{1}{\eta_{Turbine}}\left(1 - \frac{T_{t8}}{T_{t7}}\right)\right]^{\frac{\gamma}{\gamma-1}} \tag{79}$$

Station 9:

$$u_{exit} = \sqrt{2\eta_{Nozzle}\frac{\gamma}{\gamma-1}RT_{t8}\left[1 - \left(\frac{P_a}{P_{t8}}\right)^{\frac{\gamma-1}{\gamma}}\right]} \tag{80}$$

Specific Thrust and Thrust Specific Fuel Consumption Calculations:

$$Thrust = \dot{m}_a\left[\left(1 + f\right)u_{exit} + \beta u_{exit,fan} - \left(1 + \beta\right)u\right] \tag{81}$$

$$ST = \frac{Thrust}{\dot{m}_{air}} \tag{82}$$

$$TSFC = \frac{\left(\dot{m}_{fuel} + \dot{m}_{fuel,ITB}\right)}{Thrust} \tag{83}$$

A.4 Conventional Turboshaft Cycle Analysis

The conventional on-design turboshaft cycle analysis was conducted using the

following station numbers and equations from the method outlined by Hill and Peterson

(Hill and Peterson, 1992:171-189). The amount of power produced by the engine was determined along with the fuel flow to enable a comparison to an ITB turboshaft engine. Those values were used to compute specific power and power specific fuel consumption. The compressor pressure ratio for this study was set to 15.

Table 21. Conventional turboshaft station numbers

Station #	Description
1	Atmospheric Conditions/Diffuser Inlet
2	Diffuser Outlet/Compressor Inlet
3	Compressor Outlet/Combustor Inlet
4	Combustor Outlet/HP Turbine Inlet
5	HP Turbine Outlet/Power Turbine Inlet
6	Power Turbine Outlet

Station 1:

$$T_1 = T_a \tag{84}$$

$$P_1 = P_a \tag{85}$$

Station 2:

$$T_{t2} = T_1(1 + \frac{\gamma - 1}{2}M^2) \tag{86}$$

$$P_{t2} = P_1\left[1 + \eta_{Compressor}\left(\frac{T_{t2}}{T_{t1}} - 1\right)\right]^{\frac{\gamma}{\gamma-1}} \tag{87}$$

Station 3:

$$T_{t3} = T_{t2}\left[1 + \frac{1}{\eta_{Compressor}}\left(\pi_C^{\frac{\gamma-1}{\gamma}} - 1\right)\right] \tag{88}$$

$$P_{t3} = P_{t2}\pi_C \tag{89}$$

Station 4:

$$T_{t4} = Turbine\ Inlet\ Temperature\ Limit \tag{90}$$

$$P_{t4} = P_{t3} \pi_{Burner} \tag{91}$$

$$f = \cfrac{\cfrac{T_{t4}}{T_{t3}} - 1}{\cfrac{\eta_{Burner} Q}{C_{p,Burner}} T_{t3} - \cfrac{T_{t4}}{T_{t3}}} \tag{92}$$

$$\dot{m}_{fuel} = f \dot{m}_{air} \tag{93}$$

Station 5:

$$T_{t5} = T_{t4} - \frac{\dot{m}_{Compressor} C_{p,Compressor} \left(T_{t3} - T_{t2} \right)}{\dot{m}_{Turbine} C_{p,Turbine}} \tag{94}$$

$$P_{t5} = P_{t4} \left[1 - \frac{1}{\eta_{Turbine}} \left(1 - \frac{T_{t5}}{T_{t4}} \right) \right]^{\frac{\gamma}{\gamma - 1}} \tag{95}$$

Station 6:

$$P_{t6} = P_a \tag{96}$$

$$T_{t6} = T_{t5} \left[1 - \eta_{Turbine} \left(1 - \left(\frac{P_{t6}}{P_{t5}} \right)^{\frac{\gamma - 1}{\gamma}} \right) \right] \tag{97}$$

$$Power = \dot{m}_{Turbine} C_{p,Turbine} \left(T_{t5} - T_{t6} \right) \tag{98}$$

Calculation of Specific Power (SP) and Power Specific Fuel Consumption (PSFC):

$$SP = \frac{Power}{\dot{m}_{air}} \tag{99}$$

$$PSFC = \frac{\dot{m}_{fuel}}{Power} \tag{100}$$

A.5 ITB Turboshaft Cycle Analysis

The on-design ITB turboshaft cycle analysis was conducted using the following

station numbers and equations from the method outlined by Hill and Peterson (Hill and

Peterson, 1992:171-189). The amount of power produced by the engine was determined

along with the fuel flow to enable a comparison to a conventional turboshaft engine.

Those values were used to compute specific power and power specific fuel consumption.

The compressor pressure ratio for this study was set to 15.

Table 22. ITB turboshaft station numbers

Station #	Description
1	Atmospheric Conditions/Diffuser Inlet
2	Diffuser Outlet/Compressor Inlet
3	Compressor Outlet/Combustor Inlet
4	Combustor Outlet/HP Turbine Inlet
5	HP Turbine Outlet/ITB Inlet
6	ITB Outlet/Power Turbine Inlet
7	Power Turbine Outlet

Station 1:

Station 1:

$$T_1 = T_a \tag{101}$$

$$P_1 = P_a \tag{102}$$

Station 2:

$$T_{t2} = T_1(1 + \frac{\gamma - 1}{2}M^2) \tag{103}$$

$$P_{t2} = P_1\left[1 + \eta_{Compressor}\left(\frac{T_{t2}}{T_{t1}} - 1\right)\right]^{\frac{\gamma}{\gamma-1}} \tag{104}$$

Station 3:

$$T_{t3} = T_{t2}\left[1 + \frac{1}{\eta_{Compressor}}\left(\pi_C^{\frac{\gamma-1}{\gamma}} - 1\right)\right] \tag{105}$$

$$P_{t3} = P_{t2}\pi_C \tag{106}$$

Station 4:

106

$$T_{t4} = \text{Turbine Inlet Temperature Limit} \qquad (107)$$

$$P_{t4} = P_{t3}\pi_{Burner} \qquad (108)$$

$$f = \frac{\dfrac{T_{t4}}{T_{t3}} - 1}{\dfrac{\eta_{Burner}Q}{C_{p,Burner}}T_{t3} - \dfrac{T_{t4}}{T_{t3}}} \qquad (109)$$

$$\dot{m}_{fuel} = f\dot{m}_{air} \qquad (110)$$

Station 5:

$$T_{t5} = T_{t4} - \frac{\dot{m}_{Compressor}C_{p,Compressor}\left(T_{t3} - T_{t2}\right)}{\dot{m}_{Turbine}C_{p,Turbine}} \qquad (111)$$

$$P_{t5} = P_{t4}\left[1 - \frac{1}{\eta_{Turbine}}\left(1 - \frac{T_{t5}}{T_{t4}}\right)\right]^{\frac{\gamma}{\gamma-1}} \qquad (112)$$

Station 6:

$$T_{t6} = T_{t5} + \text{ITB Temp Rise } \underline{or} \text{ Maximum Turbine Inlet Temp} \qquad (113)$$

$$P_{t6} = P_{t5}\pi_{Burner} \qquad (114)$$

$$f = \frac{\dfrac{T_{t6}}{T_{t5}} - 1}{\dfrac{\eta_{Burner}Q}{C_{p,Burner}}T_{t5} - \dfrac{T_{t6}}{T_{t5}}} \qquad (115)$$

$$\dot{m}_{fuel,ITB} = f\dot{m}_{air} \qquad (116)$$

Station 7:

$$P_{t7} = P_a \qquad (117)$$

$$T_{t7} = T_{t6}\left[1 - \eta_{Turbine}\left(1 - \left(\frac{P_{t7}}{P_{t6}}\right)^{\frac{\gamma-1}{\gamma}}\right)\right] \qquad (118)$$

$$Power = \dot{m}_{Turbine}C_{p,Turbine}\left(T_{t6} - T_{t7}\right) \qquad (119)$$

Calculation of Specific Power (SP) and Power Specific Fuel Consumption (PSFC):

$$SP = \frac{Power}{\dot{m}_{air}} \qquad (120)$$

$$PSFC = \frac{\left(\dot{m}_{fuel} + \dot{m}_{fuel,ITB}\right)}{Power} \qquad (121)$$

A.6 Off-Design Point Matching Method

The fuel consumption rates for the off-design points needed during the mission analysis were calculated using the following method detailed below in this flow chart. This method assumes that the gas generator turbine temperature ratio is fixed, as described in the text of Chapter 2, and the engine operates at sea level static, so stagnation temperatures are known at the compressor inlet. The gases are expanded to atmospheric pressure to represent the maximum amount of work that can be extracted. The station number corresponds to a Non-ITB turboshaft engine shown previously in Table 21.
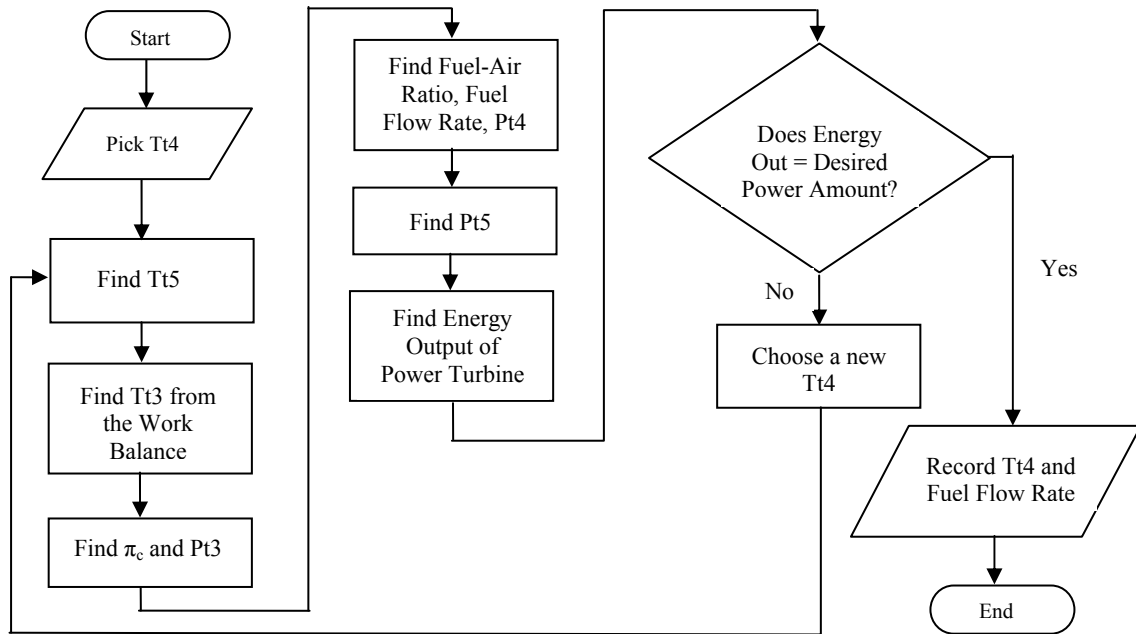
Figure 42. Off-design calculation iteration method

Appendix B: Effective Area Calculation

B.1 Effective Area Equation Derivation

The effective area of the UCC is calculated from the following equation.

$$A_{CD} = \frac{\dot{m}_{a,total}}{1.099} \frac{1}{\sqrt{\dfrac{P_3\left(P_3 - P_4\right)}{T_{ave}}}} \sqrt{\left(1 - \left(\frac{A_{CD}^{2}}{A_3^{2}}\right)\right)} \tag{122}$$

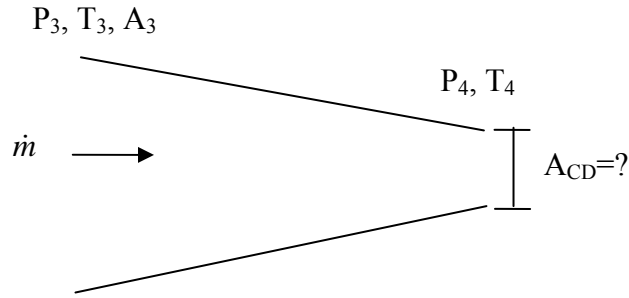Figure 43 illustrates the flow scenario for this derivation.

Figure 43: Effective area flow scenario

This equation is derived from Bernoulli's Law and Continuity. It assumes Mach numbers are much less than one and constant density. In this scenario an average density is computed from the average temperature. The derivation follows below:

Bernoulli:

$$P_3 + \rho\frac{V_3^{2}}{2} = P_4 + \rho\frac{V_4^{2}}{2} \tag{123}$$

Continuity:

$$A_3 V_3 = A_4 V_4 \tag{124}$$

$$\frac{\dot{m}}{\rho} = \frac{\dot{m}}{\rho} \tag{125}$$

Derivation from starting from above:

$$P_3 - P_4 = \frac{\rho V_4^2}{2} - \frac{\rho V_3^2}{2} \tag{126}$$

$$P_3 - P_4 = \frac{\rho}{2}\left(\frac{\dot{m}}{\rho A_{CD}}\right)^2 - \frac{\rho}{2}\left(\frac{\dot{m}}{\rho A_3}\right)^2 \tag{127}$$

$$P_3 - P_4 = \frac{\dot{m}^2}{2\rho A_{CD}^2} - \frac{\dot{m}^2}{2\rho A_3^2} \tag{128}$$

$$P_3 - P_4 = \frac{\dot{m}^2}{2\rho A_{CD}^2}\left(1 - \frac{A_{CD}^2}{A_3^2}\right) \tag{129}$$

$$A_{CD} = \frac{\dot{m}}{\sqrt{2\rho(P_3 - P_4)}}\sqrt{\left(1 - \frac{A_{CD}^2}{A_3^2}\right)} \tag{130}$$

$$A_{CD} = \frac{\dot{m}}{\sqrt{\dfrac{2P_3(P_3 - P_4)}{RT_{ave}}}}\sqrt{\left(1 - \frac{A_{CD}^2}{A_3^2}\right)} \tag{131}$$

For the desired units on A_{CD} to be in square inches, the following unit conversions are made to the first division of Equation 130, the radical involving the area ratio of A_{CD} to A_3 is dimensionless.

$$\frac{A_{CD}\left(ft^2\right)}{144\left(ft^2/in^2\right)} = \frac{\dot{m}\left(lbm/s\right)\Big/ 32.2\left(\dfrac{lbm \cdot ft}{lbf \cdot s^2}\right)}{\sqrt{\dfrac{2}{1716\left(\dfrac{ft^2}{s^2 \cdot R}\right) \cdot T_{ave}(R)} P_3\left(\dfrac{lbf}{in^2}\right)\cdot 144\left(\dfrac{ft^2}{in^2}\right)\cdot (P_3 - P_4)\left(\dfrac{lbf}{in^2}\right)\cdot 144\left(\dfrac{ft^2}{in^2}\right)}} \tag{132}$$

$$A_{CD}\left(in^2\right) = \frac{\dot{m}\left(144/32.2\right)}{\sqrt{\dfrac{2}{1716}\cdot 144^2}\sqrt{\dfrac{P_3}{T_{ave}}(P_3 - P_4)}} \tag{133}$$

The unit conversions simplify down to the constant included in the final equation shown here:

$$A_{CD} = \frac{\dot{m}_{a,total}}{1.099} \frac{1}{\sqrt{\dfrac{P_3\left(P_3-P_4\right)}{T_{ave}}}} \sqrt{\left(1-\left(\frac{A_{CD}^{\;2}}{A_3^2}\right)\right)}$$

(134)

Units for pressure are in psia, temperature is in Rankine, and mass flow rate is in lbm/s. This equation was unfortunately derived in English units, making it necessary to convert the resulting square inches to cm^2 for reporting in this thesis.

Appendix C: Rayleigh Flow Calculation Details

C.1 Bulk Mach Calculations

The preliminary calculations for the entrance and exit Mach numbers using incompressible flow and bulk parameters were completed using the method outlined below.

$$\rho = \frac{P}{RT} \tag{135}$$

$$U = \frac{\dot{m}}{\rho A} \tag{136}$$

$$a = \sqrt{\gamma RT} \tag{137}$$

$$M = \frac{U}{A} \tag{138}$$

C.2 Boundary Layer Displacement Calculations

The boundary layer displacement thickness is calculated from gathered testing data and the boundary layer relation found in Anderson (Anderson, 2001:810).

$$\mathrm{Re}_x = \frac{\rho U x}{\mu} \tag{139}$$

$$\delta^* = \frac{1.72x}{\sqrt{\mathrm{Re}_x}} \tag{140}$$

C.3 Rayleigh Flow Calculation and Computer Code

The theoretical exit Mach numbers for Rayleigh flow through the UCC were computed from the code described in the main text of Chapter 4. The code employed constants such as the entrance and exit area, the ratio of specific heats, the temperature

ratio, the initial temperature, the entrance Mach number, and the number of desired

iterations, N. Using this information the code first computes the step size for the area

contraction and temperature increase.

$$\Delta A = \left. \frac{A_2}{A_1} \right|_k = \frac{A_{Entrance} - A_{Exit}}{N} \tag{141}$$

$$\Delta T = \left. \frac{T_{t2}}{T_{t1}} \right|_k = \frac{T_{initial}\left(\frac{dT}{T}+1\right)}{N} \tag{142}$$

Then it computes the exit Mach number of an isentropic nozzle for a given area

contraction. The isentropic area relations are from Anderson (Anderson, 2001:567).

$$\frac{A_1}{A^*} = \left[\frac{1}{M_k^2} \left\{ \frac{2}{\gamma+1}\left(1+\frac{\gamma-1}{2}M_k^2\right) \right\}^{\frac{\gamma+1}{\gamma-1}} \right]^{\frac{1}{2}} \tag{143}$$

$$\frac{A_2}{A^*} = \frac{A_1}{A^*}\frac{A_2}{A_1} \tag{144}$$

$$\frac{A_2}{A^*} = \left[\frac{1}{M_a^2} \left\{ \frac{2}{\gamma+1}\left(1+\frac{\gamma-1}{2}M_a^2\right) \right\}^{\frac{\gamma+1}{\gamma-1}} \right]^{\frac{1}{2}} \tag{145}$$

The intermediate Mach number, M_a, is the value that is used at the beginning of the

Rayleigh flow calculation and it is found by using an iterative solver. The exit Mach

number for the Rayleigh heat addition is found using equations found in Zucker with a

known temperature ratio for that iteration (Zucker, 1977:291).

$$\frac{T_{t1}}{T_t^*} = \frac{2(1+\gamma)M_a^2}{\left(1+\gamma M_a^2\right)^2}\left[1+\frac{\gamma-1}{2}M_a^2\right] \tag{146}$$

$$\frac{T_{t2}}{T_t^*} = \frac{T_{t1}}{T_t^*} \frac{T_{t2}}{T_{t1}} \tag{147}$$

$$\frac{T_{t2}}{T_t^*} = \frac{2(1+\gamma)M^2_{k+1}}{\left(1+\gamma M_{k+1}^2\right)^2}\left[1+\frac{\gamma-1}{2}M^2_{k+1}\right] \tag{148}$$

The Mach number at the exit of the Rayleigh heat addition, M_{k+1}, is found with an iterative solver. Using this new Mach number the code repeats the steps for the area calculation followed by the Rayleigh calculation for the set number of iterations.

C.4 Rayleigh Pressure Losses

With the information garnered from the Rayleigh flow code, the pressure drop due to Rayleigh heat addition can be calculated. Using the entry and exit Mach numbers and assuming one dimensional Rayleigh flow through a constant area duct, the employment of the following equations from Zucker are used to find the stagnation pressure loss (Zucker, 1977:291).

$$\frac{P_{t1}}{P_t^*} = \frac{1+\gamma}{1+\gamma M_1^2}\left[\frac{1+\frac{\gamma-1}{2}M_1^2}{\frac{\gamma+1}{2}}\right]^{\frac{\gamma}{\gamma-1}} \tag{149}$$

$$\frac{P_{t2}}{P_t^*} = \frac{1+\gamma}{1+\gamma M_2^2}\left[\frac{1+\frac{\gamma-1}{2}M_2^2}{\frac{\gamma+1}{2}}\right]^{\frac{\gamma}{\gamma-1}} \tag{150}$$

$$\frac{dP_t}{P_t} = \frac{P_{t2}}{P_t^*}\frac{1}{\frac{P_{t1}}{P_t^*}} - 1 \tag{151}$$

C.5 Pressure Loss through Combustor

The pressure loss through the combustor is corrected to total pressure loss by use of isentropic flow relations. The instrumentation collects static pressures and they are used in the following calculations to determine the pressure loss percentage.

$$P_{t3} = P_3 \left(1 + \frac{\gamma - 1}{2} M_3^{\,2} \right)^{\frac{\gamma}{\gamma - 1}} \tag{152}$$

$$P_{t4} = P_4 \left(1 + \frac{\gamma - 1}{2} M_4^{\,2} \right)^{\frac{\gamma}{\gamma - 1}} \tag{153}$$

$$\frac{\Delta P}{P} = \frac{P_{t3} - P_{t4}}{P_{t3}} \tag{154}$$

Appendix D: Extra Emissions Plots

D.1 Emissions Plots for CW Configuration

The following plots provide more details about the combustion efficiency of the UCC in both configurations. These plots display g-loading versus efficiency broken down by cavity equivalence ratio, which is another method of repeating the information in Figure 34, Figure 35, Figure 36, and Figure 37 starting on page 82.
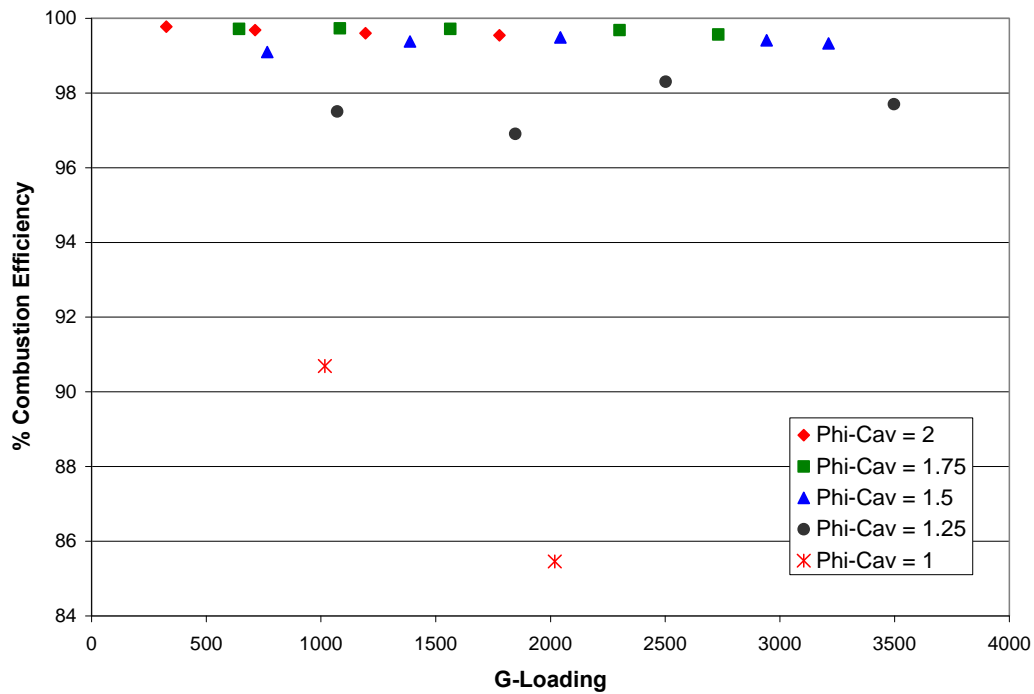

Figure 44. Efficiencies of the UCC in the JP-8 CCW configuration as a function of g-loading
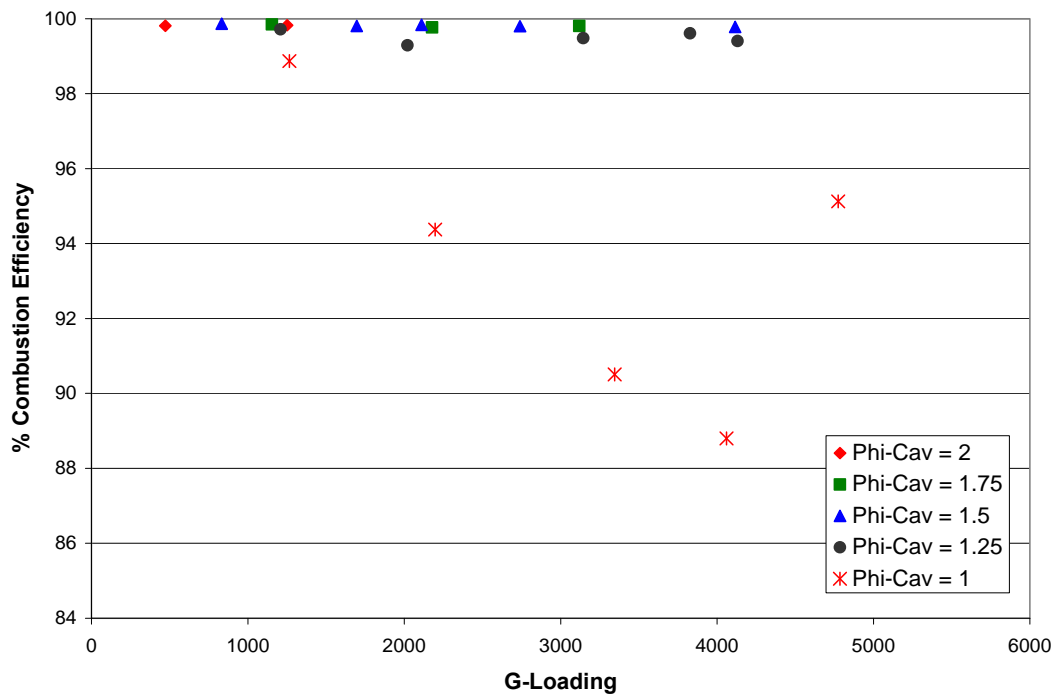
Figure 45. Efficiencies of the UCC in the FT CCW configuration as a function of g-loading
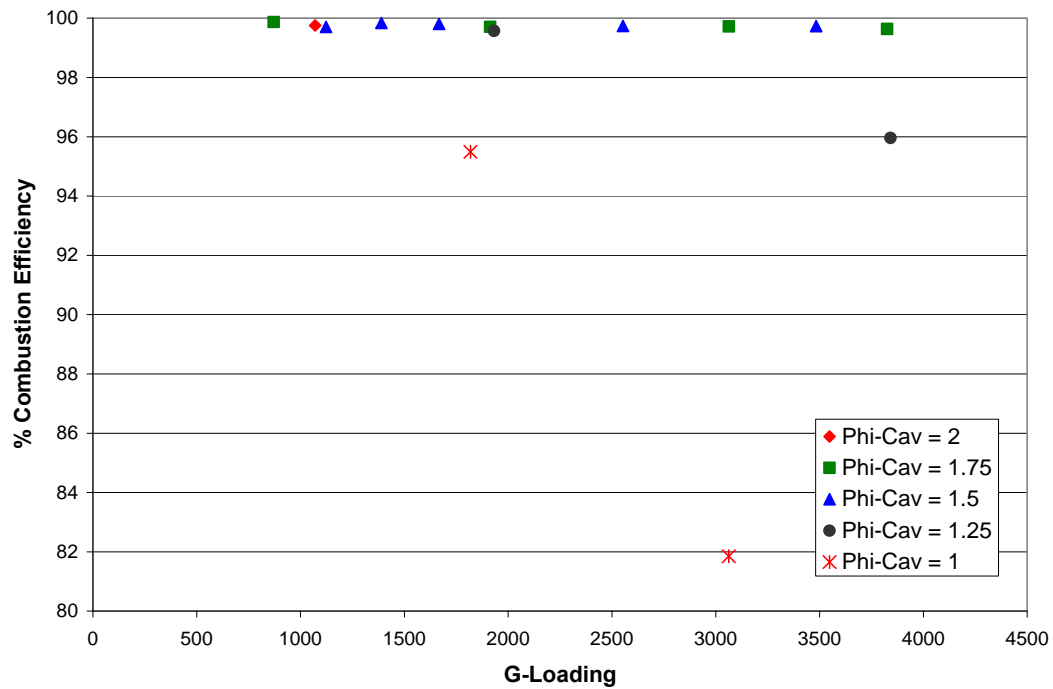

Figure 46. Efficiencies of UCC in the JP-8 CW configuration as a function of g-loading
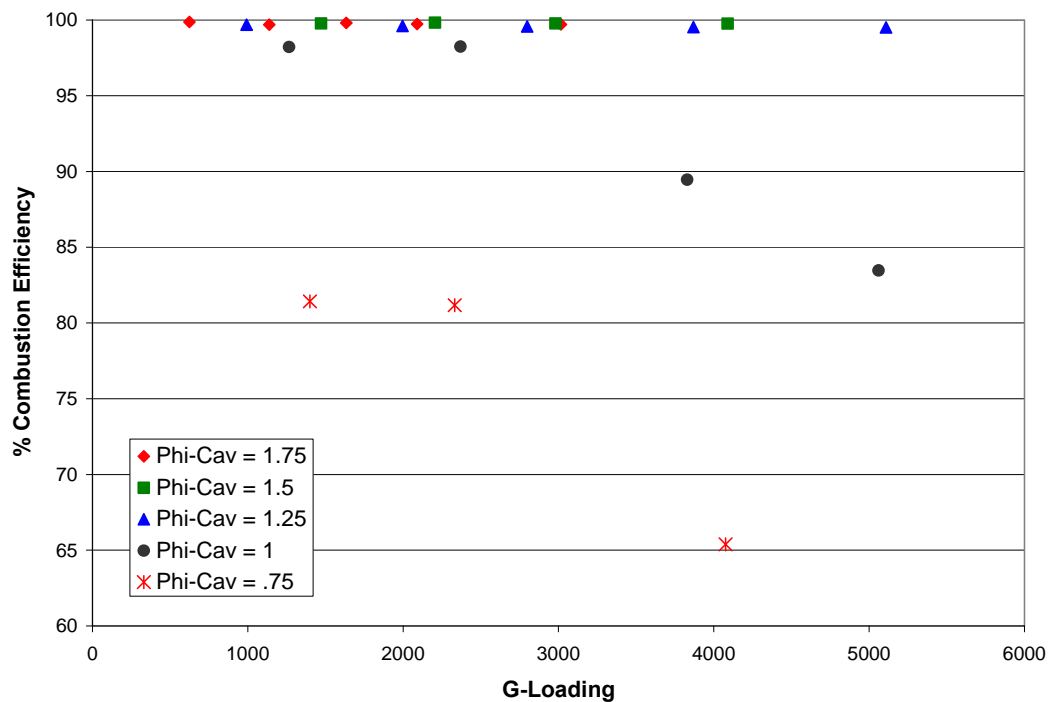
Figure 47. Efficiencies of the UCC in the FT CW configuration as a function of g-loading

D.2 More Efficiency Plots

The following figures provide more information on the operating efficiencies of the UCC. Each plot depicts a different cavity equivalence ratio and are included to supplement the information provided in Chapter 4.

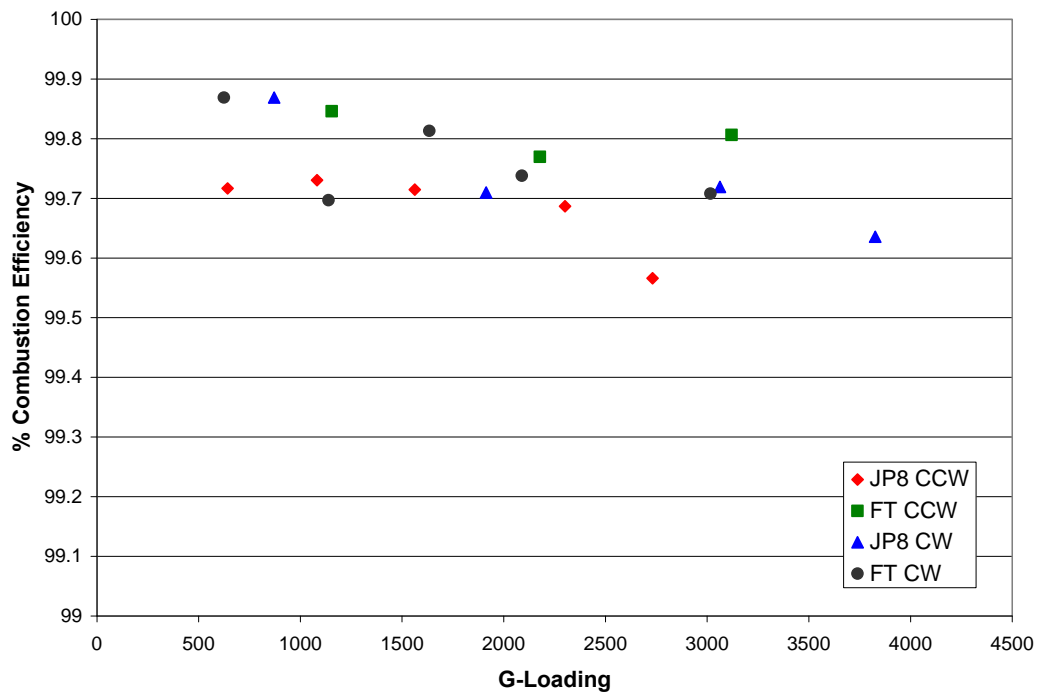**Figure 48. Efficiencies of the UCC for all configurations at a cavity equivalence ratio of 1.75**
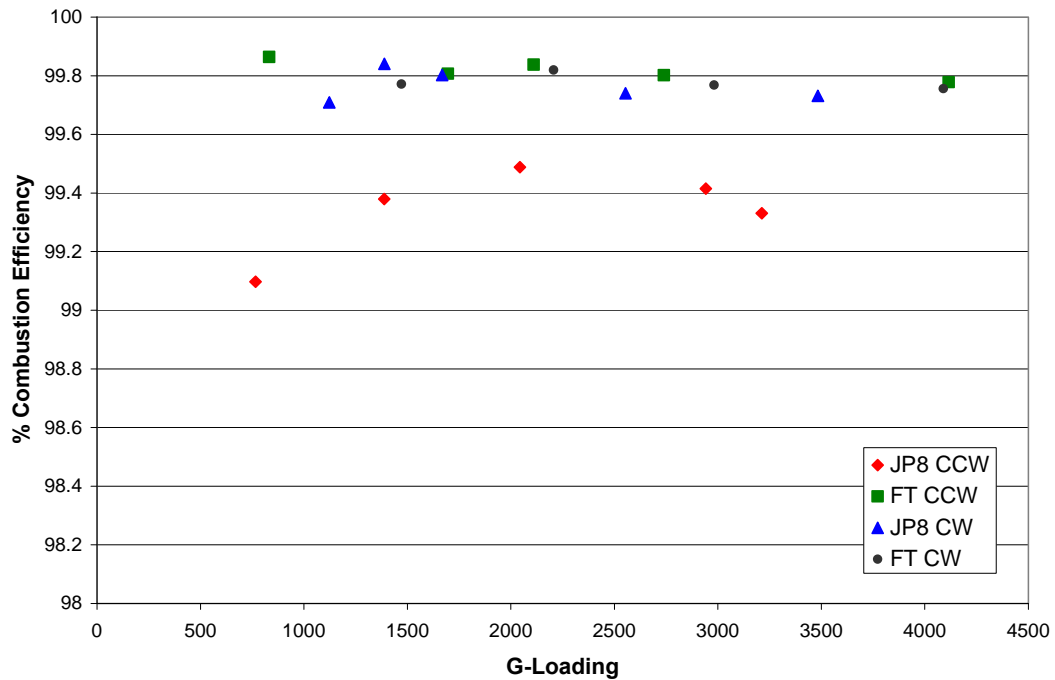

Figure 49. Efficiencies of the UCC for all configurations at a cavity equivalence ratio of 1.5
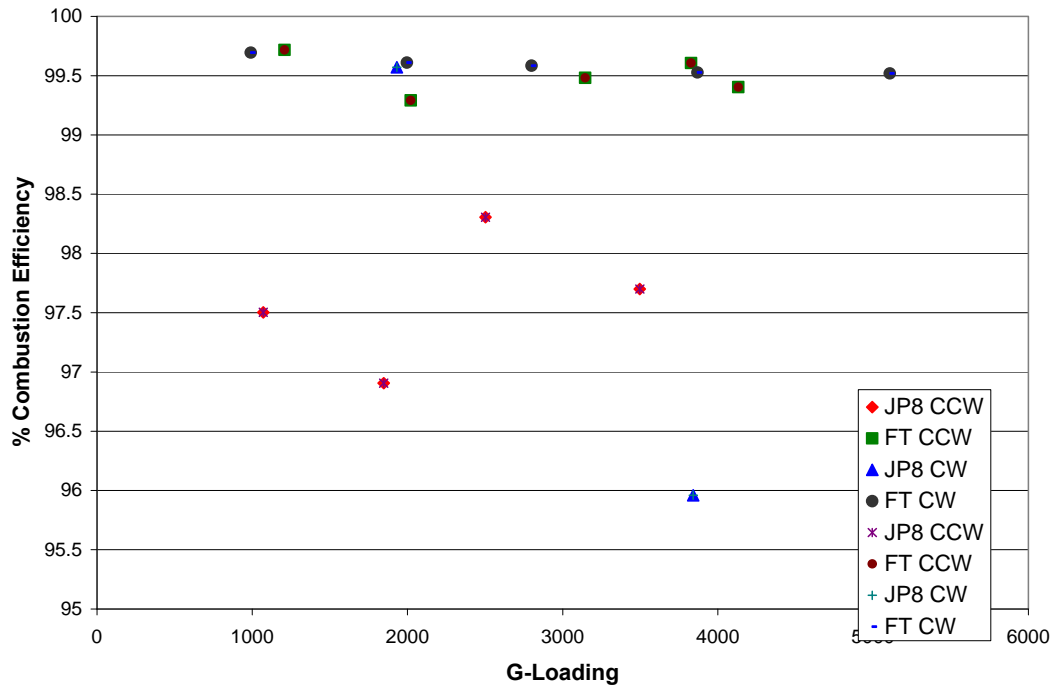
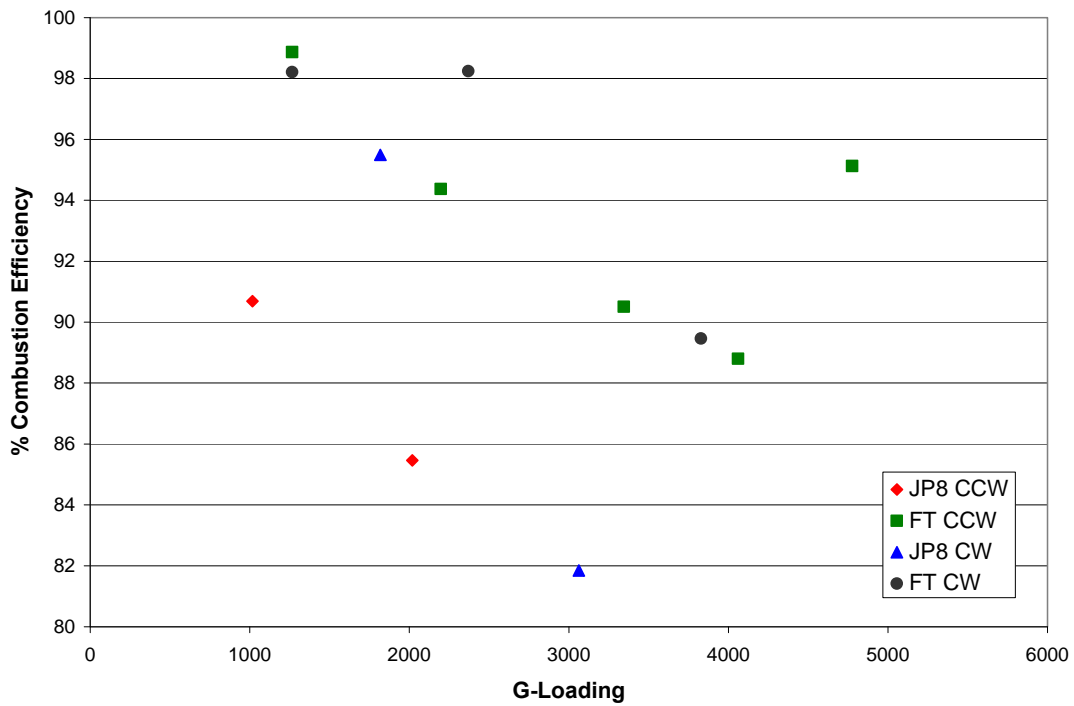**Figure 50. Efficiencies of the UCC for all configurations at a cavity equivalence ratio of 1.25**

Figure 51. Efficiencies of the UCC for all configurations at a cavity equivalence ratio of 1.0

Bibliography

Anderson, John D, *Fundamentals of Aerodynamics* (Third Edition), New York: McGraw Hill, 2001

Anisko, Jonathan F., Ralph A. Anthenien, and Joseph Zelina, "Numerical Investigation of Cavity-Vane Interactions within the Ultra Compact Combustor," 44th AIAA Aerospace Sciences Meeting & Exhibit, AIAA 2006-805, Reno, NV: January 2006

Anthenien, Ralph A. and Joseph Zelina, "Experimental Results on the Turbulent Regimes within a Small-Scale Atmospheric Pressure High-g Combustor," Proceedings of 2006 Technical Meeting of the Central States Section of The Combustion Institute, WPAFB, OH, 2006.

Barnard, J. A. and J. N. Bradley, *Flame and Combustion* (Second Edition), New York: Chapman and Hall, 1985.

Corporan, Edwin, Matthew J. DeWitt, Vincent Belovich, Robert Pawlik, Amy Lynch, James Gord, and Terrence Meyer, "Emissions Studies of a Turbine Engine and Research Combustor Burning a Natural Gas Derived Fischer-Tropsch Jet Fuel," Draft awaiting publication after review in *Energy and Fuels* as of May 2007.

Ehret, J., "Design Optimization of a High-G Loaded Ultra-Compact Combustor," M.S. Thesis, Wright State University, Dayton, OH, 2002.

Greenwood, Roger T., "Numerical Analysis and Optimization of the Ultra Compact Combustor," MS Thesis, AFIT/GAE/ENY/05-M10, Graduate School of Engineering and Management, Air Force Institute of Technology (AU), Wright-Patterson AFB, OH: March 2005.

Hill, Philip and and Carl Peterson, *Mechanics and Thermodynamics of Propulsion* (Second Edition), New York: Addison-Wesley, 2002.

Koch, Pete, Aerospace Engineer AFRL/PRTT, Personal Communications with the author May 2007

Lefebvre, Arthur H., *Gas Turbine Combustion* (Second Edition), Philadelphia, PA: Taylor & Francis: 1999

Lewis, George D, "Swirling Flow Combustion – Fundamentals and Application," 9th AIAA/SAE Propulsion Conference, AIAA 73-1250. Las Vegas, NV: 1973

Lewis, George D, "Centrifugal-Force Effects on Combustion," Fourteenth Symposium on Combustion, 413-419, Pittsburgh, PA: The Combustion Institute, 1972.

Liu, Feng and William A. Sirignano, "Turbojet and Turbofan Engine Performance Increases Through Turbine Burners," 38th AIAA Aerospace Sciences Meeting & Exhibit. AIAA-2000-0741, Reno NV: January 2000

Mao, Chien-Pei, Delevan TFT Chief Technologist, Personal Communications with Dr. Joseph Zelina, PhD, 2003

Mattingly, Jack D., William H. Heiser, and David T. Pratt, Aircraft *Engine Design* (Second Edition), Reston, VA: 2002.

Quaale, Ryan J., Ralph A Anthenien, Joseph Zelina, and Jeffrey Ehret, "Flow Measurements within a High Swirl Ultra Compact Combustor for Gas Turbine Engines," ISABE-2003-1141, WPAFB, OH: 2003

Roquemore, W.M., Dale Shouse, Dave Burrus and others, "Trapped Vortex Combustor Concept of Gas Turbine Engines," 39th AIAA Aerospace Sciences Meeting & Exhibit, AIAA 2001-0483, Reno, NV: January 2001

Saad, Michel A., *Compressible Fluid Flow,* Englewood Cliff, NJ: Prentice-Hall, 1985

Saravanamutto, HIH., GFC Rogers, and H. Cohen, *Gas Turbine Theory* (Fifth Edition), Harlow, England: Pearson Education Limited, 2001.

Sirignano, W. A. and F. Liu, "Performance Increases for Gas-Turbine Engines Through Combustion Inside the Turbine," *Journal of Propulsion and Power,* Vol 14 No 6 (December 1998).

Society of Automotive Engineers, Inc., "Aerospace Recommended Practice: Procedure for the Calculation of Gaseous Emissions from Aircraft Turbine Engines." ARP1533, Warrendale, PA: 1994

Sturgess, G.J and K.Y. Hsu, "Combustion Characteristics of a Trapped Vortex Combustor," Contract F33615-95-C-2507, Beavercreek, OH: Innovative Scientific Solutions, Inc., October 1998

Zelina, J., R.T. Greenwood, and D.T. Shouse, "Operability and Efficiency Performance of Ultra-Compact, High Gravity (g) Combustor Concepts," Proceedings of ASME TURBO EXPO '06: 51st ASME International Gas Turbine and Aeroengine Congress and Exposition, GT2006-90119, Barcelona, Spain: May 2006a

Zelina, J., D.T. Shouse, and R.D. Hancock, "Ultra-Compact Combustors for Advanced Gas Turbine Engines," Proceedings of ASME TURBO EXPO '04: 49th ASME International Gas Turbine and Aeroengine Congress and Exposition, 2004-GT-53155, Vienna, Austria: June 2004a

Zelina, J., Dale T. Shouse, and Craig Neuroth, "High-Pressure Tests of a High-g, Ultra-Compact Combustor," 41st AIAA/ASME/SAE/ASEE Joint Propulsion Conference and Exhibit, AIAA 2005-3779, Tucson, AZ: July 2005

Zelina, J., D.T. Shouse, J.S. Stutrud, G.J. Sturgess, and W.M. Roquemore, "Exploration of Compact Combustors for Reheat Cycle Aero Engine Applications," Proceedings of ASME Turbo Expo '06 51st ASME International Gas Turbine and Aeroengine Congress and Exposition, GT2006-90179, Barcelona, Spain: May 2006b

Zelina, J., G.J. Sturgess, and D.T. Shouse, "The Behavior of an Ultra-Compact Combustor (UCC) Base on Centrifugally-Enhanced Turbulent Burning Rates," 40th AIAA/ASME/SAE/ASEE Joint Propulsion Conference and Exhibit, AIAA 2004-3541, Fort Lauderdale, FL: July 2004b

Zucker, Robert D., *Fundamentals of Gas Dynamics,* Chesterfield OH: Matrix Publishers, 1977

Vita

Ensign James T. Radtke graduated from Pike High School in Indianapolis, IN. He entered undergraduate study in the Fall of 2002 at Purdue University in West Lafayette, IN where he graduated with a Bachelor of Science in Aeronautical and Astronautical Engineering in May of 2006. He was commissioned through the Navy ROTC program at Purdue University.

His first assignment was to the Graduate School of Engineering and Management at the Air Force Institute of Technology, Wright-Patterson Air Force Base, Ohio. Upon graduation, he will begin training to become a Naval Aviator in Pensacola, Florida.

REPORT DOCUMENTATION PAGE		*Form Approved* *OMB No. 074-0188*

The public reporting burden for this collection of information is estimated to average 1 hour per response, including the time for reviewing instructions, searching existing data sources, gathering and maintaining the data needed, and completing and reviewing the collection of information. Send comments regarding this burden estimate or any other aspect of the collection of information, including suggestions for reducing this burden to Department of Defense, Washington Headquarters Services, Directorate for Information Operations and Reports (0704-0188), 1215 Jefferson Davis Highway, Suite 1204, Arlington, VA 22202-4302. Respondents should be aware that notwithstanding any other provision of law, no person shall be subject to an penalty for failing to comply with a collection of information if it does not display a currently valid OMB control number.
PLEASE DO NOT RETURN YOUR FORM TO THE ABOVE ADDRESS.

1. REPORT DATE *(DD-MM-YYYY)* 14 Jun 07	2. REPORT TYPE **Master's Thesis**	3. DATES COVERED *(From – To)* **Jun 2006 – Jun 2007**	
4. TITLE AND SUBTITLE Efficiency and Pressure Loss Characteristics of an Ultra-Compact Combustor with Bulk Swirl		5a. CONTRACT NUMBER	
		5b. GRANT NUMBER	
		5c. PROGRAM ELEMENT NUMBER	
6. AUTHOR(S) Radtke, James T., Ensign, USN		5d. PROJECT NUMBER	
		5e. TASK NUMBER	
		5f. WORK UNIT NUMBER	

7. **PERFORMING ORGANIZATION NAMES(S) AND ADDRESS(S)** Air Force Institute of Technology Graduate School of Engineering and Management (AFIT/EN) 2950 Hobson Way WPAFB OH 45433-7765	8. PERFORMING ORGANIZATION REPORT NUMBER **AFIT/GAE/ENY/07-J18**
9. SPONSORING/MONITORING AGENCY NAME(S) AND ADDRESS(ES) AFRL/PRTC Attn: Dr. Joseph Zelina 1790 Loop Road North (937)255-7487 DSN: 986-4570	10. SPONSOR/MONITOR'S ACRONYM(S)
	11. SPONSOR/MONITOR'S REPORT NUMBER(S)

12. DISTRIBUTION/AVAILABILITY STATEMENT
APPROVED FOR PUBLIC RELEASE; DISTRIBUTION UNLIMITED.

13. SUPPLEMENTARY NOTES

14. ABSTRACT
    Research was conducted on a novel combustor design using a highly centrifugal loaded circumferential cavity to enhance flame speeds and lower mixing time to lower overall combustion time achieving improved efficiency and stability. This Ultra-Compact Combustor (UCC) is fed air with a bulk swirl, resembling gas leaving a compressor without the final set of compressor guide vanes to straighten the flow, at higher than normal Mach numbers for a combustor. The larger Mach numbers in the combustor do not cause a total pressure loss in excess of what Rayleigh theory would dictate for the given heat addition taking place within the combustor.
    Tests were conducted on the UCC with a clockwise or counter-clockwise swirl direction in the circumferential cavity using JP-8 and natural gas derived Fischer-Tropsch synthetic jet fuel with each direction. The results for lean blow out stability, combustion efficiency, and emissions proved that the best configuration uses counter-clockwise swirl. The two fuels performed equally with no noticeable differences between JP-8 and the synthetic Fischer-Tropsch fuel.

15. SUBJECT TERMS
High-g Combustion, Ultra-Compact Combustor, Inner-Turbine Burner

16. SECURITY CLASSIFICATION OF:			17. LIMITATION OF ABSTRACT	18. NUMBER OF PAGES	19a. NAME OF RESPONSIBLE PERSON Dr. Paul King (AFIT/ENY)
REPORT **U**	ABSTRACT **U**	c. THIS PAGE **U**	**UU**	144	19b. TELEPHONE NUMBER *(Include area code)* (937) 255-3636, ext 4628 e-mail: paul.king@afit.edu

Standard Form 298 (Rev: 8-98)
Prescribed by ANSI Std. Z39-18